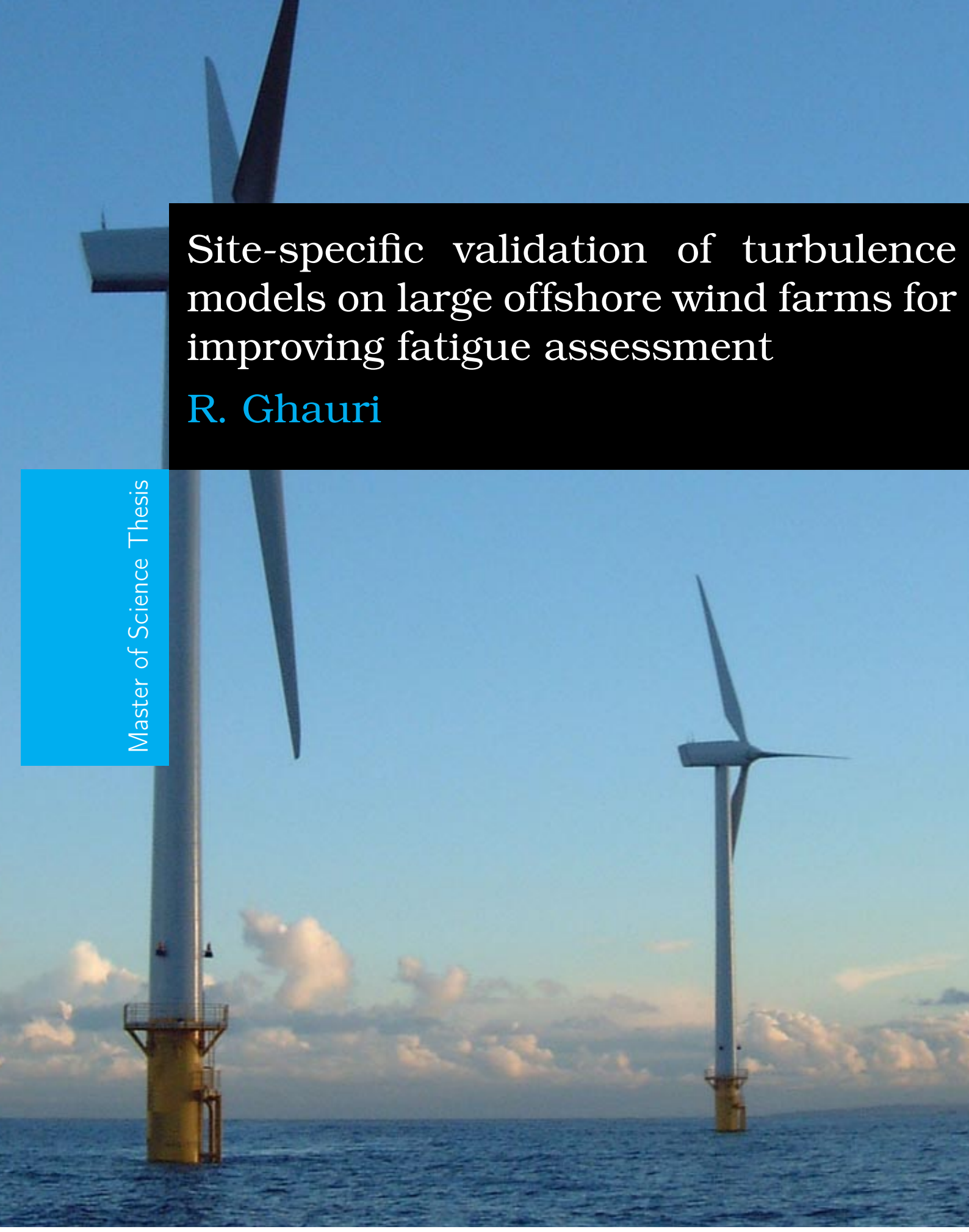

Site-specific validation of turbulence models on large offshore wind farms for improving fatigue assessment

R. Ghauri

Master of Science Thesis

TU Delft Delft University of Technology

SIEMENS Gamesa RENEWABLE ENERGY

Site-specific validation of turbulence models on large offshore wind farms for improving fatigue assessment

Master of Science Thesis

For the degree of Master of Science in Sustainable Energy Technology at Faculty of Electrical Engineering, Mathematics and Computer Science, Delft University of Technology

Autonomous systems

Author:	Rameen Ghauri	
Committee:	Prof. Simon Watson	TU Delft
	Dr Laura Valldecabres Sanmartin	Siemens Gamesa Renewable Energy
	Dr Alexandros Iliopoulos	Siemens Gamesa Renewable Energy

March 5, 2021

TU Delft Delft University of Technology

SIEMENS Gamesa RENEWABLE ENERGY

Abstract

Wind turbines installed in a wind farm are typically subject to increased turbulence because they are in the wake of upstream wind turbines that generate additional turbulence. Accurate prediction of turbulence in wind farms is critical as it is proportional to wind turbine fatigue loads, power losses and prediction of wind farm lifetime. IEC Standard 61400-1 suggests the use of the semi-empirical turbulence model called Frandsen model, which was originally proposed in 1999. Since the development of the Frandsen model, the size of wind turbines and wind farms has increased significantly. Therefore, this work aims to determine the accuracy of two versions of the Frandsen model: Standard and Modified, when applied to large offshore wind farms experiencing a combination of atmospheric stability conditions. This is done by comparing the estimated wind farm turbulence under specific atmospheric stability conditions with measurements from Westermost Rough and Horns Rev 2. It was found that the atmospheric stability distribution and the distance of the upstream wake inducing wind turbine at the offshore site plays a significant role in the accuracy of the estimated turbulence from the Frandsen models. The estimated turbulence intensity from the Standard and Modified Frandsen models was found to be under-predicted with respect to the measured turbulence for all atmospheric stability conditions at both wind farms. For wind directions with wake flow for upstream wind turbines more than 10 rotor diameters away, the Modified Frandsen model showed better prediction of turbulence intensity compared to the Standard Frandsen model. On the other hand, for wind directions with wake flow for upstream wind turbines less than 10 rotor diameters away, the Standard Frandsen model showed better turbulence intensity estimation compared to the Modified Frandsen model. Among all atmospheric stability conditions, the turbulence intensity estimate was closest to the measured data for unstable conditions. It is suggested that this fact can be attributed to the presence of a significant number of unstable conditions in the offshore wind farms used for the design of the semi-empirical Frandsen model.

Acknowledgements

First and foremost, I thank ALLAH for giving me the strength and opportunity to complete this project.

I would like to express my sincere gratitude to my thesis supervisors from TU Delft University, Professor Simon Watson and from Siemens Gamesa Renewable Energy, Dr. Laura Valldecabres Sanmartin and Dr. Alexandros Iliopoulos for their invaluable guidance, patience, motivation, enthusiasm and immense knowledge sharing. They very patiently listened to my doubts, questions and concerns and gave me the guidance at every step of this exciting journey into the world of wind turbulence. I would also like to thank Laurant Beaudet for helping me and providing me with the necessary data and guidance for this analysis. These months have been a great learning experience where I have not only developed academically but also made some new friends.

My sincere thanks also go to Dr. Pim Versteijlen, who provided me with the opportunity for a summer internship in Siemens Gamesa, which ultimately led to me being able to work on this diverse and exciting project. It was an honor for me to be a part of this highly professional team at SGRE. My sincere thanks also go to all the SGRE team members who contributed to my thesis and supported me throughout this process.

A special thanks goes to my friends in Delft, without whom I would not have been able to cope with the stressful moments during the last year. I really appreciate their support and will always have pleasant memories of them.

I am very grateful to my parents for their love, prayers and for giving me the emotional support and strength during those difficult times of isolation and fear due to the pandemic. I also thank my brother and sister for their invaluable support in helping me through this. Without the support of my family, this would not be possible. I thank them for their never-ending care and love.

Contents

List of Figures

List of Tables

Nomenclature

Latin symbols

A	Axial induction factor	m/s
g	Acceleration due to gravity	
s	Normalized turbine spacing	
k	Weibull scale parameter	
k	Von Karman Constant	
ρ	Density	kg/m^3
σ	Standard deviation	
ψ_m	Stability Correction Function	
β_0	Wake expansion constant ranging from 0.15-0.2	
ζ	Dimensionless Stability Parameter	
θ	Wind Direction	
θ_{wj}	View angle of the turbine J seen from the wake of the affected turbine	
θ_j	Wind Turbine alignment with respect to the wind turbine of interest	
θ	Mean Virtual Potential Temperature	
θ_*	Surface layer temperature scale	
$\overline{\theta_v}$	Mean virtual potential temperature	
$(\overline{w`\theta`})$	Surface virtual potential heat flux	
f_{wd}	Probability of wind coming from wind direction θ for free stream wind U	
c	Weighting-factor less than unity	
D	Width of the wake at a downstream distance of S	
D_0	Rotor diameter normalised by rotor diameter	m
I	Turbulence intensity	$\%$
L	Obukhov Length	
N	Number of Wind Turbines	
Ri	Richardson Number	
U	Mean wind speed	m/s
U_*	Friction Velocity	
X	Distance	m

Subscripts

c	Critical

j	Upstream Wind Turbine
n	Near wake
t	Thrust
u	Wind speed
w	Wake
x	Streamwise
y	Spanwise
z	Height
wf	Wind farm
add	Added
amb	Ambient
$char$	Characteristic
dir	Directional
eff	Effective
ref	Reference
rep	Representative
sec	Sector

Abbreviations

HR2	Horns Rev 2
WMR	Westermost Rough
ABL	Atmospheric boundary layer
CFD	Computational Fluid Dynamics
ECN	Energy Research Centre of the Netherlands
IEC	International Electrotechnical Commission
LES	Large Eddy Simulation
TKE	Turbulent Kinetic Energy
LCoE	Levelized Cost of Electricity
RANS	Reynolds Averaged Navier Stokes
SGRE	Siemens Gamesa Renewable Energy
TMDB	Turbine Measurement Database
WAsP	Wind Analysis and Application Program
WFDB	Wind Farm Database
IRENA	International Renewable Energy Agency
LIDAR	Light Detection and Ranging System
SCADA	Supervisory Control and Data Acquisition

Chapter 1

Introduction

1.1 Scope of the Thesis

With global warming at its peak, the focus is on decarbonizing the energy sector to limit climate change. The Paris Agreement set a climate goal of limiting global temperature rise to below $2°C$ [1]. To achieve this goal, it required the transformation of the current energy sector with the rapid development of sustainable energy generation sources. This has led to an accelerated deployment of wind energy, with an increasing number of wind turbines and wind farms being installed mainly offshore due to their higher potential. According to a recent study by IRENA (International Renewable Energy Agency), energy development pathways to 2050 were investigated in order to meet the Paris climate targets. It was found that the future wind power sector alone would contribute to more than a quarter of the total emission reductions required [2]. With the developed pathways and current trends, a tenfold increase in global cumulative installed offshore wind energy is expected by 2030, approaching 1000 GW by 2050 [2]. This increased demand in the future, in addition to the current growing number of wind farms installed worldwide, requires efficient wind farm design.

Wind turbines installed in a wind farm are typically subject to increased turbulence because they are in the wake of upstream wind turbines that generate added turbulence. This increased turbulence is a combination of the free stream ambient and the turbine added turbulence. Its accurate prediction is critical because it is proportional to the wind turbine fatigue loads [3], power losses, and the lifetime prediction of a wind farm [4]. All these factors contribute to an efficient wind farm design. Since fatigue loads are known as the main design driver for the support structure, their good estimation based on increased turbulence will act as a key factor to reduce the overdesign and increase the lifetime of the wind turbine and consequently reduce the LCoE.

To estimate the fatigue loads for an offshore wind turbine in a wind farm, the Frandsen model explained in the IEC Standard 61400-1 [5] is used. This semi-empirical model was proposed back in 1999, where Frandsen calculates a design variable called effective turbulence intensity assuming neutral atmospheric stratification to determine the fatigue loads [3]. The effective turbulence is a

function of the wind probability, ambient turbulence intensity and wake added turbulence intensity [3]. As the size of wind turbines and wind farms increased, the accuracy of the model became questionable [6]. Therefore, in conjunction with established work within SGRE (Siemens Gamesa Renewable Energy), this thesis aims to determine the accuracy of the Frandsen model for calculating turbulence within the offshore wind farm under different atmospheric stability conditions. This research will help to identify the factors contributing to the inaccuracy of the model which, if removed, would improve the turbulence estimation and consequently the fatigue load estimation and support structure design.

1.2 Literature review

Wind turbines operating in a wind farm encounter two main problems when exposed to the wake of an upwind turbine: Power losses due to the velocity deficit and an increased fatigue load due to the generation of added turbulence intensity [7, 8]. Several studies [9, 10, 11, 12] show that induced vortices increase the turbulence intensity in the wake with respect to the turbulence level of the incoming atmospheric boundary layer flow. Recent studies show that the wake decay is affected by ambient turbulence and turbine-induced turbulence [13]. The wake recovery rate is proportional to the turbulence intensity, since higher turbulence increases the momentum transfer between the wake and the outer region [14, 15]. Therefore, wakes decay faster at locations with a higher roughness length than in a smooth boundary layer[16]. This effect explains the higher wake recovery rate for onshore sites due to higher turbulence and roughness length compared to offshore sites, where the wake recovery rate is more dependent on turbine generated turbulence due to the lower ambient turbulence level [14]. These wake characteristics - increased turbulence and reduced velocity - are highlighted in an offshore wind farm due to a lower wake recovery rate, leading to severe impacts - increased fatigue load and reduced energy production. Therefore, to improve the lifetime and power efficiency of the wind turbine, an accurate assessment of wake effects is essential for the design of an offshore wind farm.

1.2.1 Wake turbulence models

Over the past few years, several researchers have worked on developing models to accurately predict the wind speed deficit caused by wind turbine wake. However, very little work has been done on developing models to predict the wake added turbulence intensity. The wake of a wind turbine is divided into two regions: the near wake and the far wake [7]. In the downwind direction, the near wake region extends over 2 to 4 diameters [17], followed by the far wake region. Flow in the near wake region is influenced by tip vortices, stalled flow, and also by the geometry of the blades, nacelle, and tower [18]. Since it is difficult to model this region, most models focus on the fully developed wake in the far wake region. Here, the velocity deficit and the added turbulence intensity are assumed to have a self-similar distribution and symmetric behaviour across the wake centre [7] as shown in Figure1.1.

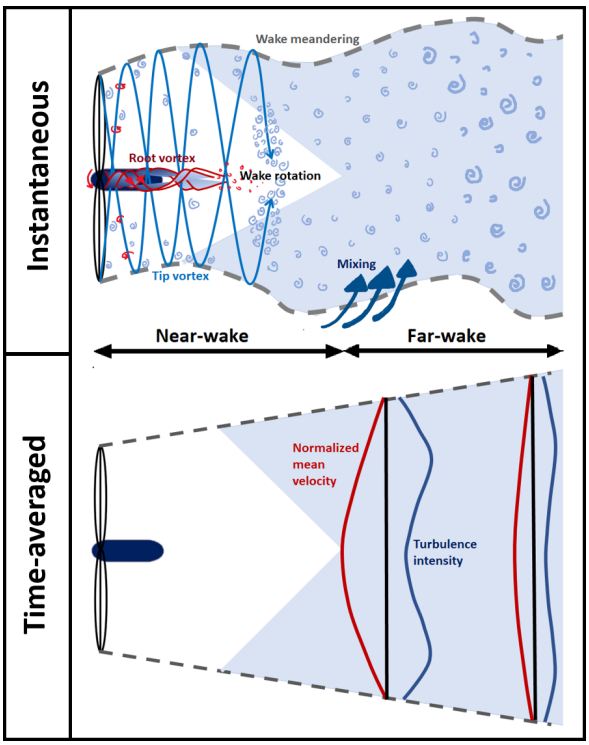

Figure 1.1: Schematic top view of the evolution of the wake structure and characteristics behind the wind turbine at hub height (Adapted from [19, 20])

Several numerical, analytical and empirical models are proposed to estimate and study the turbulence intensity of wind farms. Numerical models are capable of making predictions under highly controlled boundary conditions, using methods such as RANS (Reynolds-averaged Navier-Stokes) equations and LES (large-eddy simulation). A detailed review of numerical approaches was provided by Sanderse et al. in 2011 [21]. Here, LES was the popular method that had to run thousands of cases for data accuracy. However, this also made it computationally expensive [22].

In contrast, analytical and empirical models are simple and fast and provide quantitative predictions based on available knowledge and measurements of practical relevance [18]. Initially, these models were developed and tested for predicting turbulence intensity behind a single wind turbine [17, 22]. Next, research was extended to focus on the analysis of turbulence from multiple wakes in arrays. Since the combined effect of wakes has an impact on the structure of the boundary layer. This is the order in which the previous models will be presented.

Models based on single wind turbine wake

Several empirical and semi-empirical models have been proposed that looked into the prediction of added turbulence intensity in the far-wake region of the wind turbine. Amongst others, Quarton and Ainslie(1990) [23] (Equation 1.1), followed by Crespo and Hernandez (1996) [24] (Equation 1.2), were the first to present an

empirical model. Their models were based on wind tunnel and full-scale measurements from an individual wind turbine wake. They showed a proportional relation of ambient turbulence (I_{amb}), thrust coefficient (C_t) [23] and axial induction factor (a) [24] with the added turbulence intensity. The assess the above mentioned models they were validated with experimental data. The validation studies [13, 25] showed consistent over prediction of turbulence intensity in the far-wake region.

$$I_{add} = 4.8 C_t^{0.70} I_{amb}^{0.68} \frac{X_x}{X_n}^{-0.57} \tag{1.1}$$

where,
X_x - Downstream distance from wind turbine,
X_n - estimated near wake length[26]

$$I_{add} = 0.73 a^{0.8325} I_{amb}^{0.0325} \frac{X_x}{D}^{-0.32} \tag{1.2}$$

where,
D - Diameter of the wind turbine rotor

Xie and Archer [27] presented another single wind turbine wake empirical model (Equation 1.3) which was based on the fitting of LES results. The study of LES results showed that the peak added turbulence intensity was at a downstream distance of 4-5 turbine diameters.

$$I_{add} = 5.7 C_t^{0.5} I_{amb}^{0.68} \frac{X_x}{X_n}^{-0.96} \tag{1.3}$$

Lastly, in 2018, Ishihara and Qian [28] proposed a 3-dimensional wake model for a single wind turbine. This model was validated using LES. Compared to the previous models, the model of Ishihara and Qian showed the highest correlation between the predicted wake and the simulations. However, this model still needs to be validated with measured or experimental data. In general, all the aforementioned models show a gradual decrease in the added turbulence intensity with increasing downstream position, in agreement with observations.

Models based on multiple wind turbine wakes

In the literature on wind turbine wake modelling, Lissaman, in 1979 [29] was the first to propose the idea of linear superposition, i.e., the addition of the turbulence variance of the various interacting turbulent flows. It is a very strong first assumption given the fact that it ignores the dynamic interactions between the turbulent flows. However, it serves as a modelling approach. This assumption was seen to fail for larger turbulence variance, due to its overestimation when multiple wakes superimposed. Later, in 1987, Katic et al. [30] proposed the second idea - linear superposition of the square of the turbulence variance of the wind flow. In this proposal, the cumulative effect of multiple wakes was smaller than the results obtained by the linear superposition of turbulence. In addition, this assumption had better agreement with experimental data.

In 1992, Teknisk Grundlag [31] presented the assumption that fatigue loading is proportional to the standard deviation of wind speed fluctuations divided by the mean wind speed (Equation 1.4), also known as the turbulence intensity. It was also shown from measurements that this proportionality holds for both wake and non-wake conditions.

$$I = \frac{\sigma_u}{U} \tag{1.4}$$

The aforementioned assumptions later motivated the definition of resultant turbulence intensity in the wake, I_w, as a combination of ambient turbulence intensity, I_{amb}, and added wake turbulence intensity, I_{add}, [24]. The resultant wake turbulence intensity and effective turbulence intensity were then calculated as[32]:

$$I_w = \sqrt{{I_{amb}}^2 + {I_{add}}^2} \tag{1.5}$$

$$I_{eff} = \sqrt{{I_{amb}}^2 + c^2{I_{add}}^2} \tag{1.6}$$

where,
I_{eff} - Effective turbulence intensity,
I_w - Maximum Wake turbulence intensity,
c - weighting-factor less than unity [32]

Based on the assumption by Teknisk Grundlag [31], Frandsen [3], in 1999, presented a semi-empirical model for calculating added wind farm ambient turbulence intensity (Equation 1.7) in a fully developed indefinitely large wind farm. The added wind farm ambient turbulence is the turbulence intensity added due to the presence of the wind farm, where wind turbines are considered as roughness elements. It was estimated based on the following approximation since it was noted to be fairly insensitive to geostropic wind speed, hub height and surface roughness.

$$I_{add,wf,amb} = \frac{1.8\sqrt{C_t}}{5\sqrt{C_t} + \sqrt{s_x s_y}} = \frac{0.36}{1 + 0.2\sqrt{\frac{s_x s_y}{C_t}}} \tag{1.7}$$

where,
s_x - Streamwise turbine spacing normalized by the rotor diameter,
s_y - Spanwise turbine spacing normalized by the rotor diameter

Here 1.8 and 5 are empirically estimated coefficients. In an attempt to link the model of added wind farm ambient turbulence to turbulence in the individual wakes, in 2007, Frandsen [32] proposed a relation (Equation 1.8) for calculating added wake turbulence intensity for a narrowly spaced wind farm. In this case, the wind turbines were installed at 2 rotor diameter or less, perpendicular to the wind direction [32]. It was also demonstrated by Frandsen [32] that the observed turbulence intensity was dominated by the added turbulence from the closest wind turbine.

$$I_{add,wake} = \frac{1}{1.5 + s\frac{0.8}{\sqrt{C_t}}} \tag{1.8}$$

where,
s - Turbine spacing normalized by the rotor diameter,

Later, in 2015, Niayifar and Porte-Agel [33] proposed a model for the wind farm turbulence intensity based on the maximum added turbulence intensity resulting from the closest wind turbine. However, since this model was based on the single wind turbine wake model, it would require modifications when applied to a wind farm with greater than 5 rows [5].

1.2.2 Validation of wake turbulence model

Frandsen and Madsen, in 2003, validated the added wind farm ambient turbulence intensity (Equation 1.7) with met mast measurements from the Norrekaer Enge II [34]. A comparison between the modelled and the measured wind farm ambient turbulence was performed at multiple heights using met mast data inside and outside the wind farm. That showed a good correlation between the two compared turbulence values above the rotor height. It was noted that the added wind farm ambient turbulence model neglected the variation of turbulence intensity over the rotor as a function of height and assumed that the spatially averaged shear forces acted on the flow at hub height. Whereas based on measured data the shear force imposed by the wind turbine was noted to be vertically distributed across the rotor. This observation led to the concept of wind farm ambient turbulence intensity, as an average of above and below rotor turbulence intensity (Equation1.9). Here, turbulence was assumed to vary linearly across the rotor with an assumption of constant turbulence above and below the rotor. The turbulence below the rotor was chosen to be equal to ambient turbulence (I_{amb}).As a general rule, this formula is used for locations within the wind farm where there are more than five turbines present upstream. This is when the internal boundary layer (IBL) is fully developed and reaches the height of the atmospheric boundary layer (ABL).

$$I_{wf,amb} = \frac{1}{2}(\sqrt{I_{add,wf,amb}{}^2 + I_{amb}{}^2} + I_{amb}) \tag{1.9}$$

In 2007, Barthelmie and Frandsen conducted another comparative study of modelled added turbulence intensity with measured data from Middlegrunden offshore wind farm, comprising of a single gently curved row of wind turbines [35]. Here, due to lack of met mast data, the ambient turbulence was estimated based on nacelle measurements. The unique part about this study was the relatively close spacing of 2.4D in the wind farm that was noted to be beyond the limit of the wake model. During this study, the modelled added turbulence intensity was calculated using the expression of Frandsen added turbulence intensity (Equation 1.8) [32]. The results showed a common trend between the measured and modelled added wake turbulence intensity with respect to wind direction. However, an under-prediction of the absolute value of modelled wake turbulence was noted. This could have resulted from the negligence of stability and coastal effects during the calculation of ambient turbulence intensity provided by Wind Analysis and Application Program (WAsP). Another similar study with relatively close spacing of 3.8D in Energy Research Centre of the Netherlands (ECN) wind turbine test site Wieringermeer was conducted [36]. There, the comparison between measured and modelled wind speed standard deviation was observed down a line of five 2.5MW wind turbines. The turbulence was modelled in terms of the standard deviation of velocity. The single

turbine velocity variance, $\sigma_u(r,x)^2$, across the rotor radius and downstream distance was modelled as the sum of ambient velocity variance, ${\sigma_{amb}}^2$, and wind turbine added velocity variance, $\sigma_{add}(r,x)^2$:

$$\sigma_u(r,x)^2 = {\sigma_{amb}}^2 + \sigma_{add}(r,x)^2 \tag{1.10}$$

The wind turbine added velocity variance was modelled using two sub-components - decay in stream-wise direction with a power function and production of two peaks originating at the edge of the rotor disk merging 8D downstream of the rotor. In the power-law decaying function, the initially added turbulence was based on the Gunner C. Larsen GCL model [37], taking into account the thrust of the rotor. The results did not show a good correlation between the modelled and measured standard deviation, which originated from "*un-modeled spatial variations in wind speed, the un-modelled effect of turbine nacelle on wind speed, un-modelled effect of upstream turbulence on the decay of added turbulence, and too gradually modelled decay of wind speed deficit and added turbulence*"[36]. The next validation study, presented by Argyle et al, stands out because it was conducted on a large offshore wind farm (Greater Gabbard offshore wind farm) with an average wind turbine spacing of 8D [6]. Here, the modelled turbulence intensity based on the Fradsen model and its proposed simplified version were validated with measured data. The simplified model disregarded the wind farm turbulence relation proposed by Frandsen (Equation 1.9), and consequently, the fully developed wind farm added turbulence intensity (Equation 1.7). Generally, both the original and the simplified Frandsen model showed good performance in predicting turbulence intensity. However, the simplified model proved more reliable for the Greater Gabbard offshore wind farm. Although this research paved the path with great findings, it is deemed necessary to analyze a greater number of large offshore wind farms in order to reach definite conclusions.

In addition to the comparison of measured and calculated turbulence from wake models, another study that dealt exclusively with the measured turbulence of wind farms yielded interesting results. In this study, wind farm turbulence was estimated using the rotor effective wind speed from SCADA data obtained at the Lillgrund offshore wind farm [38]. In this farm with a turbine spacing of 3.3D, SCADA measurements showed a significant increase in turbulence intensity in the first two rows, which stabilized in the back rows. In addition, the measurements from Horns Rev I with a turbine spacing of 7D showed an increase in turbulence intensity for the first five rows in the wind farm. These results confirmed the guidelines of the Frandsen model, which suggests that the position of the overall wind farm background turbulence intensity, representing sufficiently diffused wakes, depends on the turbine spacing in the wind farm [32].

To further investigate the effects of turbine spacing on wake turbulence intensity, several wind tunnel experiments were conducted with different wind field configurations. Chamorro and Porté-Agel [39] found in the experimental wind tunnel tests with a regularly aligned array (10x3) that the increase in turbulence intensity became constant after five rows in the wind farm. This finding was consistent with

the general Frandsen model rule [32] for accounting wind farm turbulence (equation 1.9) when turbulance is calculated for more than five rows into the wind farm. However, in the same wind tunnel, another experimental study was conducted with staggered array which showed no significant increase in turbulence intensity after the first row of wind turbines [40]. This was due to the doubled wake recovery distance in the staggered configuration compared to the regular one. To further evaluate the performance of the fully developed wind farm added turbulence (equation 1.7) in a staggered and aligned configuration, the modelled and measured hub-height turbulence behind the 11th row were compared [41]. Both configurations showed good agreement between the experimental and calculated turbulence values.

Besides comparing wake turbulence values with full scale or wind tunnel measurements, modelled turbulence based on the Frandsen proposed relation in equation 1.8 was also validated with CFD measurements. Andersen and Sørensen compared the predicted turbulence with the results obtained from LES of 16 wind turbines in the streamwise direction [42]. Furthermore, Ishihara and Qian also ran a comparative study of the modelled turbulence based on the Frandsen proposed relation in equation 1.8 with LES for wind turbines positioned closer than 2D [28]. Both of these studies were run for a range of ambient turbulence intensities, adding to which Ishihara and Qian expanded the study for multiple thrust coefficients. Overall, the modelled turbulence showed good correlation with measured turbulence in the far wake region but resulted in over-prediction in the near wake region. This over-prediction was noted to increase for smaller thrust coefficients. The results show that the Frandsen proposed relation of added turbulence (equation 1.8) is conservative when it comes to predicting near wake turbulence intensities with smaller thrust coefficients. Based on this literature review on the validation of wake turbulence models, it is evident that little work has been done on the development and validation of large offshore wind farm turbulence models. To add to that, the performed studies were constrained by limited data from relatively moderate-sized wind farms, computationally expensive CFD simulations or wind tunnel experiments.

1.2.3 Wind farms under complex conditions

Another important factor that influences the wind farm turbulence and consequently the fatigue load is the stability of the atmospheric boundary layer. All of the aforementioned studies are focused on modelling turbulence in wind farms under neutral flow conditions over smooth ocean surfaces or flat terrains. To study the effects of stability conditions apart from neutral conditions, wind tunnel experiments[43], full-scale measurements [44, 45] and numerical simulations are conducted [46, 47, 48]. All these studies propose better wind farm performance in unstable, convective conditions due to increased wake recovery as opposed to the stable conditions. These conclusions are further supported when the diurnal cycle of a wind farm is studied [49, 50]. It shows that there are relatively high turbulence levels in the ambient flow, promoting turbulent mixing and consequently faster wake recovery due to the positive buoyancy fluxes, creating an unstable atmosphere during the day. On the contrary, during the night, in a stable atmosphere, relatively lower turbulence levels in the ambient flow result in slow wake recovery.

All these studies on the stability conditions look into the effects on wind speed deficit and consequently the power output. In this concern, no past work of validation is done on exploring the effect of unstable or stable conditions on the wind farm turbulence.

1.3 Research questions

With respect to the existing literature, Frandsen model [32] gives a relatively good prediction of the wind farm turbulence intensity, although it was designed for estimating fatigue loads. This observation is based in the validation studies that were constrained by limited data from relatively moderate-sized wind farms, computationally expensive CFD simulations or wind tunnel experiments. Furthermore, most of these studies have been conducted for neutral wind farm conditions disregarding the effects of the stable and unstable atmosphere on these validation studies.

To the best knowledge of the author at the moment, no research has been conducted that evaluates the performance of the Frandsen model in different atmospheric stability conditions for the calculation of wind farm turbulence and consequently fatigue loads in an offshore wind farm. Hence, the comparison of estimated wind farm turbulence under specific atmospheric stability condition with measurements is the main objective of this thesis. This leads us to the main research question that will be answered upon the successful completion of this research:

Is the Frandsen model accurate for estimating of turbulence intensity inside a wind farm under specific atmospheric stability conditions in a large offshore wind farm?

To answer this main research question it has been sub-divided further into the following main objectives:

1. Validate the accuracy of the standard Frandsen model and the modified Frandsen model for different wind farm layouts.
2. Determine factors affecting the accuracy of turbulence in the wind farm.
3. Quantify the change in the validity of the two models for different wind farm layouts under varying atmospheric stability conditions.
4. Provide insights into the limitations and future recommendations for estimation of turbulence under varying wind farm atmospheric stability conditions.

1.4 Structure of the thesis

In order to achieve the objectives of this thesis, theoretical background knowledge in various fields is required. After acquiring the knowledge, the required data modeling can be better understood and appropriate conclusions can be drawn. For this reason, this report has been organized as follows:

Chapter 1- Defines the scope of this thesis by presenting the previous literature studies. Finally, the research question to be answered is stated.

Chapter 2- In this chapter, the theoretical background on two key areas - Frandsen wind farm turbulence model and atmospheric boundary layer with its classification has been presented.

Chapter 3- In this chapter, the available wind farm data and modeling are explained. The wind farm layout, its surroundings, wind turbine specifications and wind distribution of the selected offshore wind farms are presented. Then, the available data, their filtering and the estimation of the undisturbed conditions are discussed. Furthermore, the correction considering the external disturbances for each of the selected wind farms is presented. Finally, based on the filtered data sets, a set of wind turbines is selected for detailed analysis.

Chapter 4 - In this chapter, the used atmospheric stability classification is defined, followed by the validation of the turbulence models. The validation study is first performed for a given wind speed, followed by another validation study for each individual atmospheric stability conditions.

Chapter 5 - Finally, the last chapter provides an answer to the research question along with recommendations for future research.

Chapter 2

Theoretical background

In a wind farm, wind turbines are subjected to an added turbulence, caused by wake effects. Therefore, for sound fatigue design of large offshore wind farms, an accurate prediction of the increased wind farm turbulence is essential. This study focuses on the calculation of the wind farm turbulence using Frandsen model, which is widely used by the industry and had also been adopted by the IEC standards[5]. Based on literature, it is seen that the turbulence intensity estimation from the Frandsen model is primarily based on wind speed, ambient turbulence intensity, wind farm spacing and thrust coefficient. Ambient turbulence intensity that serves as the reference for the wind farm turbulence is highly impacted by atmospheric boundary layer stability [44]. This chapter will hence, focus on providing the theoretical background of the two main focus areas- Frandsen wind farm turbulence model and the atmospheric boundary layer with its classification.

2.1 Atmospheric boundary layer stability and its classification

Overall ambient TI is dependent on atmospheric stability [44] and shear. Turbulence intensity at an offshore site is higher at low wind speeds, decreasing to a minimum at wind speeds between 8-12 m/s, and then increases with increasing wind speeds [51, 52]. The initial increase in turbulence at low wind speeds is seen due to thermally derived turbulence, whereas the increase at higher wind speeds is due to the rise in surface roughness resulting in mechanically driven turbulence [52]. This changing nature of turbulence intensity, associated with the thermal and mechanical processes, highlights its dependence on the structure and dynamics of the Atmospheric Boundary Layer (ABL).

2.1.1 ABL Stability

ABL is defined as the lowest part of the troposphere, typically up to the height of 1km. Its characteristics, such as wind speed, wind shear and turbulence intensity, are influenced by surface properties like aerodynamic roughness, thermal stratification and topography. In the past years, wind turbines operated in the

surface layer of the ABL, which ranges up to 100m from the earth surface. Here, localized turbulence is driven by both mechanical and thermal processes. As a result, all wind farm turbulence models were based on the study of the surface layer of the ABL. In this concern, traditionally, all these models considered neutral conditions, where turbulence is mainly produced mechanically by shear of the mean wind profile. The mean wind profile is defined with the logarithmic profile law for neutral stability conditions as shown in Equation 2.1.

$$U(z) = \frac{u_*}{k} ln(\frac{z}{z_0}) \tag{2.1}$$

where,
$U(z)$ - Wind speed at height z
u_* - Friction velocity
k - von Karman constant
z - Height of wind speed
z_0 - roughness length

In a neutral ABL, wind shear results in the inelastic collisions between eddies (i.e mixing of air parcel with different velocities) transforming the mean flow kinetic energy into turbulent kinetic energy (TKE). This process continues till the large scale TKE is transformed into smaller scales and eventually into heat during the process of turbulent energy cascade. In reality, apart from neutrally stratified ABL, the atmospheric boundary layer also faces unstable and stable conditions. In both of these cases, turbulence is produced thermally by vertical heat flux. The unstable or convective atmospheric condition is observed when the surface is warmer than the air, leading it to get heated. This heating and consequent lifting of the air parcel add potential energy to the atmosphere, which is later converted to kinetic energy, while producing a positive buoyancy effect. The added kinetic energy is expressed as random thermally induced TKE that enhances vertical transport of momentum and increases atmospheric turbulence intensity [53]. The stable atmospheric conditions are observed when the surface is cooler than the air. This situation causes negative heat flux resulting in negative thermally induced TKE, which acts as a drain, dampening the shear generated TKE. As a result, in comparison to the neutral and unstable conditions, the stable atmosphere has lower turbulence.

These effects of varying ABL stability, traditionally, are not considered when modelling wind turbine loads. Neutral conditions with shear generated turbulence is assumed to be the only case. This assumption was proven to be wrong when simulations for NREL 5MW wind turbine were run considering diabatic wind conditions [54]. There was a significant difference of 17% in tower loads and 13% in rotor loads compared to loads obtained assuming neutral conditions. For wind turbines operating in wind farm conditions, the impact of ABL stability on loads was seen to be further increased [55]. To summarise, the thermal effects on the wind flow in the ABL cannot be seen as a small variation to neutral conditions, and therefore, they call for consideration of unstable and stable cases. Since this consideration leads to changes in turbulence, and consequently in the wake dynamics and wind farm flows, it plays a significant role in wind turbine loading.

2.1.2 ABL stability quantification and classification

Having recognized the importance of considering ABL stability, it calls for accurate quantification and characterization based on available measured data. The ABL stability classification is typically done using Obukhov length(L).

Obukhov length is used as a scaling parameter (Equation 2.2), L, indicating the atmospheric mixing conditions in the surface ABL. Obukhov length itself is the height at which the buoyant production of TKE is more than that produced by wind shear. A negative value indicates unstable cases, a positive value indicated stable cases and an infinite value indicates neutral cases. Its absolute value reveals deviation from neutral conditions, where a small absolute value represents large deviation from neutral conditions.

$$L = -\frac{\overline{\theta_v} {u_*}^3}{kg(\overline{w`\theta`})_s} = \frac{\overline{\theta_v} {u_*}^2}{kg\theta_*} \tag{2.2}$$

where,
$\overline{\theta_v}$ - Mean virtual potential temperature
g - Acceleration due to gravity
$(\overline{w`\theta`})_s$ - Surface virtual potential heat flux
θ_* - Surface layer temperature scale

ABL Stability quantification: Obukhov length from measured data

Direct calculation of Obukhov length requires an input of surface virtual potential heat flux (Equation 2.2). This heat flux is determined based on the eddy-covariance method using high frequency observation data. However, when this data isn't present, Obukhov length is estimated using the following empirical methods (dependent parameters):

1. RI methods (Richardson number)
2. Profile methods (Wind and temperature profiles)

These empirical methods can be sub divided into two methods- Bulk method and the Gradient method. The bulk method considers the atmosphere as one bulk layer by using surface and atmospheric measurements of wind speed [with $U(z_0) = 0 m/s$] and temperature. On the other hand, the gradient method considers the gradient of wind speed and temperature by using measurements at two heights in the atmosphere.

RI methods are dependent on the Richardson number (Ri) that shows the formation of turbulence as a ratio of the buoyancy turbulence to the shear generated turbulence. In order for the flow to be turbulent, the Richardson number must drop below the critical value Ri_c. The glossary of American Meteorological Society defines the critical Richardson number as "*The value of the Richardson number below which air becomes dynamically unstable and turbulent. This value is usually taken as Ri_c = 0.25, although suggestions in the literature range from 0.2 to 1.0.*" [56].

$$Ri = \frac{\text{buoyancy term}}{\text{flow shear term}} = \frac{g \triangle \overline{\theta_v} \triangle z}{\overline{\theta_v} (\triangle \overline{U})^2} \tag{2.3}$$

Where,
g - gravitational acceleration ($9.81 m/s^2$)
z - height
$\overline{\theta_v}$ - mean virtual potential temperature
$\overline{U}$ - mean wind speed

Richardson number is calculated by using wind speed and temperature measurements from two different heights within the atmosphere. These selection of these two measurement heights then defines the bulk-Richardson number (with z_1 = 0 and z_2 >0) or the gradient-Richardson number(with z_1 and z_2 > 0). The Richardson number is then used estimate Obukhov length by Bulk-RI method (Equation 2.4) and Gradient-RI method (Equation 2.5), implying a critical Richardson number of 0.2. Here, the dimensionless Obukhov stability parameter, z/L, is calculated where z represents the average height between the two selected measurement heights.

Bulk-RI method [57]:

$$\frac{z}{L} = \begin{cases} \frac{10Ri}{1-5Ri}, & \text{if } Ri \geq 0 \\ Ri, & \text{if } Ri \leq 0 \end{cases} \tag{2.4}$$

Gradient-RI method [58]:

$$\frac{z}{L} = \begin{cases} \frac{Ri}{1-5Ri}, & \text{if } Ri \geq 0 \\ Ri, & \text{if } Ri \leq 0 \end{cases} \tag{2.5}$$

Profile methods are based on estimation of surface layer temperature scale (θ_*) and friction velocity (U_*), assuming that the stability corrected logarithmic wind and temperature profile is valid. Since the logarithmic wind profile (Equation 2.1) only addressed neutral conditions, the Monin-Obukhov similarity theory introduced a stability correction function (ψ_m). This incorporated the changes in wind shear profile for non neutral cases by adding a stability correction function, ψ_m. The stability correction function (ψ) was introduced to account for the deviation of the wind profile from the logarithmic function under increasingly unstable or stable atmospheric conditions. For a neutral atmosphere (ψ_m), it is equal to zero, resulting in a logarithmic wind profile. Monin and Obukhov stated that the value of the stability correction function can be derived from experimental data. In the past, many empirical studies have been conducted to determine the shape of (ψ_m) as a function of ($\frac{z}{L}$) . Table 2 summarizes most of the widely used empirically fitted functions for the stability correction function found in the literature.

Table 2.1: Empirical stability correction functions found in the literature

ψ_m: STABLE ATMOSPHERE (L>0)		
BUSINGER-DYER (KANSAS EXPERIMENT) [59]	$-\beta\frac{z}{L}$	$\beta = 4.7$
HOGSTRUM [60]		$\beta = 6$
HOLTSLAG [61]	$-\frac{z}{L} - \frac{2}{3}(\frac{z}{L} - \frac{5}{0.35})(\exp(-0.35\frac{z}{L})) - \frac{10}{1.05}$	-
ψ_m: UNSTABLE ATMOSPHERE (L<0)		
BUSINGER-DYER (KANSAS EXPERIMENT) [59]	$2\ln(\frac{1+x}{2}) + \ln(\frac{1+x^2}{2}) - 2\arctan(x) + \frac{\pi}{2}$	$\gamma = 15$
HOGSTRUM [60]	$x = \gamma\frac{z}{L}$	$\gamma = 19.3$
GRACHEV-FAIRALL-BRADLEY [62]	$\frac{3}{2}\ln(\frac{y^2+y+1}{3}) - \sqrt{3}\arctan(\frac{2y+1}{\sqrt{3}}) + \frac{\pi}{3}$ $y = (1+\gamma\frac{z}{L})^{\frac{1}{3}}$	$\gamma = 10$

Similar to the wind speed stability correction function a stability correction, ψ_t, is applied to the logarithmic temperature profile.

$$U(z) = \frac{u_*}{k}\left[ln\frac{z}{z_0} - \psi_m(\frac{z}{L}) + \psi_m(\frac{z_0}{L})\right] \tag{2.6}$$

$$\theta(z) = \theta(z_0) + \frac{\theta_*}{k}\left[ln\frac{z}{z_0} - \psi_t(\frac{z}{L}) + \psi_t(\frac{z_0}{L})\right] \tag{2.7}$$

The profile methods calculates Obukhov length by iteratively solving the following equation for surface layer temperature scale (θ_*-Equation2.9), friction velocity (U_*-Equation2.8) and Obukhov length (L-Equation 2.2).

$$U_* = \frac{\triangle U k}{ln\frac{z_2}{z_1} - \psi_m\frac{z_2}{L} + \psi_m\frac{z_1}{L}} \tag{2.8}$$

$$\theta_* = \frac{\triangle\overline{\theta_v}k}{ln\frac{z_2}{z_1} - \psi_t\frac{z_2}{L} + \psi_t\frac{z_1}{L}} \tag{2.9}$$

Where,
z_1 - Lower height
z_2 - Upper height

Since friction velocity and surface layer temperature scale estimation assume validity of stability corrected logarithmic profile, the observation must be carried out in the surface layer- lower 10% of ABL. Here, wind speed and temperature measurements from two different heights are required. The selection of these two measurement heights then defines the bulk-profile method(with $z_1 = 0$ and $z_2 > 0$) or the gradient-profile method(with z_1 and $z_2 > 0$).

ABL Stability classification: Obukhov length and ζ

Having defined Obukhov length as the variable for ABL stability quantification the next challenge is defining the thresholds for unstable, neutral and stable conditions. Table 2.2 summarizes multiple Obukhov length (L) and ζ (z/L) thresholds proposed in the previous studies.

Table 2.2: Ranges for stability classes based on Obukhov length and ζ present in the literature[63]

Study	Very Unstable	Unstable	Neutral	Stable	Very Stable	Notes
Van Wijk et al.(1990) [64]	-200 <L< 0	-1000 <L< -200	|L| >1000	200 <L< 1000	0 <L< 200	North sea offshore sites - air temp and wind sensors at 70m
Motta et al.(2005) [65]	-200 <L< 0	-1000 <L< -200	|L| > 1000	200 <L< 1000	0 <L< 200	North sea danish offshore sites - air temp and wind sensors at various heights; max 47m
Gryning et al(2007) [66]	-100 <L< -50	-500 <L< -100	|L| > 500	50 <L< 500	10 <L< 50	Inland; 10 or 50m sonics
Sathe et al.(2011) [67]	-100 <L< -50	-500 <L< -100	|L| > 500	50 <L< 500	10 <L< 50	Two North sea offshore sites - air and sea temp at various heights; max 21m
Högström(1988) [68]		ζ < -0.1	-0.1 < ζ < 0.1	ζ > 0.1		Inland - wind sensors at 3,6,14m
Metzger et al.(2007) [69]		ζ < -0.1	-0.1 < ζ < 0.1	ζ > 0.1		Inland - 1.4, 26m sonics
Rajewski et al.(2013) [70]		ζ < -0.05	-0.05 < ζ < 0.05	ζ > 0.05		Inland - 4.5, 6.5m sonics

ABL stability categorization based on Obukhov length defines five categories introducing limits for very stable and very unstable conditions. Two main thresholds for identifying neutral conditions are used with the largest as 1000m followed by a lower threshold of 500m. Gryning et al [66] based the stability classification on the respective wind profiles: straight for neutral, curving downwards for unstable and curving upwards for stable conditions. ABL stability categorization based on ζ defines three categories: Unstable, Neutral and Stable.

Very unstable and unstable classes represent ABL conditions with low wind shear and low wind speeds due to the increased mixing. However, high turbulence is present due to large buoyant eddies. In contrast, very stable and stable classes represent ABL conditions with high wind shear and low turbulence with an exception of high turbulence during the presence of low-level jets. Lastly, neutral conditions represent moderate turbulence and highest wind speeds increasing logarithmically with height across the rotor. Based on the ranges of Obukhov length L used in the literature, two main thresholds for defining neutral conditions shown in Table 2.2 are considered for this study. The final value used for the stability classification used for the stability classification are reported in Chapter 4.

2.2 Sten Frandsen wind farm turbulence model

The Sten Frandsen model recommended by the IEC Standard 61400-1 [5] is a semi-empirical model designed for estimating fatigue loads for wind turbines located in a wind farm. Wind turbines positioned in a wind farm are normally subjected to increased turbulence intensity due to wake effects from neighboring wind turbines. Frandsen based his model on the assumption that "fatigue loading under both wake and non-wake conditions is proportional to the turbulence intensity"[32]. The validity of this assumption in terms of fatigue loading was assessed by Frandsen. The model was proved to be feasible based on satisfactory agreement with measurements. In order to determine fatigue loads Frandsen calculates a design variable known as effective turbulence intensity:

$$I_{eff}(U) = \left[\int_{-180}^{180} f_{wd} I_{dir}^{m}(\theta, U) d\theta \right]^{1/m} \tag{2.10}$$

Where,
I_{eff} - Effective turbulence intensity for freestream wind speed U.
f_{wd} - Probability of wind coming from wind direction θ for freestream wind speed U.
I_{dir} - Directional turbulence intensity.
m - Wohler slope
θ - Wind direction
U - Wind speed

Since the Frandsen model was developed for determining fatigue loads while designing a wind farm, it normalizes the turbulence intensity to the freestream (ambient) wind speed instead of local wind speed at the point of interest. As a result, the modelled turbulence intensity cannot be compared directly with the measured turbulence within the wind farm, which accounts for changes in wind speed due to wake included wind speed deficit.

For design purposes the Frandsen model calculates effective turbulence intensity based on a representative turbulence intensity which is assumed to be the 90th quantile of the measured ambient turbulence intensity. The probabilistic distribution of ambient turbulence in a 10min basis is assumed to follow a normal distribution, thus enabling the use of the formula:

$$I_{rep}(\theta, U) = I_{amb}(\theta, U) + \frac{1.28 \sigma_{\sigma_{amb}}}{U}(\theta, U) \tag{2.11}$$

Where
$I_{rep}(\theta, U)$ – Representative turbulence intensity
$I_{amb}(\theta, U)$ – Mean ambient turbulence intensity
$\sigma_{\sigma_{amb}}(\theta, U)$ – Standard deviation of ambient turbulence

Since turbulence is a function varying with height, for design purpose, the directional turbulence intensity is determined at hub height. Frandsen assumes that

the hub-height directional turbulence is representative of the loads caused by the spatially varying turbulence. For this research two different implementations of the Frandsen model are used for determining directional turbulence intensity. The first implementation, known as the Standard Frandsen model, is based on the general concept shared in the IEC Standard 61400-1. The second implementation, on which this research work is based, is a simplified version of the Standard Frandsen model.

2.2.1 Standard Frandsen model

Standard Frandsen model implementation defines directional turbulence intensity for a wind direction (θ) based on three different cases that can be present within a wind farm. Case 1 represents freestream conditions, whereas case 2 and 3 represent conditions with increased turbulence due to wake of upstream wind turbines. In order to determine wind directions exposed to increased turbulence, the wake inducing wind turbines are identified based on a view angle (θ_{wj}) which is introduced in the next subsection.

Wake inducing wind turbine identification

View angle calculated for each wake inducing wind turbine as seen from the wake facing wind turbine, represents the maximum range of wind directions that result in wake on the wind turbine of interest. Frandsen model assumes the wake effects on the wind turbine of interest are present, when more than half of the rotor is within the wake of the upstream wind turbine. The view angle is derived on the basis of the wake width, which is defined by the linearly expanding wake model proposed by Jensen (1983)[]:

$$\frac{D}{D_0} = \frac{1}{1+\beta_0 s} \tag{2.12}$$

Where,
D - Width of the wake at a downstream distance of s
D_0 - Rotor diameter
β_0 - Wake expansion constant ranging from 0.15-0.2
s - Normalized spacing between wind turbines

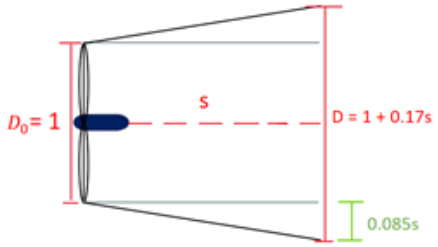

Figure 2.1: Jensen linear wake expansion model implemented by Frandsen for view angle calculation

Figure 2.1 shows the linear expansion of the wake width with increasing downstream distance as defined by Jensen wake model. Frandsen assumes a constant wake expansion coefficient of $\beta_0 = 0.17$, from the proposed range of 0.15-0.2 by Jensen that varies with increasing ambient turbulence intensity. This assumption made by Frandsen results in an increase in the wake width, defined as 17% of the downstream distance (s) with respect to the rotor diameter (D_0).

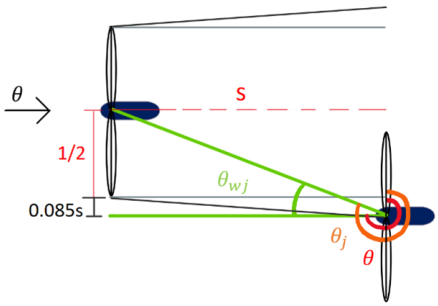

Figure 2.2: View angle as seen from the wake affected wind turbine

Figure 2.2 shows the visual representation of how the view angle is defined by Frandsen. Here, in order to determine the maximum range of wake-facing wind directions represented by the view angle, the center of the wake facing wind turbine is assumed to be positioned at the edge of the wake. The view angle can then be computed as:

$$\begin{aligned} \theta_{wj,calc} &= \left[tan^{-1}\left(\frac{1}{2s_j} + 0.085\right)\right] \approx tan{-}1\left(\frac{1}{2s_j} + 5\right) \\ &= \frac{1}{2}\left[2tan{-}1\frac{1}{2s_j} + 10\right] \end{aligned} \tag{2.13}$$

Where,
$\theta_{wj,calc}$– Calculated View angle of the upstream wind turbine j

s_j– Normalized spacing between wind turbine j and wind turbine of interest

Frandsen further simplifies the view angle formulation, using a small angle approximation resulting in the following equation.

$$\theta_{wj} = \frac{1}{2}\left[tan{-}1\frac{1}{s_j} + 10\right] \tag{2.14}$$

Where,
θ_{wj}– Frandsen proposed View angle of the wind turbine j seen from the wake effected turbine.

It can be seen in Figure 2.3 that both formulations converge for normalized spacings greater than 4D. This results in similar view angle values for a greater range of normalized spacing. Therefore, for all comparisons and calculations made in this research work, the view angle for each wind turbine is determined using the Frandsen simplified formulation, which is also recommended by the IEC 61400-1 Standards[5].

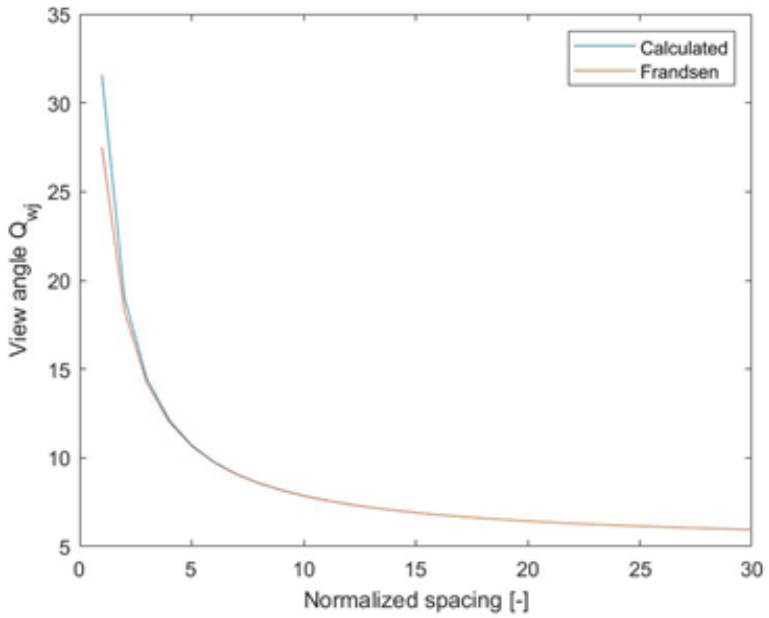

Figure 2.3: Calculated view angle and modified Frandsen view angle vs normalized spacing between wind turbines

Lastly, for each wind direction, wind turbines inducing wake on a turbine of interest are identified using the following condition:

$$If|\theta_j - \theta| \leq \theta_{wj} \tag{2.15}$$

Where,
θ_j – Alignment direction of wind turbine j with respect to wake effected turbine.
θ – Wind direction.
θ_{wj} – View angle of the wind turbine j seen from the wake effected turbine.

Direction turbulence intensity calculation

Case 1: Freestream turbulence

The location of interest is assumed to experience freestream turbulence when the following conditions are met:

1. Minimum normalized distance of surrounding wind turbines is greater than 10D – ensures enough dissipation of wake induced by upstream wind turbine.

2. Large wind farm effects are not present: Large wind farm effects are considered when there are more than 5 wind turbines upstream or the spacing in the rows perpendicular to the predominant wind direction is less than 3D.

$$I_{dir}(\theta,U) = I_{rep}(\theta,U) = I_{amb}(\theta,U) + \frac{1.28\sigma_{\sigma_{amb}}}{U}(\theta,U) \tag{2.16}$$

Case 2: Wind farm turbulence

For wind directions with more than five upstream wind turbines, where a wind turbine of interest is not in direct wake of an upstream wind turbine and large wind arm effects are present [5], ambient wind farm turbulence in experienced. Since turbulence is a function of height, in order to determine the ambient wind farm turbulence and consequently the directional turbulence, Frandsen makes the following assumptions based on measured data:

1. Constant turbulence intensity above the rotor ($\sqrt{I_{add,wf}(\theta,U)^2 + I_{amb}(\theta,U)^2}$
2. Constant ambient turbulence intensity below the rotor I_{amb}
3. Linearly varying turbulence intensity across the rotor

$$\begin{aligned} I_{dir}(\theta,U) &= I_{wf,amb}(\theta,U) + \frac{1.28\sigma_{\sigma_{amb}}}{U}(\theta,U) \\ I_{wf,amb}(\theta,U) &= \frac{A+B}{2} = \frac{1}{2}(\sqrt{I_{add,wf}(\theta,U)^2 + I_{amb}(\theta,U)^2} + I_{amb}(\theta,U)) \\ I_{add,wf}(\theta,U) &= \frac{0.36}{1+0.2\sqrt{\frac{S_x S_y}{C_t(U)}}} \end{aligned} \tag{2.17}$$

Where,
S_x - Streamwise normalized wind turbine spacing.
S_y - Spanwise normalized wind turbine spacing.

Case 3: Direct wake turbulence

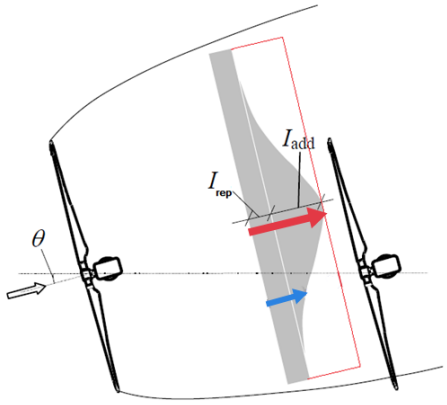

Figure 2.4: Direct wake turbulence intensity as seen by the downstream wind turbine. Red line represents the turbulence intensity as modelled by the standard Frandsen model. Blue line represents the turbulence intensity as modelled by the modified frandsen model[32]

For wind directions where the minimum normalized distance of surrounding wind turbines is less than 10D, direct wake turbulence is experienced from the nearest wake inducing wind turbine. Frandsen model represents the direct wake turbulence as the superposition of the hub height representative turbulence and added wake turbulence. Added wake turbulence as sensed by the downstream wind turbine is represented by the bell-shaped curve as seen in Figure 2.4.

In the standard Frandsen model implementation maximum added turbulence intensity (I_{add}) is assumed to be constant horizontally across the rotor at hub height (red line in Figure 2.4). Therefore, the centered hub-height directional turbulence intensity is represented as:

$$I_{dir}(\theta,U) = \sqrt{I_{add}^2(\theta,U) + I_{rep}^2(\theta,U)}$$
$$I_{add} = \frac{1}{1.5 + s_j \frac{0.8}{\sqrt{C_t(U)}}} \tag{2.18}$$

Where,
I_{add} – Maximum direct wake added turbulence intensity
s_j – Normalized spacing between wind turbine j and wind turbine of interest.

2.2.2 Modified Frandsen model

Modified Frandsen model does not implement the 10D cut off but at the same time it considers the direct wake added turbulence intensity for all wind directions in the wake of upstream wind turbines, independent of their distance to the turbine of interest. The maximum turbulence out of all the direct wake inducing wind turbines

is considered. Since the direct wake is being considered for all wind directions the assumption of wind farm turbulence beyond 10D is considered unnecessary.

Frandsen represents the rotor-averaged wake turbulence profile as a superposition of wake added turbulence and vertical ambient turbulence intensity. Figure 2.4 illustrates the case where the downstream wind turbine is exposed to a non-symmetric turbulence field. Modified Frandsen model assumes that considering constant turbulence intensity across the whole rotor as in the center (blue line in Figure 2.4) results in the same response as the spatially distributed turbulence intensity.

Assuming a bell-shaped profile for the wake added turbulence intensity:

$$I_{dir}(\theta,U) = \max_{j=1:N}\left[I_{rep}\left[1+\alpha exp\left[-\left(\frac{\theta-\theta_j}{\theta_{wj}}\right)^2\right]\right]\right] \tag{2.19}$$

Where,
j – Upstream wind turbines
N – Numbers of wake inducing wind turbines
α – Constant

For the case where $\theta = \theta_j$, the downstream wind turbine is exposed to a symmetric turbulent field:

$$\begin{aligned} I_{rep}(1+\alpha) &= \sqrt{{I_{add}}^2 + {I_{rep}}^2} \\ \alpha &= \sqrt{\left(\frac{I_{add}}{I_{rep}}\right)^2 + 1} - 1 \end{aligned} \tag{2.20}$$

For wind directions with multiple wind turbines inducing wake on the reference wind turbine, modified Frandsen model considers the wind turbine with the maximum wake added turbulence. The figure below represents the directional turbulence intensity with varying normalized spacing between wind turbines for 2 different wind speed levels and consequently Ct parameters. The black line represents the representative turbulence intensity assumed to be 0.06 for this example. Significant increase in directional turbulence intensity is observed for lower normalized spacing, which decreases exponentially with increased spacing due to dissipation of the wake. It is also observed that increased directional turbulence intensity is faced by the downstream wind turbine for higher thrust coefficient present at lower wind speeds in the below rated region.

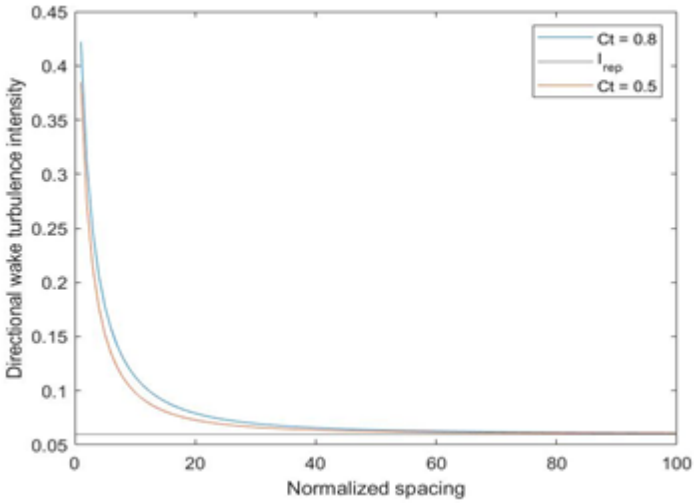

Figure 2.5: Directional turbulence intensity for the case where θ=θ_j with varying thrust coefficient and normalized spacing

2.2.3 Example of wind farm turbulence in a regular wind farm

Having described the theory behind the two implementations of the Frandsen model, this section exemplifies the estimation of the directional turbulence intensity with the application of the two models. The artificial wind farm considered is a regular array consisting of 7x7 wind turbines with a uniform normalized spacing of 8D (Figure 2.6). The analysis is performed for wind speed of 7m/s assuming a thrust coefficient C_t =0.826 and a constant mean freestream turbulence intensity of 0.058 along with its standard deviation equal to 0.028.

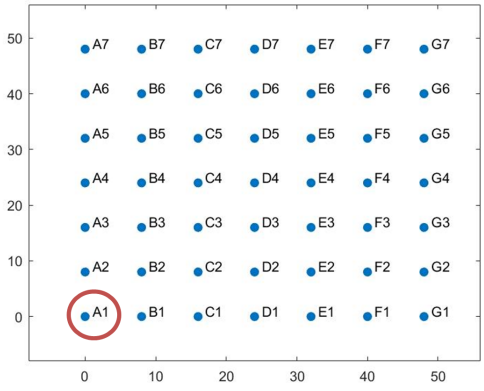

Figure 2.6: Artificial wind farm layout

The wind turbine of interest for which the analysis is performed is A1 for which all the 3 cases for determining directional turbulence intensity are considered. The

standard directional turbulence intensity is determined for every 5-degree sector, whereas the simplified directional turbulence is computed for every degree.

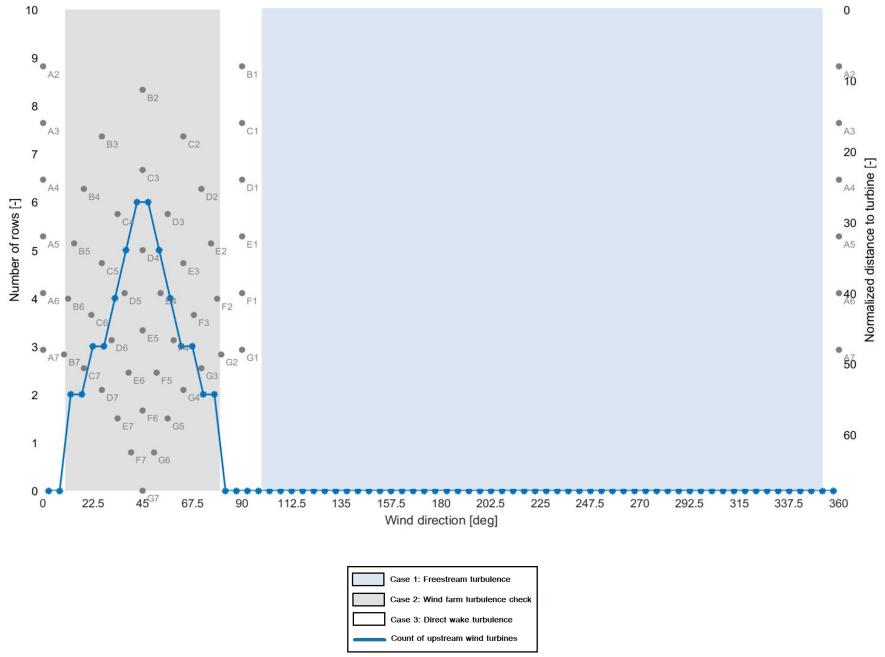

Figure 2.7: Count of rows upstream of A1 to determine sectors where wind farm turbulence is considered as per the standard Frandsen model implementation

Figure 2.7 represents the positioning of the neighboring wind turbines with respect to A1 for all wind directions. Based on the positioning of neighboring turbines, wind directions from 100-350 degrees represented by the blue shaded region have no upstream wind turbines. Hence for wind flow from these directions, A1 is exposed to freestream turbulence. Wind direction sectors in white have wake effects from turbines positioned at less than 10D. Therefore, for these wind directions the standard Frandsen model considered direct wake turbulence. The shaded wind direction sectors in grey are where wind turbines are positioned at a normalized spacing greater than 10D. Here, to ensure if the standard Frandsen model will consider wind farm turbulence or representative turbulence, the number of rows of upstream wake inducing wind turbines is counted. Figure 2.7 shows that for the range of inflow wind direction from 40-50 degrees the number of upstream rows is greater than 5D, as a result standard Frandsen model considers wind farm turbulence.

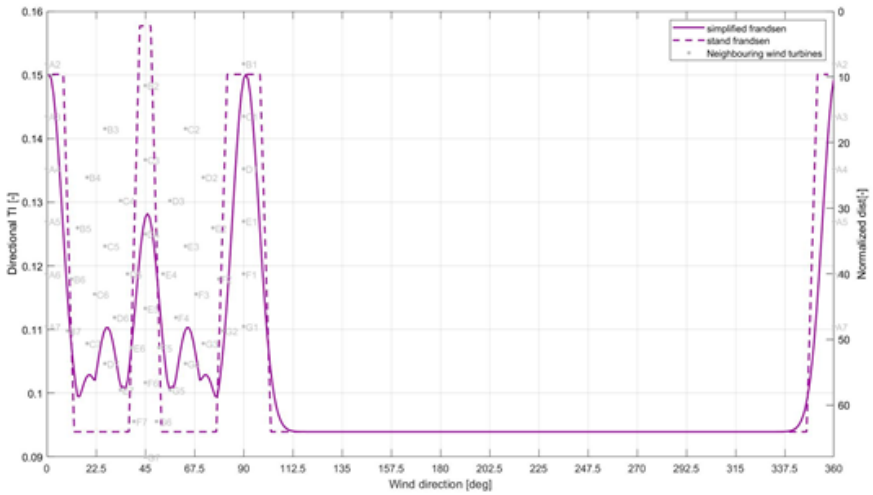

Figure 2.8: Standard Frandsen model and Modified Frandsen model based directional turbulence intensity 0-360 degrees for A1 wind turbine for a 7m/s freestream wind speed

Figure 2.8 shows the direction turbulence intensity calculated based on the two Frandsen model implementations. Using standard Frandsen model implementation highest directional turbulence is recorded for 40-50 degree where wind farm turbulence in considered since it accounts for the multiple wakes from upstream wind turbines. Modified Frandsen model on the other hand only considers the direct wake turbulence intensity from the nearest wind turbines and it estimates a lower value of turbulence than the Standard Frandsen model. The Standard Frandsen model is seen to result in constant maximum direct wake turbulence across the range of wake effected wind directions. Lastly, the modified Frandsen model's directional turbulence intensities are also noted to capture increased turbulence due to upstream wind turbines in the wind direction range of 10-40 degrees and 50-80 degrees. Whereas, for these wind directions standard Frandsen model disregards any increase in turbulence due to less than or equal to 5 rows of upstream wind turbines that are positioned greater than 10D.

2.3 Conclusion

The focus of this research is to assess the accuracy of the Frandsen model in predicting turbulence levels and fatigue loads within in a large offshore wind farm under specific atmospheric stability conditions. The model is validated for offshore wind farms with varying spacing and wake situations(single or cumulative) as a function of wind direction. To assess the accuracy of the predicted turbulence levels, the representative turbulence intensity (90^{th} percentile) from the Standard Frandsen model and the modified Frandsen model are compared to the measured values under specific atmospheric stability conditions. The ABL stability quantification and classification are based on Obukhov Length L as mentioned in Section 2.1.2. The modified Frandsen model is similar to the standard Frandsen model (Section 2.2) except for the following differences:

1. Unlike Standard Frandsen model the modified Frandsen model considers direct wake added turbulence intensity for all wind direction sectors.

2. It assumes a bell shaped profile for the wake added turbulence intensity.

3. As the previous change already gives a picture of the wake-related added turbulence, the use of wind farm turbulence intensity for cases where 5 wind turbines are upstream is regarded as unnecessary.

Chapter 3

Wind farm overview: Data description and modelling

To validate the turbulence models, ambient undisturbed turbulence intensity, wake added turbulence intensity, and wind speed data are needed. Two offshore wind farms Horns Rev II and Westermost Rough were selected for this study. In this chapter, the wind farm layout, its surroundings, wind turbine specifications and wind distribution of the selected offshore wind farms are presented. Subsequently, the available data, their filtering and the estimation of the undisturbed conditions are discussed. Furthermore, the correction considering the external disturbances for each of the selected wind farms is presented. Finally, based on the filtered data sets, a set of wind turbines is selected for a detailed analysis.

3.1 Wind Farms

Horns Rev 2 (HR2) and Westermost Rough (WMR) are wind farms owned by Ørsted (formerly Dong Energy). Both of these farms are located in the North Sea. HR2, which became operational in September 2009, is located 30 km west of the coast of Southern Denmark and 60 km from Esbjerg, as shown in Figure 3.1.

Figure 3.1: HR2 location aerial view

WMR was commissioned in May 2015 and is located 8 km northeast of Yorkshire Coast, north of Hull, UK, as shown in Figure 3.2.

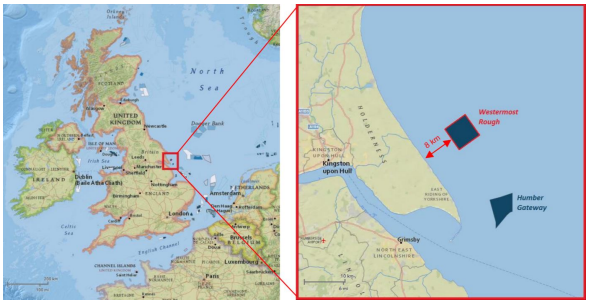

Figure 3.2: WMR location aerial view

The specific details for the wind farms are provided in the sections 3.1.1 and 3.1.2

3.1.1 Horns Rev II

The wind farm contains 91 SWT-2.3-93 turbines with a capacity of 2.3 MW and a total generation of 209 MW. The operating range of the wind turbines is from 3 m/s to 25 m/s, with rated power at 13 m/s. In its vicinity, almost 15 km to the southeast, is another wind farm, Horns Rev 1. It consists of 80 Vestas V80-2.0 MW turbines with a cumulative wind farm capacity of 160 MW.

The wind turbines at the HR2 wind farm are arranged in a fan-shaped formation of 35 km^2. There are 13 rows along the south-north axis and 7 rows along the east-west axis with a minimum spacing between turbines of about 5.8 diameters (about 540 m). The layout of the wind farm is shown in Figure 3.3.

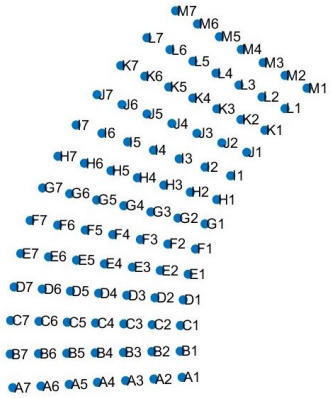

Figure 3.3: HR2 wind turbine layout and naming

The wind turbine names consist of a letter and a number. Along the south-north

axis, a letter is given from A to M, depending on the row. Along the east-west axis, a number from 1 to 7 is given, depending on the row. The wind distribution at a hub height of 68 m is approximated by a Weibull distribution with a scale parameter (A) of 10.52 m/s and a shape parameter (k) of 2.309, giving a mean wind speed of 9.32 m/s. The average air density is 1.24 kg/m^3. The wind rose is shown in Figure 3.4, where the prevailing wind from the southwest till north west wind directions, which is an open sea wind.

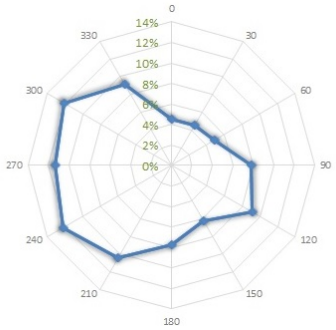

Figure 3.4: HR2 wind rose

3.1.2 Westermost Rough

The wind farm contains 35 SWT-6.0-154 turbines with a capacity of 6 MW, reaching a total combined generation of 210 MW. The operating range of the wind turbines is between 3 m/s and 25 m/s, with rated power at 13 m/s. In its vicinity, almost 20 km to the southeast, there is another wind farm, Humber Gateway. It consists of 73 Vestas V112 3.0 MW turbines with a cumulative wind farm capacity of 219 MW.

The outer boundaries of the WMR wind farm frame a 5.9 km square. There are 7 rows along the southeast to northwest axis with an approximate row spacing of 6.4 diameters and 6 rows along the southwest to northeast axis with an approximate row spacing of 7.6 diameters. This wind farm layout (Figure 3.5) is unique in that it leaves a gap in the middle of the farm.

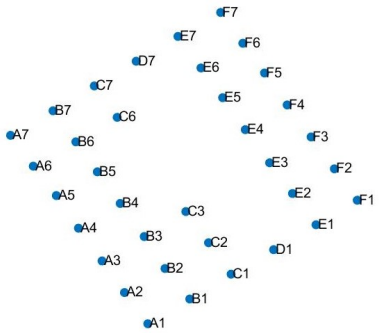

Figure 3.5: WMR wind tubrine layout and naming

Wind turbine names consist of a letter and a number. Along the southwest to northeast axis, a letter is given from A to F, depending on the row. Along the south-east to north-west axis, a number from 1 to 7 is given, depending on the row. The wind distribution at a hub height of 105.52 m is approximated by a Weibull distribution with a scale parameter (A) of 10.45 m/s and a shape parameter (k) of 2.39, giving a mean wind speed of 9.26 m/s. The mean air density is 1.235 kg/m^3. The wind rose is shown in Figure 3.6, where the prevailing wind is from the southwest direction, this is the coastal wind.

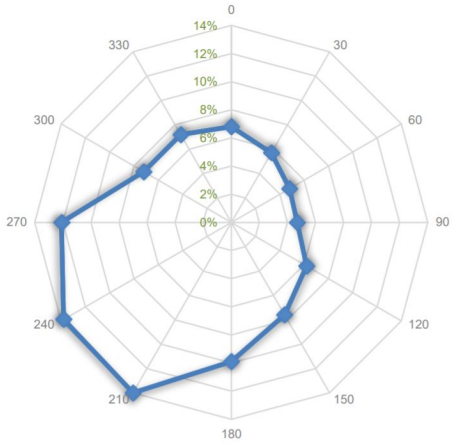

Figure 3.6: WMR wind rose

All the information provided above is summarized in Table 3.1 below.

Table 3.1: Summary of Wind farms and its surroundings

		WMR	HR2
Wind farm layout	Area	34.8 km^2	35 km^2
	Wind turbines	35	91
	Min spacing	6.4D	5.8D
	Pattern (rowsxcolumns)	7x6	13x7
Wind turbine properties	Wind tubrine	SWT-6.0-154	SWT-2.3-93
	Rated power	6 MW	2.3MW
	Rotor diameter	154 m	93m
	Hub height	105.52 m	68m
	Cut in wind speed	3 m/s	3 m/s
	Cut out wind speed	25 m/s	25 m/s
	Rated wind speed	13 m/s	13 m/s
Wind farm operating conditions	Weibull scale parameter, A	10.45	10.52
	Weibull shape parameter, k	2.39	2.309
	Mean wind speed, U	9.26 m/s	9.32 m/s
	Mean air density, ρ	1.235 kg/m^3	1.24 kg/m^3
	Prevailing wind direction	South west	West

3.2 Measurement data

The turbulence intensity is calculated using the measured mean and standard deviation of wind speed over a 10-minute interval. To estimate undisturbed ambient turbulence, the required measurements are usually provided by a meteorological met mast, Light Detection and ranging (Lidar) system, or Sonic detection and ranging (SODAR) system. However, the accuracy of these measurements is questionable since they are point measurements at a location distant from the turbine of interest. In addition, depending on the wind direction, these readings could be in the wake of upstream wind turbines.

The wind farms selected for this study are not equipped with a meteorological met mast, Lidar or SODAR system. Therefore, the only data available are the signals from the Supervisory Control and Data Acquisition (SCADA) system. SCADA is designed to perform control updates using real-time wind farm data. The signals from SCADA provide measurements affected by the wake of upstream wind turbines along with the rotor of the wind turbine being investigated. The measured data (mean, min, max, standard deviation) for HR2 and WMR consist of 10-minute samples, and the duration was approximately 1-3 years respectively.

The measured turbine data are obtained from two types of measurement databases: Wind Farm Database (WFDB) and Turbine Measurements Database (TMDB). WFDB consists of basic operational parameters that include wind speed measurement from the nacelle anemometer, wind direction from the wind vane, yaw position, blade pitch positions, rotor speed, power and nacelle accelerations for each of the turbines in the wind farm. TMDB contains additional data provided by a set of distributed sensors in the rotor-nacelle assembly and the tower-foundation structure of selected turbines in the wind farms. At WMR, only one turbine is equipped with the advanced measurement system that provides the TMDB signals, while HR2 has multiple turbines with available TMDB signals. Table 3.2 provides a summary of the available signals at the HR2 and WMR wind farms.

The two assumptions that have been made with respect to the wind direction are as following:

1. The Yaw misalignment is always assumed to be zero. This allows the yaw position (measured with the yaw sensor) to be used instead of the wind vane as a better estimate of the wind direction. In addition, the yaw position is likely to be more reliable since it depends mainly on the ability of the control system to align the rotor with the wind direction within 10 minutes. Unfortunately, the yaw signals cannot be used as is because they need to be calibrated to north (equal to zero degrees) by applying one offset per wind turbine. The yaw position offsets were previously derived by SGRE based on the ratio of the power deficit between two adjacent wind turbines.

2. The measured yaw position should be the same across all turbines in a wind farm. Thus, by measuring the yaw direction of only one wind turbine, the wind direction for the entire farm can be determined. This is true as long as the wind direction gradients are small at wind farm scale. For large scale wind farms, this would be a rough assumption, but still reasonable as long as the

wind speed is high enough. So some small errors can be attributed to this assumption and further improvements can be part of future thesis reports.

Table 3.2: Measurement data available at HR2 and WMR

Wind Farm Database (WFDB)	HR2	WMR
Wind speed	✓	✓
Wind direction		
Yaw position		
Blade pitch position		
Rotor speed		
Generator speed		
Wind turbine operational status		
Power		
Turbine Measurements Database (TMDB)	HR2	WMR
Blade root edgewise bending moment (blades A, B, C)		✓
Blade root flapwise bending moment (blades A, B, C)	✓	
Tower-top bending moment		
Tower-top torsion		
Calculated channels	HR2	WMR
Wind speed estimate	✓	✓
Turbulence intensity estimate		

For both wind farms, "WinAvail" and "TurbEst" are the two calculated SCADA signals provided by SGRE. Both represent signals faced by the turbine. WinAvail represents wind speed and TurbEst represents turbulence intensity. Compared to anemometer measurements, they have lower fluctuations and are less sensitive to the fluctuations caused by the operating turbine. These signals are calculated from estimators based on mean values and standard deviations of power, pitch and rotor speed, calibrated with BHawC simulations. Using the BHawC simulations, the estimated wind speed is modified until the simulations and measurements give identical power. Similarly, the estimated turbulence intensity is modified until identical power is obtained for wind speeds below rated and identical pitch variation is obtained for wind speeds above rated. It is assumed that this method is accurate for moderate values of turbulence intensity (less than 25%) and wind speeds between cut-in and cut-out. It is also assumed that this turbulence estimator may be slightly inaccurate in the tower resonance exclusion zone.

3.3 Data filtering

This master thesis is mainly concerned with wind turbines operating under normal wind conditions with normal turbulence intensity (NTM). Therefore, there is a need to define filters that ensure that these conditions are met, which consequently reduces the amount of available 10-minute samples. Subsequently, this section presents the trade-off between sufficient amount of data and satisfactorily filtered data. The filtering is based on a combination of 7 criteria as follows:

1. Reasonably reliable values of wind speed and TI from the estimators
2. A valid operation status
3. No significant curtailment
4. A reasonable yaw activity
5. A reasonable generator speed activity
6. A reasonable pitch activity
7. No yaw steering test

All these filters are applied sequentially, i.e., each filter is applied to the data filtered by the previous filters. The measured dataset of WMR was filtered with all 7 criteria, while for HR2 only the first 5 filter criteria are applied.

The criterion *'reasonably reliable values of wind speed and TI from the estimators'* is met by setting upper and lower bounds on wind speed and keeping only positive values of turbulence intensities. In this case, the bounds are set at the cut-in and cut-out speeds. The wind speed estimates that fall outside this range are not considered reliable.

The *'valid operation status'* relies on the wind turbine operational signal, where a different value is given for each state. Keeping samples with normal production operational status removes all cases where the wind turbine is idling, encounters faults or when a power boost is activated.

The *'no significant curtailment'* criterion is established by selecting only samples for which the 10-minute minimum power limitation value is greater than 95% of the rated power. The power limitation channel indicates the maximum power that the wind turbine can produce at a given time. If the value is significantly below the rated power and the wind speed is sufficient, then the turbine can be throttled.

The next criteria are filtered by using one or both of the methods below:

1. Selection of 10-minute samples in which the difference between the maximum and minimum values of the measured variables is between the defined parameters.
2. Selection of 10-minute samples of the measured variables for which the difference between the standard deviation and the mean standard deviation per wind speed is smaller than a defined factor of the standard deviation per wind speed.

A *'Reasonable yaw activity'* for WMR is ensured by using Method 1, and the defined parameter for the yaw direction is chosen to be 10°. This method also filters out cases where the wind direction changes gradually (these are cases where the standard deviations of the wind direction are large, but the resulting fatigue is small). For HR2, *'reasonable yaw activity'* is ensured by applying method 2, and the factor chosen is 3 times the standard deviation of the standard deviation of the yaw position. This results in the equation shown below:

$$|SY_i - \text{mean}(SY_i)| < 3\text{std}(SY_i)$$

Where,
SY_i - std($Yaw\ position$)

i - 10 min sample i

A *'reasonable generator speed activity'* for WMR is ensured in two ways. First, by using Method 1 and using 3 rpm as the defined parameter. Secondly, by using method 2 and keeping 6 as a factor for the standard deviation of the standard deviation of the rotor speed:

$$|SRS_i - \text{mean}(SRS_i)| < 6\text{std}(SRS_i)$$

Where,
SRS_i - std($Rotor\ speed$)
i - 10min sample i

For HR2, *'reasonable generator speed activity'* was ensured by applying method 2 used in WMR. However, the factor was set lower, to 3 times the standard deviation of the standard deviation of the rotor speed:

$$|SRS_i - \text{mean}(SRS_i)| < 3\text{std}(SRS_i)$$

A *'reasonable pitch activity'* for WMR is ensured by the same methods as *'reasonable generator speed*. But instead of using 3rpm, the factor 10° is chosen because *'reasonable pitch activity'* deals with blade pitch values. As for the second method, the factor is kept the same at 6 times the standard deviation of the standard deviation of the blade pitch.

$$|SP_i - \text{mean}(SP_i)| < 6\text{std}(SP_i)$$

Where,
SP_i - std($Blade\ pitch$)
i - 10min sample i

All data from the last year has been removed from this analysis to ensure that *'no yaw steering test'* was performed during the available measurement data for WMR.

After the process of sequential filtering, 77% of HR2 and 57% of WMR initial data was kept.

3.4 Ambient undisturbed conditions

To validate the Frandsen and modified Frandsen model, the undisturbed ambient wind conditions are required as input. These conditions are encountered by the wind turbine when there is no velocity deficit or additional turbulence due to the upstream wake of the wind turbine.

The wind speed measurements obtained from the nacelle anemometer and the wind speed estimator describe only the local wind characteristics and not the free-stream

wind characteristics of the selected turbine. For this reason, the free stream wind conditions are based on the measurements provided by the upstream undisturbed wind turbines. The following process is followed to determine the ambient undisturbed conditions for each 10-minute sample:

1. ***Identify wake inducing wind turbines:*** It is assumed that all wind turbines in the farm have the same wind directions (taken as yaw direction, see Section 3.2) as the selected turbine. For each 10-minute sample, all wind turbines (j) that induce wake on the turbine under study are identified based on the following search criterion::

$$abs[\theta - \theta_j] < 3\theta_{w,j} \text{ for } \theta$$

Where,
θ - wind direction
θ_j - Alignment direction of wind turbine j with respect to wake effected turbine.
$\theta_{w,j}$ - Frandsen proposed view angle of wind turbine j (Equation 2.14)

2. ***Remove invalid 10-min samples:*** According to the filtering criteria defined in Section 3.3, any wind turbine that falls outside of these parameters will be rejected. Failure to meet these parameters indicates that the wind turbine is not operating normally under normal turbulence. Therefore, there is no guarantee that the upstream wind turbine would induce wake on the investigated turbine. Examples of such rejected 10-minute samples for WMR are shown below in Figure 3.7a and Figure 3.7b.

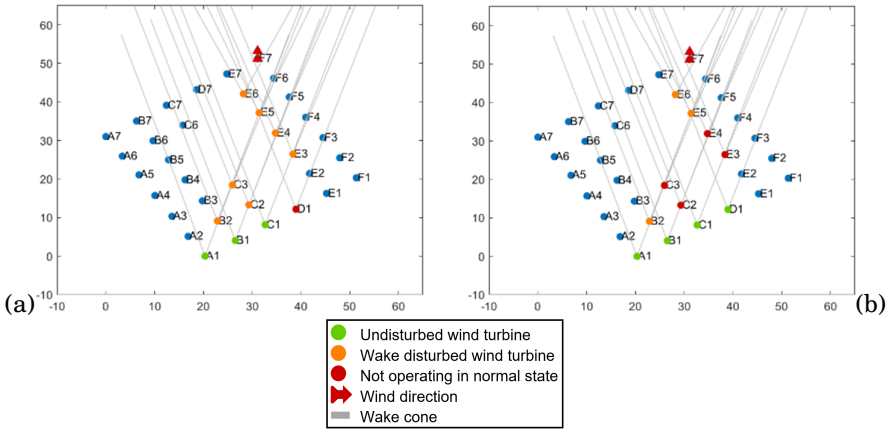

Figure 3.7: WMR examples of invalid 10-min samples where at least one wind turbine that is not operating normally generates a wake that could potentially affect F07. The wind turbine not operating in normal state are D1 in (a) and C2,C3,E3,E4 in (b) for a wind direction of 180°

For HR2, the same 10-minute sample rejection criteria are applied, but with an additional threshold. The threshold states that any turbine that is within the 20D distance must be operating under normal operating conditions. Any turbine operating outside the 20D threshold, whether operating normally or not, is assumed to be far enough to not affect the results of the wind turbine

under study. An example of a valid and invalid 10-min sample for D5 in HR2 is shown in Figure 3.8.

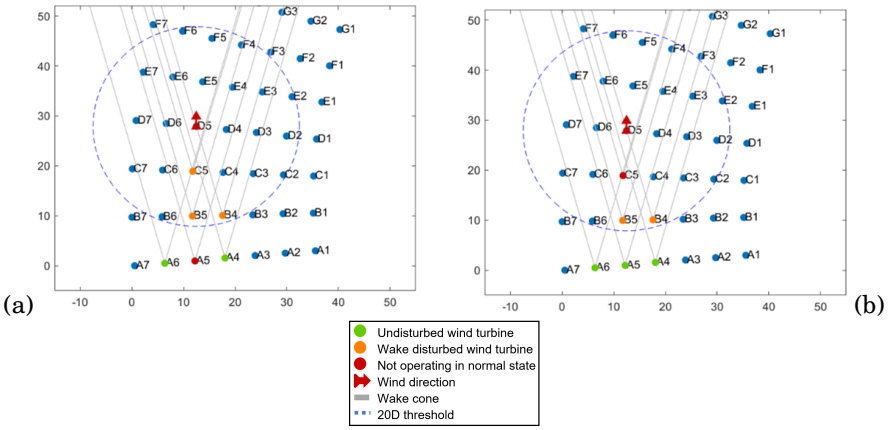

Figure 3.8: HR2 examples of (a) valid 10-min samples where at least one wind turbine(A5) outside of the 20D threshold may not be operating normally (b) invalid 10-min sample where at least one wind turbine(C5) within 20D may not be operating normally

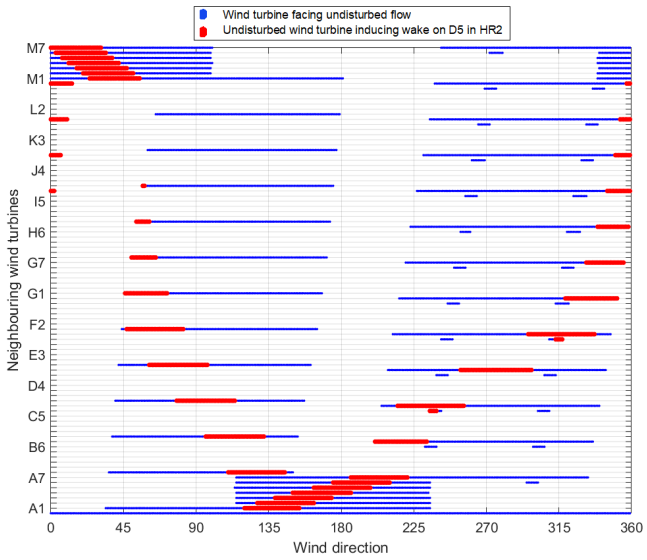

Figure 3.9: Wind turbines facing undisturbed free-stream flow (in blue) with respect to wind direction for HR2. Red markers represent wind directions where the undisturbed wind turbine induce wake on D5 in HR2

3. ***Determine ambient undisturbed conditions:*** If a 10min sample is valid, then among all the wake-inducing wind turbines the ones which are experiencing undisturbed free stream conditions are found. From the selected turbines, the median value of the wind measurements representing the

ambient conditions is calculated. An example of such a case is shown in Figure 3.8 a, where the undisturbed measurements are based on the median of measured values from A6 and A4. Figure 3.9 and 3.10 shows all wind turbines exposed to wake free flow (in blue) in relation to wind direction and highlights the wind directions (in red) where they induce a wake on the wind turbine of interest (i.e. F07 in WMR and D5 in HR2).

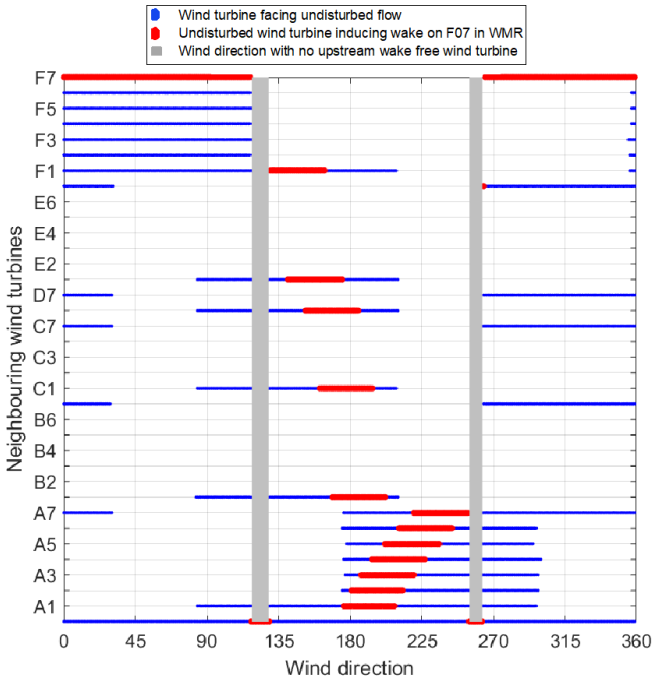

Figure 3.10: Wind turbines facing undisturbed free-stream flow (in blue) with respect to wind direction for WMR. Red markers represent wind directions where the undisturbed wind turbine induce wake on F07 in WMR. Grey area highlights the wind direction where no free-stream facing wind turbines are present

4. ***Special cases:*** Listed below are special conditions that are not covered by steps 1-3.

   (a) When the wind turbine under investigation is not exposed to wake flow, then the values measured on this turbine represent the undisturbed wind conditions (Figure 3.11a).

   (b) To be used as a reference for estimating the undisturbed wind speed the wind turbine must be wake-free. However, if all wake-inducing wind turbines themselves experience disturbed conditions, the value measured on the investigated turbine is used (Figure 3.11b). This rare situation only appears when the wind is almost aligned with the rows. It only concerns a very small portion of the data and is not considered to be affecting the overall results. For WMR this situation occurs for wind directions $118 - 129°$ and $255 - 263°$ (shown in Figure 3.10)

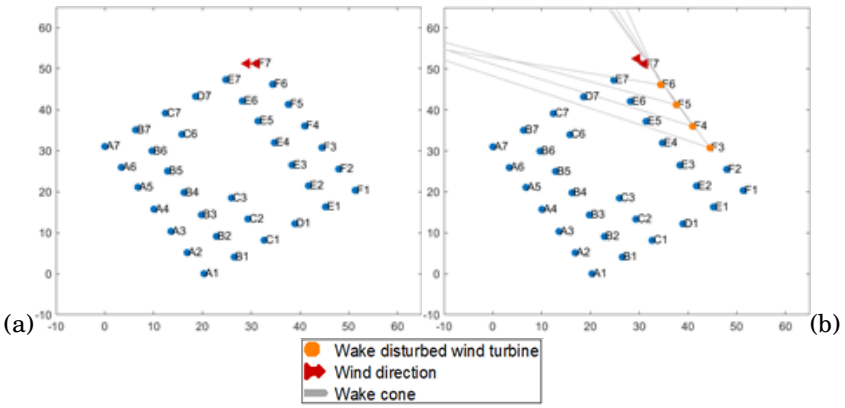

Figure 3.11: Special case (a) F07 is not in the wake of another wind turbine, (b) F07 is in the wake of wind turbines that encounter disturbed conditions

(c) This scenario, while specific to HR2, states that if all the wake-inducing wind turbines that face undisturbed wind conditions are not operating in the normal condition, no estimate of ambient wind conditions can be found. Therefore, the corresponding 10-minute sample from this study is discarded (Figure 3.12).

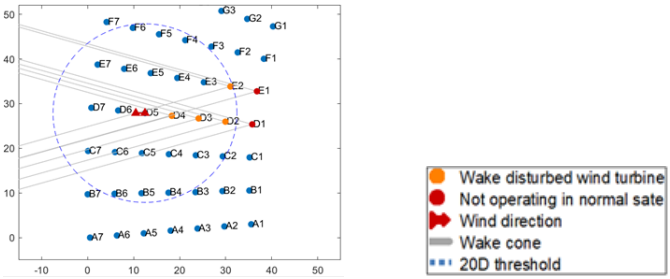

Figure 3.12: Special case (c) D05 is in the wake of wind turbines that cant be considered undisturbed

3.5 Correcting effects of external disturbances

The undisturbed wind speed for the examined wind turbine is calculated based on measurements from upstream undisturbed wind turbines (see section 3.4). When there are more than one undisturbed wind turbines the median of their measurements is calculated to represent the ambient conditions faced by the wind turbine under investigation. However, the calculated ambient needs to be corrected since some velocity gradients are found on the scale of the wind farm. It must be noted that only the wind speed gradients were corrected herein.

3.5.1 Westermost Rough (WMR)

For WMR wind speed gradients were found in south west direction due to wind flows from the shore and in the southeastern wind direction due to the wake of the neighbouring wind farm (Humber Gateway seen on Figure 3.2). Figure 3.13 illustrates the magnitude of the two observed external disturbances experienced at WMR. Here the wind speed difference between the wind turbines present in row 1 and row 7 are calculated with respect to wind turbine 'A'. Figure 3.10 shows that row 1 wind turbines experience wake free flow from wind direction 90-200 degrees. For row 7 wind turbines the wake free flow is present for wind directions ranging from 270-20 degrees.

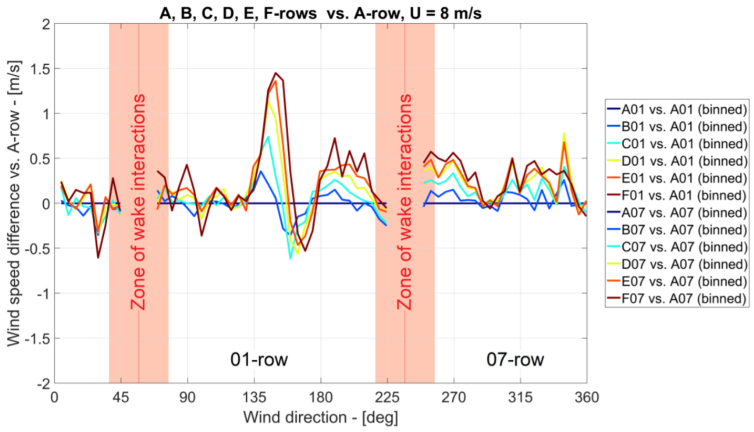

Figure 3.13: Wind speed differences of row 1 and row 7 wind turbines with respect to the first wind turbine in the row [71]

Even though wind turbine in row 1 face wake flow for the wind direction of 237 degrees, a positive velocity gradient with a maximum increase in wind speed of 0.5m/s with respect to A1 can be determined based on the trend in Figure 3.13. This increase in wind speed can be either coastal effect or wind farm blockage effect. However, since no increase in wind speed was recorded for the wind coming from the sea, the positive velocity gradient around 237 degrees was identified as coastal effect.

The second velocity gradient observed by WMR due to the wake of the neighbouring wind farm reaches a magnitude of 1.5m/s for the wind speed of 8m/s. Unlike the coastal gradient this disturbance results in increasing and decreasing wind speeds centered around the wind direction of 160° (relative position of Humber gateway). The variation in the wind speed gradient can be explained by the position of the wake experienced by WMR from Humber Gateway. For the wind direction of less than 150 degrees a positive velocity gradient is seen in Figure 3.13, since A1 experiences low wind speeds as it is in the wake. However, as the wind direction increases the position of the wake moves to the right side of the wind farm falling on F1. As a result the velocity gradient becomes negative.

For wind directions where ambient wind speed is based on upstream wind turbines a correction factor is applied to correct for the velocity gradients. This velocity gradient correction is based on a formula developed in-house by SGRE for the WMR site. It

includes both the southwest velocity gradient correction for coastal effects and the southeast velocity gradient correction for Humber Gateway's wake.

3.5.2 Horns Rev II

For HR2 one wind speed gradient was found for the wind flow from the southeasterly wind direction due to the wake of the neighbouring wind farm (Horns Rev 1 seen on Figure 3.1). In order identify the magnitude of the wind speed gradient, the wind speed difference was checked for all 4 sides of the wind farm. That is between column M wind turbines, column A wind turbines, row 1 wind turbines and row7 wind turbines. Figure 3.9 shows the wind directions where each of the column and rows in HR2 experience wake free flows.

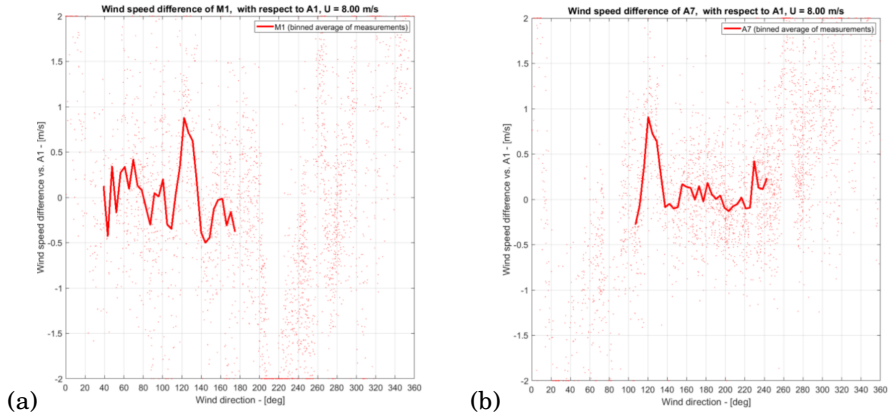

(a) (b)

Figure 3.14: Wind speed difference along the (a) Eastern side of the wind farm between M1 and A1 (b) Southern side of the wind farm between A7 and A1 [71]

Figure 3.14 shows the wind direction range where significant speed gradients were detected (100° till 160°). Similar to wind speed gradient observation due to wake flow on WMR, HR2 also experienced a variation of increasing and decreasing wind speed gradient with respect to wind direction. The magnitude of wind speed gradient is observed to reach a maximum of +1m/s for a wind direction of 119 degree at the wind speed of 8 m/s. That is when the wake of HR1 falls on A1 whereas M1 experiences free stream flow. As the wind direction increases to 142 degrees the wake of HR1 is shifted onto M1, as a result the wind speed gradient of -0.5m/s is observed. These wind speed gradients are also faced by the wind turbine in column A resulting in wind speed gradient of +1m/s for the wind directional range of 114-119 degrees.

To correct for the identified wind speed gradient in the measurements of upstream wind turbines (section3.4), a simplified wind farm wake model developed in-house by SGRE was used. This modeled the wind speed deficit caused by the Horns Rev 1 wind farm as a Gaussian curve with an amplitude and a width calculated from site characteristics (turbine type and geometric parameters). The wake is assumed to propagate linearly and affect only the wind speed (and not the turbulence property). For HR2 coastal wind speed gradients may have been present, however insufficient evidence were found to build a corrective model.

3.6 Selection of wind turbine to investigate

After describing the corrected wind speed and filtering the 10-minute data samples, a number of wind turbines were selected to further analyze. This selection was based on several criteria that ensured that the available data for the selected turbine was sufficient and comprehensive. The criteria are as follows:

1. Sufficient number of 10-min samples to obtain statistically meaningful results
2. Stability of the load measurements over the observed time period
3. Consistent measurements between the three blades of the same wind turbine
4. Multiple wake conditions with respect to wind directions (to test the validity of direct wake or wind farm turbulence as defined by the Frandsen model)

Based on the criteria, the following wind turbines were shortlisted from the respective wind farms:

1. HR2: The wind turbine selected is D5, whose final data set is 71.4% of the initial data.

2. WMR: The wind turbine selected is F7, as it is the only wind turbine with available data. Its data set amounts to 39.5% of the initial data.

Compared to the percentages of available data after filtering (77% for HR2 and 57% for WMR see section3.3), these data sets are even more reduced. This reduction in data is due to the additional filtering introduced while estimating undisturbed wind conditions. As a consequence the resulting wind rose of the filtered data is no longer representative of the wind rose of the site as shown in Figure 3.15.

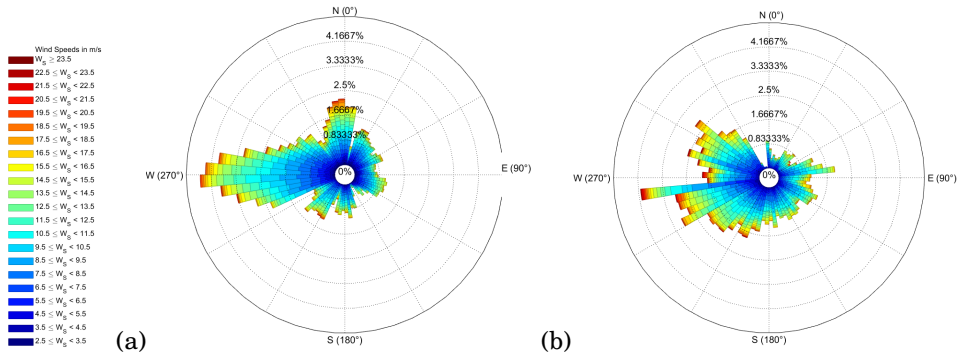

Figure 3.15: Approximated wind rose of the final dataset (a) F07 WMR (b) D5 HR2

The estimated ambient undisturbed wind conditions for the selected wind turbines were also validated against the meteorological data (measured) collected prior to the installation of the wind farm. The 90th percentile of the estimated ambient TI (Figure 3.16 and 3.17) was compared to the 90th percentile of the measured ambient TI per wind speed. For WMR and HR2, the trend of the estimated TI per wind speed

was consistent with that of the measured data within the range of 5-13m/s. Looking at the correlation per wind speed, for both wind farms, the estimated ambient TI was higher (+0.01 for WMR and +0.005 for HR2) than the measured TI at 10m/s, probably because of the limitation of the wind speed and TI estimator. Moreover, for HR2, the estimated ambient TI was smaller than the measured TI for 6-9m/s. This means that when the estimated ambient TI is used as an input in the Frandsen model, it will result in the same difference in the comparison of TI and loads from wake flows.

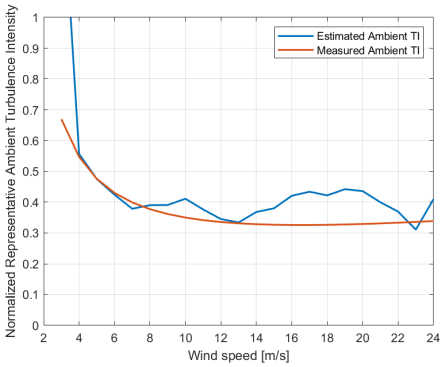

Figure 3.16: Normalized Representative ambient turbulence per wind speed for F7 in WMR

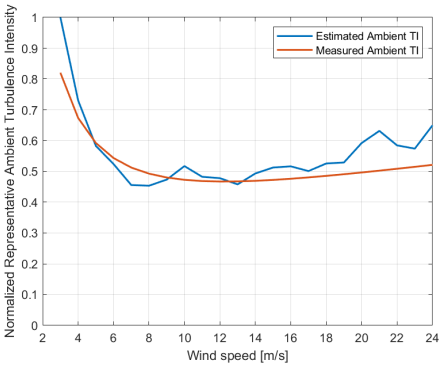

Figure 3.17: Normalized Representative ambient turbulence per wind speed for D5 in HR2

Lastly the estimated ambient turbulence for each 10min observation was also compared with the measured turbulence level as seen in Figure 3.18 and 3.19. Some estimated ambient turbulence values were observed to be higher than the measured wake effected turbulence. This could be because of no TI dissipation effects being considered while estimating values of TI based on upstream wind turbines or due to some flow acceleration around turbines (between the rows) which increases wind speed and thus reduces TI values (e.g. the effect of D06 in HR2 around 300 degrees). For F7 in WMR this overestimation in ambient turbulence levels was mainly in the southwesterly wind direction sectors with coastal winds. Whereas, for D5 in HR2 the overestimation in ambient turbulence levels was mainly present in winds direction sectors (225-315 degrees) facing open sea wind. The wind turbine being investigated experienced wake flow in the identified wind direction sectors. Therefore, to quantify the turbulence dissipation on the scale of the wind farm the difference of turbulence between the upstream wind turbine and the wind turbine being investigated were calculated for below cut-in and above cut-out wind speed. However due to limited number of observation no significant evidence of the turbulence dissipation was found to build a correction model.

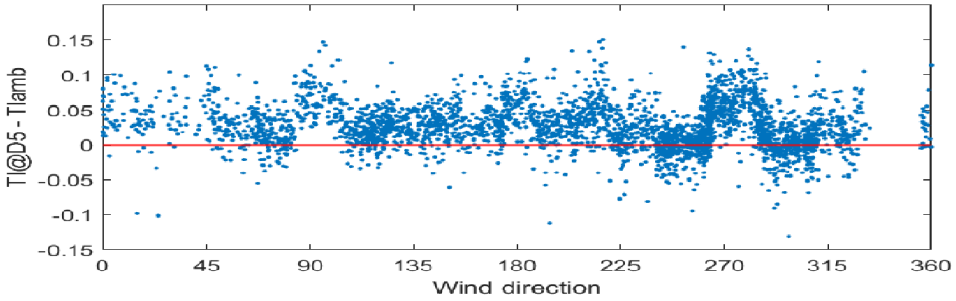

Figure 3.18: Difference between the 10min estimated ambient and measured turbulence intensity for D5 in HR2 at a wind speed of 9m/s

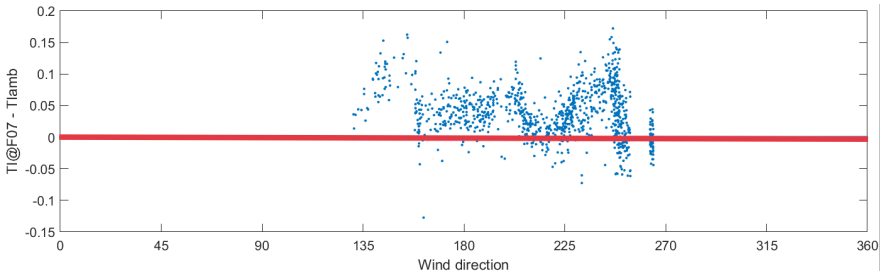

Figure 3.19: Difference between the 10min estimated ambient and measured turbulence intensity for F7 in WMR at a wind speed of 9m/s

Chapter 4

Turbulence model validation

The goal of this study is to assess the accuracy of the Standard Frandsen model and the Modified Frandsen model described in Section 2.2 for estimating wake affected directional turbulence intensity under specific atmospheric stability conditions. This chapter initially defines the used atmospheric stability classification, followed by the comparative study of the directional turbulence intensity at two specific wind farm locations.

4.1 ABL stability categorization

The ABL stability classification used in this study is based on the Obukhov length, which can be estimated using the RI methods or Profile methods (see section 2.1.2). All of these methods require the input of temperature and wind speed readings at two different altitudes. Since air and sea temperature data were not available for this study, the required measurements are obtained using hind-casting mesoscale models. The New European Wind Atlas (NEWA) dataset based on mesoscale simulations with the Weather, Research and Forecasting (WRF) model at a resolution of 3 km x 3 km x 30 min is used for this analysis [72]. The purpose of using the downscaled dataset is to define the atmospheric stability for each of the 10-min observations. Table 4.1 provides a summary of the height of the extracted wind speed and temperature readings from NEWA. The height of the extracted NEWA readings was chosen to be closest to the hub height of each wind farm.

Table 4.1: NEWA wind speed and temperature recording height

	HR2 (hub height: 68m)		WMR (hub height: 105.52m)	
NEWA	75m	10m	100m	10m

The Obukhov length used for stability categorization is provided as a calculated variable in the NEWA dataset. Before the SCADA observations are categorized into the atmospheric stability classes, the accuracy of the NEWA dataset is checked. This is done by comparing the measured undisturbed wind speeds at HR2 and WMR with the wind speed data provided by NEWA. Since the NEWA wind speed readings represent 30-minute instantaneous values, they are compared to the 30-minute

SCADA observations for the respective time stamp. To obtain the wind speed at hub height from the NEWA dataset, the power law was used (equation 4.1), using the maximum recording height as a reference. Here, the wind shear was determined using the wind speed readings from the two recording heights given in Table 4.1. Figures 4.1 and 4.2 show a correlation plot with the correlation coefficient for the wind speed recordings at HR2 and WMR, respectively. For both wind farms, the scatter in the correlation plot is present because the high-resolution NEWA dataset (3 km x 3 km) does not capture the small-scale variations and local effects such as land-sea transitions that well. For both wind farms, the correlation coefficient represents a strong correlation, as a factor greater than 0.7 indicates highly correlated values [73].

$$U_h = U_{h_{ref}} \left(\frac{h}{h_{ref}} \right)^{\alpha} \tag{4.1}$$

Where,
h - height
α - wind shear

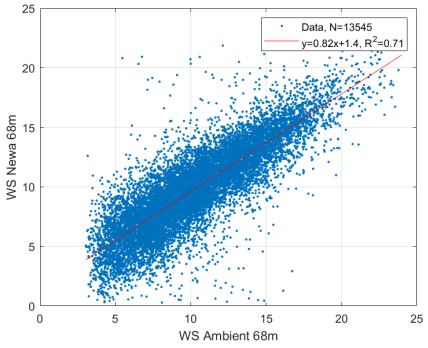

Figure 4.1: NEWA wind speed correlation plot for HR2 with SCADA hub height wind speed for D05 in HR2

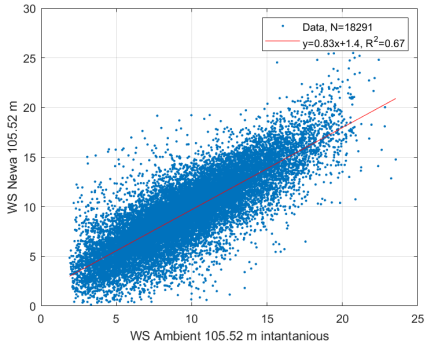

Figure 4.2: NEWA wind speed correlation plot for WMR with SCADA hub height wind speed for D05 in HR2

To ensure that the data from the SCADA observation and NEWA were synchronized, a time shift was applied to the NEWA dataset ranging from -2hrs to +2hrs. Then, the correlation coefficient between the SCADA wind speed observation and the NEWA dataset with the applied time shift was determined. Figure 4.3a and 4.4a shows that the correlation coefficient increased to a maximum when a time shift of about 60 minutes was applied to the NEWA dataset. This could be due to a mismatch in the reference time used: Coordinated Universal Time (UTC) or Western European Summer Time (WEST). The time signal in NEWA was therefore corrected to match the time signal in SCADA by applying a one-hour shift. This resulted in an increased correlation coefficient of 0.72 for HR2 and 0.68 for WMR, as shown in Figure 4.3b and 4.4b.

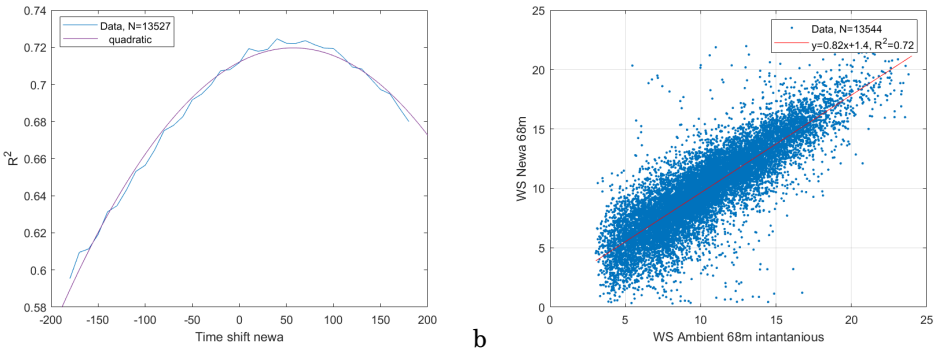

Figure 4.3: (a) HR2 wind speed correlations coefficient vs applied time shift (b) HR2 NEWA wind speed (shifted by 60 min) correlation plot with SCADA hub height wind speed for D05 in HR2.

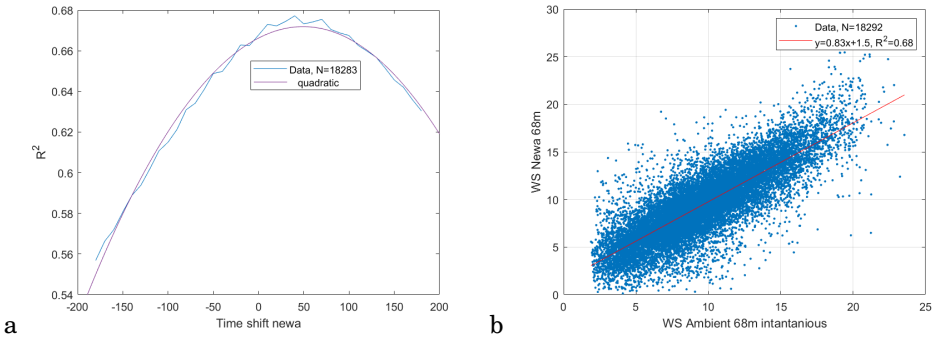

Figure 4.4: (a)WMR wind speed correlations coefficient vs applied time shift (b) WMR NEWA wind speed (shifted by 60 min) correlation plot with SCADA hub height wind speed for F07 in WMR.

The monthly distribution of available filtered 10-minute SCADA timestamps was also examined for possible bias. A significant bias in the monthly distribution of available 10-min timestamps would result in a bias in the atmospheric stability distribution present in the complete data set. Since there is an increased frequency of occurrence of unstable conditions during the summer months and stable conditions during the winter months [67].

Figure 4.5 and 4.6 show the monthly distribution of filtered 10 min SACAD timestamps for WMR and HR2. WMR shows a slightly increased number of 10min observations in the month October-December. However, when looking at the winter months as a whole, this increased number of 10-min observations is balanced by the relatively lower number of 10-min observations in the months of Jnauray-March. For HR2, the significantly increased number of available 10-min observations is seen in May, as this is the only month present two times during the one-year period of available SCADA measurements. When considering the winter and summer months for HR2 together, a roughly equal number of available 10-min observations can be seen. Since there is no significant variation in the seasonal distribution of available

10-min observations, it is assumed to have no significant effect on the distribution of atmospheric stability in the available dataset.

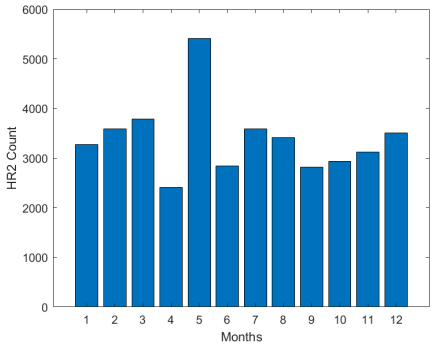

Figure 4.5: Monthly distribution of available 10min time stamps at HR2

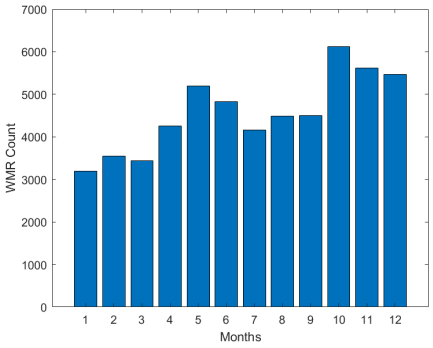

Figure 4.6: Monthly distribution of available 10min time stamps at WMR

4.1.1 Atmospheric stability classification

This section explains how the atmospheric stability classification has been conducted in order to assess the turbulence models accuracy under different stability conditions. Previous works as introduced in Section 2.1.2 have used different thresholds for neutral conditions (e.g. |L|>500 or |L|>1000). To understand the choice of the stability classification of |L|>500 or |L| >1000 to classify neutral atmosphere, a comparative study was performed between the empirical relations defining the wind profile and NEWA data. The variation in mean wind speed ratio (U2/U1) and mean stability correction function (ψ_m) for different neutral atmospheric stability classification criteria ranging between absolute value of Obukhov length of 500-1000 were investigated. Using Monin Obukhov length similarity theory in combination with the stability correction functions the wind profile is calculated as:

$$\frac{u[z_2]}{u[z_1]} = \frac{\ln(\frac{z_2}{z_0}) - \psi_m[\frac{z_2}{L}] + \psi_m[\frac{z_0}{L}]}{\ln(\frac{z_1}{z_0}) - \psi_m[\frac{z_1}{L}] + \psi_m[\frac{z_0}{L}]} \approx \frac{\ln(\frac{z_2}{z_0}) - \psi_m(\frac{z_2}{L})}{\ln(\frac{z_1}{z_0}) - \psi_m(\frac{z_1}{L})} \tag{4.2}$$

The roughness length (z_0) for the open sea is estimated to be about 0.0002 m [74], which is relatively small to the measurement height (z). Therefore, the second stability correction term, which is a function of the roughness length, is usually neglected.

Wind Speed Ratio

In Figure 4.7 and 4.8 the wind speed ratios ($\frac{U_2}{U_1}$) for WMR and HR2 as a function of $\zeta = \frac{z}{L}$ are shown. The wind speed ratios that are calculated using the empirical relations use a constant roughness length(z_o) of 0.0002 m [74]. For increasing stable conditions, the wind speed ratio increases linearly, whereas for increasing unstable conditions the wind speed ratio decreases exponentially. The wind speed ratios from

the empirical relations follow a similar trend as the observed wind speed ratios in the stable atmospheric conditions. However, under unstable atmospheric conditions the observed wind speed ratio is lower than what is calculated using the empirical relations. The term 'observed' refers to the wind speed ratio calculated using the NEWA data.

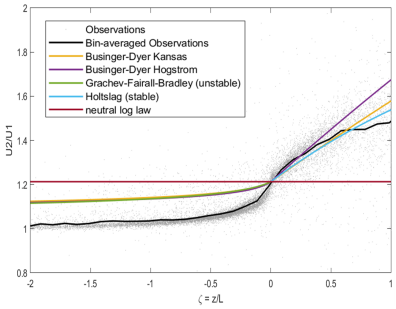

Figure 4.7: WMR wind speed ratio vs z/L

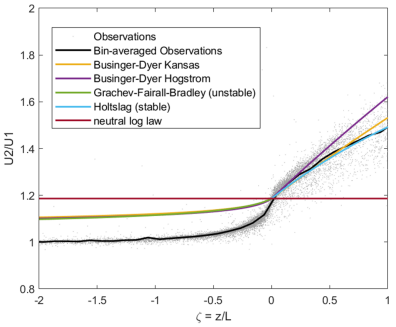

Figure 4.8: HR2 wind speed ratio vs z/L

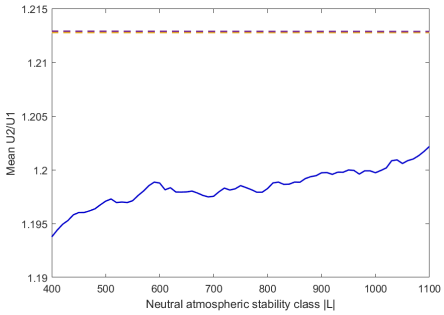

Figure 4.9: WMR mean wind speed ratio for each neutral atmospheric stability class

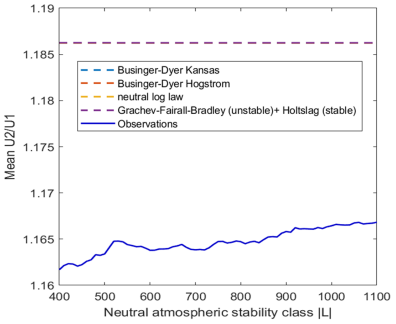

Figure 4.10: HR2 mean wind speed ratio for each neutral atmospheric stability class

In order to see the difference in the atmospheric classification depending on the threshold used for the classifying neutral samples, the mean of the wind speed ratio was calculated from a selected range of ζ defined using the Obukhov length. In the literature the atmosphere is considered neutral when the absolute value of Obukhov length ($|L|$) is greater than 500 or 1000 m. The variation of the mean wind speed ratio for the neutral conditions defined using the Obukhov length can be seen in Figure 4.9 and 4.10. It can be seen that with decreasing threshold used for the classifying neutral samples, the difference between the observed and empirically obtained mean wind speed ratio increases.

Figure 4.11 and 4.12 show how the empirically obtained mean of the wind speed ratio varies for each Obukhov length based neutral atmospheric stability classification. With increasing Obukhov length that defines the neutral stability class, the mean wind speed ratio obtained from the empirical relations deviates

further from the mean wind speed ratio defined by the neutral logarithmic wind profile. From these results it can be concluded that when the neutral atmospheric conditions are defined with $|L| > 1000$ they are more representative of the neutral atmosphere. Whereas when $|L| > 500$ is used, it considers neutral atmospheric conditions that are slightly unstable or stable.

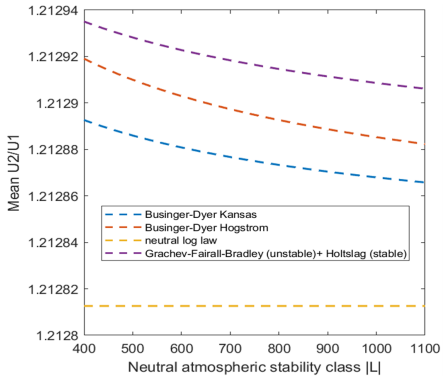

Figure 4.11: WMR empirically obtained mean wind speed ratio for each neutral atmospheric stability class

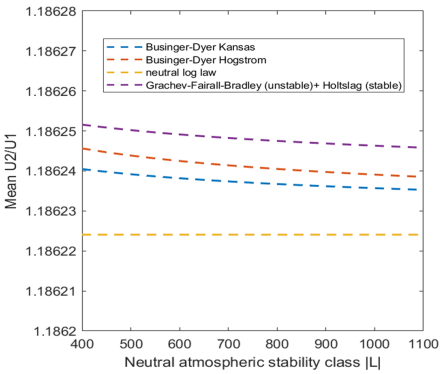

Figure 4.12: HR2 empirically obtained mean wind speed ratio for each neutral atmospheric stability class

Stability correction function

A similar comparative study like the wind speed ratio was performed for the stability correction function (ψ_m). The empirical stability correction function is determined using the equations defined in Table 2.1. The stability correction function is also calculated from the observed NEWA data set, using Monin Obukhov similarity theory with a constant roughness length of 0.0002. Figure 4.13 and 4.14 show the stability correction factor as a function of $\frac{z}{L}$. For increasing stable atmospheric conditions, the stability correction factor decreases linearly whereas for increasing unstable conditions it initially increases until it reaches a constant value of around two.

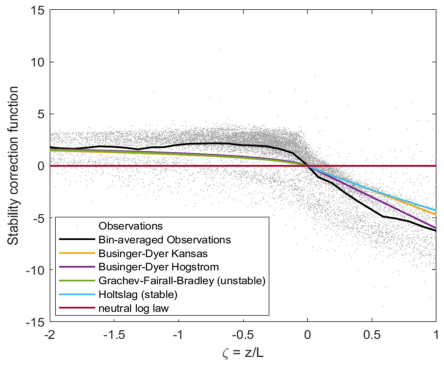

Figure 4.13: WMR stability correction factor vs z/L

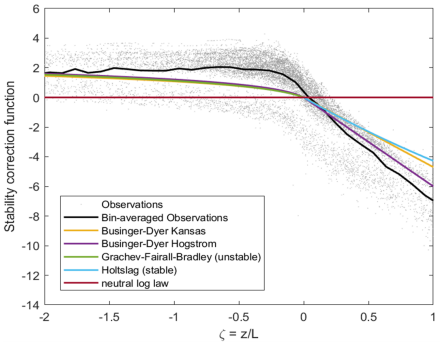

Figure 4.14: HR2 stability correction factor vs z/L

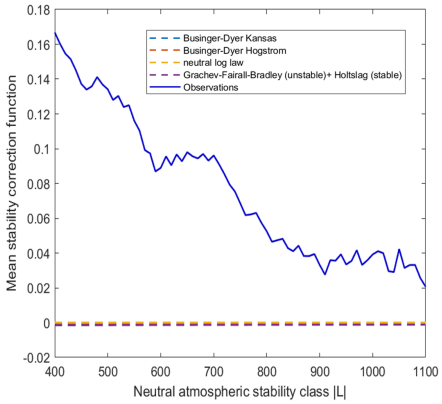

Figure 4.15: WMR empirically obtained mean stability correction factor for each neutral atmospheric stability class

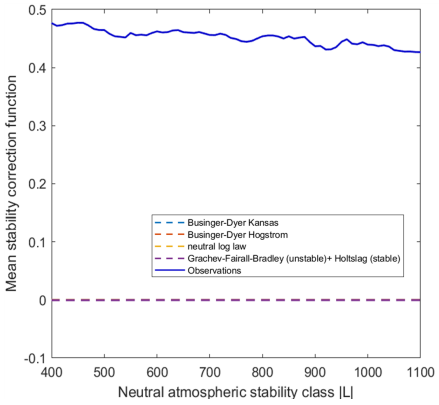

Figure 4.16: HR2 empirically obtained stability correction factor for each neutral atmospheric stability class

Figures 4.15 and 4.16 show the variation of the mean stability correction factor for neutral conditions defined using the Obukhov length. For completely neutral conditions at $\frac{z}{L} = 0$ the stability correction factor is zero since the wind profile follows the logarithmic law. The mean stability correction factor from the observations increases for both WMR and HR2 as the Obukhov length defining the neutral atmosphere is decreased from 1000 to 500. Here, the magnitude of the mean stability correction factor and its variation with increasing Obukhov length, which defines the neutral conditions, depends on the assumed roughness length and the gradient of the stability correction factor for the neutral conditions, as shown in Figure 4.13 and 4.14.

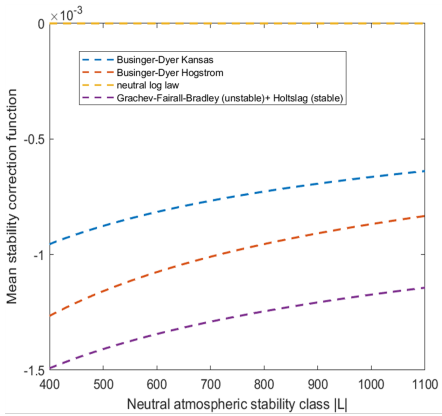

Figure 4.17: WMR empirically obtained mean stability correction factor for each neutral atmospheric stability class

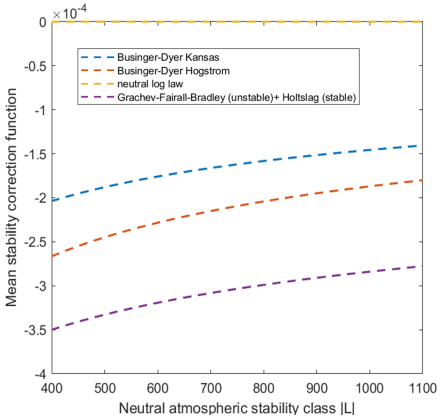

Figure 4.18: HR2 empirically obtained mean stability correction factor for each neutral atmospheric stability class

Figure 4.17 and 4.18 show a similar variation in the mean stability factor obtained

from the empirical relation. This variation in the mean neutral stability correction factor suggests that $|L| > 1000$ is a better classification for identifying neutral atmospheric conditions compared to $|L| > 500$. As the Obukhov length is inversely proportional to ζ, decreasing the Obukhov length defining neutral conditions from 1000 to 500 increases the bin range of ζ to be considered, leading to the consideration of neutral conditions that may be slightly stable or unstable.

Selected atmospheric stability classification

On the basis of the comparative study between the empirical relations defining the wind profile and NEWA data it can be conclude that a neutral atmosphere stability classification of $|L|>1000$ ensures that only neutral conditions are considered. However, when a neutral atmosphere stability classification of $|L|>500$ is used, it also considered neutral conditions that are slightly stable and unstable. Based on this understanding the atmospheric stability classes can be defined as:

Table 4.2: Proposed range of stability classes based on Obukhov length

	HR2	WMR
Unstable	$-500 < L < 0$	$-500 < L < 0$
Neutral- slightly unstable	$-1000 < L < -500$	$-1000 < L < -500$
Neutral	$\|L\| > 1000$	$\|L\| > 1000$
Neutral- slightly stable	$500 < L < 1000$	$500 < L < 1000$
Stable	$75 < L < 500$	$100 < L < 500$

However, to ensure that each class has sufficient number of 10-min observations the proposed five-stage stability classes are merged to obtain a three-stage stability classification (Table 4.3). Even though the data-set for HR2 and WMR might seem large, that won't be the case when binning is performed per wind speed, direction and atmospheric stability. In order to avoid contamination of the large scatter found at the high ends of the scale with the "very unstable" class, the unstable regime is limited to $\zeta > -2$. An additional bound is added at $\zeta < 1$ for the stable regime to exclude data with shallow boundary layer height.

Table 4.3: Finalized atmospheric stability classification based on Obukhov length used in this study

	HR2	WMR
Unstable	$-500 < L < -37.5$	$-500 < L < -50$
Neutral	$\|L\| > 500$	$\|L\| > 500$
Stable	$75 < L < 500$	$100 < L < 500$

The figures below show the atmospheric stability distribution per wind speed for HR2 and WMR, using the stability classifications defined above in Table 4.3. For both wind farms an increase in the number of observed neutral conditions is seen with increasing wind speeds. This observation is in line with the results of variation of atmospheric stability with respect to wind speed obtained for HR and OWEZ in an independent study [67].

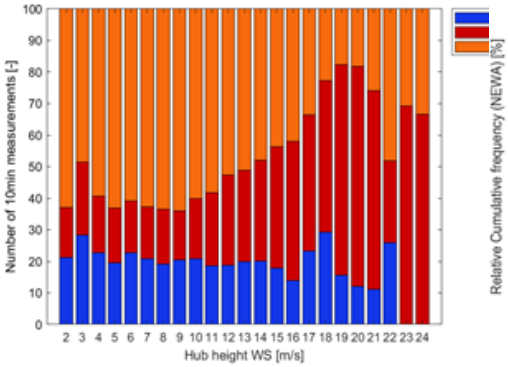

Figure 4.19: WMR atmospheric stability classes per wind speed level

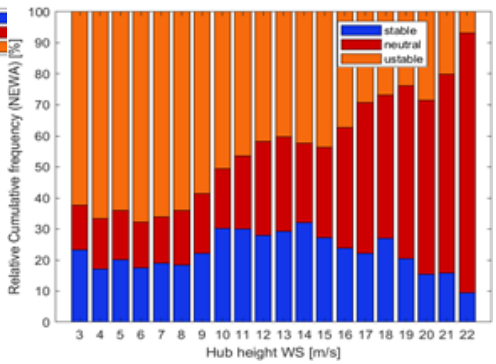

Figure 4.20: HR2 atmospheric stability classes per wind speed level

4.2 Turbulence model validation

The validation of the previously introduced turbulence models was performed by comparing the measured and modelled representative (90^{th} percentile) turbulence intensities across a 10-degree sector. The sectors width and alignment were chosen so that the wakes are perfectly aligned with the centre of the sectors. The modelled turbulence intensity is computed with the Standard Frandsen and modified Frandsen models using sectorial representative ambient turbulence intensity as the reference turbulence intensity (input into the model).

This analysis is performed for wind turbine F07 in WMR and D5 in HR2 at the free-stream wind speed of 9m/s. The value of 9m/s was chosen due to the high number of 10-min samples (Figure 4.21 and 4.22) and the significant presence of wake effects at this wind speed level due to the higher thrust coefficient. Following this line of thought and in order to expand the number of samples analysed, the data set was extended to the wind speed level of 7 to 9 m/s. This was done to ensure sufficient number of 10min observations in all the wind direction sectors for each atmospheric stability condition. As shown in Figure 3.16 3.17, these wind speed levels were selected because the variation between the representative turbulence is not significant.

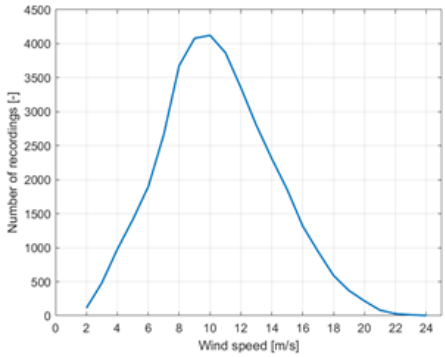

Figure 4.21: Number of 10min observation per wind speed for F7 in WMR

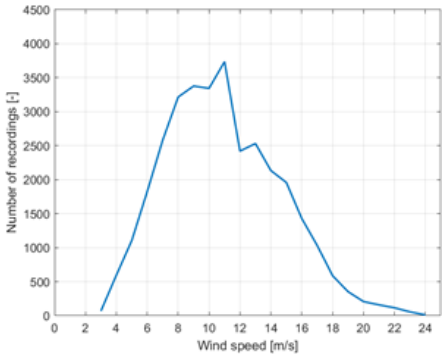

Figure 4.22: Number of 10min observation per wind speed for D5 in HR2

The selected wind turbines experience a variety of wake situations, as the distance to the upstream wind turbine strongly varies with the wind direction. Figure 4.23 and 4.24 show the layout of the upstream wind turbine with respect to the turbine being investigated in WMR and HR2. Since F07 in WMR is located at the northern edge of the wind farm, it only experiences wake flow from upstream wind turbines (determined by view angle), when the wind is coming from a range of southeastern till southwestern directions. In contrast D05 in HR2 experiences wake from all wind directions, with up to 8 rows of upstream wind turbines in the northern direction. This allows for testing the validity of the wind farm turbulence proposed by the Standard Frandsen model as case 2 (see section 2.2) for HR2.

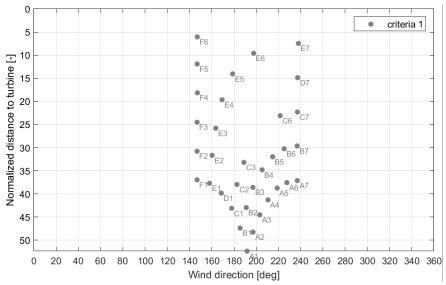

Figure 4.23: Normalized distance to upstream wind turbine (in terms of rotor diameter) with respect to the wind direction for F07 in WMR

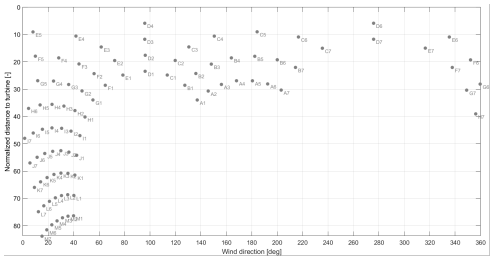

Figure 4.24: Normalized distance to upstream wind turbine (in terms of rotor diameter) with respect to the wind direction for D07 in HR2

For the implementation of the Standard Frandsen model it is initially determined which of the three defined cases are to be used for each wind direction sector. It is to be noted that for both the wind farms with reference to the wind turbine being investigated, the spacing in the rows perpendicular to the predominant western wind direction is greater than 3D. Therefore, for sectors that do not experience direct wake, the number of upstream wind turbines needs to be determined. Figure 4.25 and 4.26 show which of the three conditions in the Standard Frandsen model are used for determining directional turbulence intensity. As seen in Figure 4.25, F07 in WMR experiences a combination of freestream and direct turbulence for wind flow from 135-245 degrees. The direct turbulence faced by F07 is as a result of the wake from F06, E06 and E07, as they are located at a distance less than 10 D. Since the amount of upstream wind turbines relative to F07 is less than 5 it doesn't experience wind farm turbulence. On the contrary, D5 in HR2 does experience wind farm turbulence for wind flow from 20-50 degrees, with a combination of direct and freestream turbulence for the remaining wind directions. The direct turbulence faced by D5 is a result of the wake from upstream wind turbines E05, D04, C05 and D06.

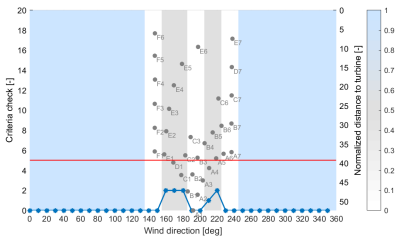

Figure 4.25: Standard Franden model identification of the case for directional turbulence intensity estimation and the count upstream wind turbines for F7 in WMR

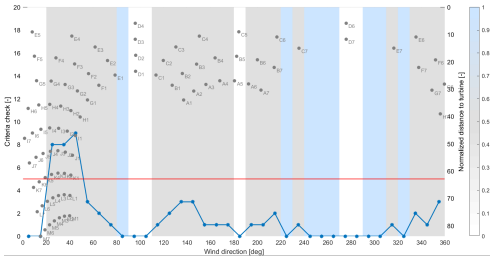

Figure 4.26: Standard Franden model identification of the case for directional turbulence intensity estimation and the count upstream wind turbines for D5 in HR2

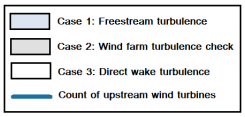

4.2.1 Directional turbulence validation for a specific wind speed

WMR and HR2 experience coastal and open sea winds for different wind directions. F07 in WMR experiences open sea winds for the north eastern wind direction. By contrast, D5 in HR2 experiences open sea winds for the wind flow from the West. Figure 4.27 and 4.28 shows the binned representative and mean ambient turbulence intensity faced by F07(WMR) and D5(HR2) for a wind speed of 9m/s.

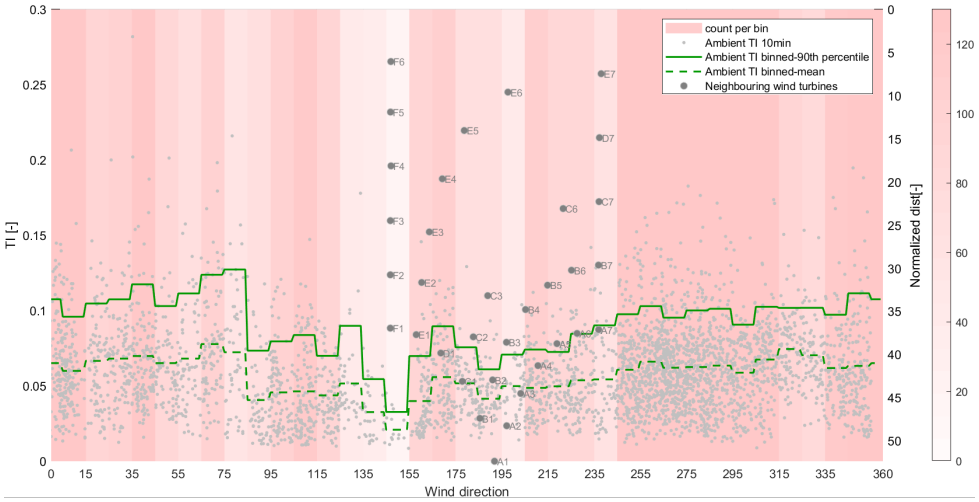

Figure 4.27: Binned 90th percentile of the ambient turbulence intensity for F07 in WMR at the wind speed of 9 m/s

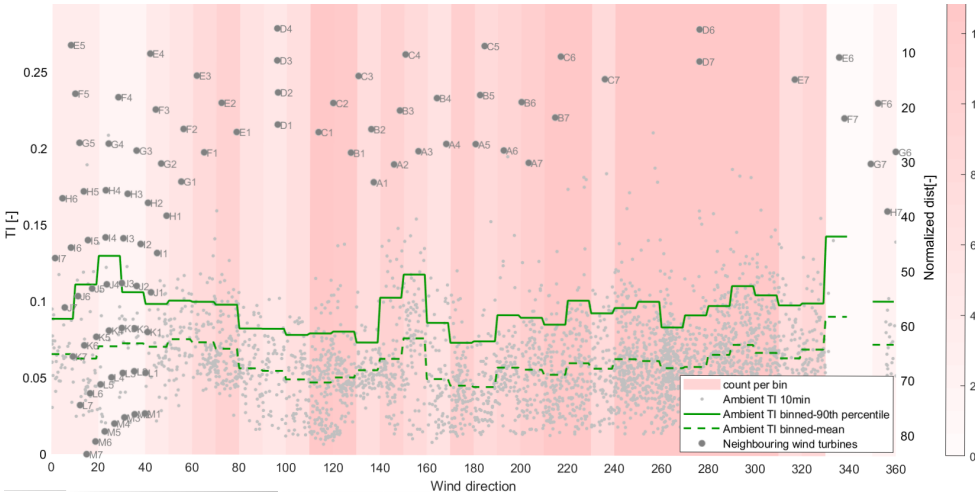

Figure 4.28: Binned 90th percentile of the ambient turbulence intensity for D05 in HR2 at the wind speed of 9 m/s

For WMR a higher ambient turbulence intensity level are seen in the Northeastern

wind direction, compared to the relatively lower representative ambient turbulence intensity in Southwestern wind direction. A significant drop in ambient turbulence in noted for wind flow from 85-125 degrees and 135-155 degrees, which can be attributed to lower offshore ambient turbulence intensity or a low number of recorded observations. For HR2 a decrease in the representative ambient turbulence intensity is observed for the wind direction ranging from 90-180 degrees, with an exception for wind direction from 140-160 degrees. This observed increase in ambient turbulence intensity is because HR2 is in the wake of HR1.

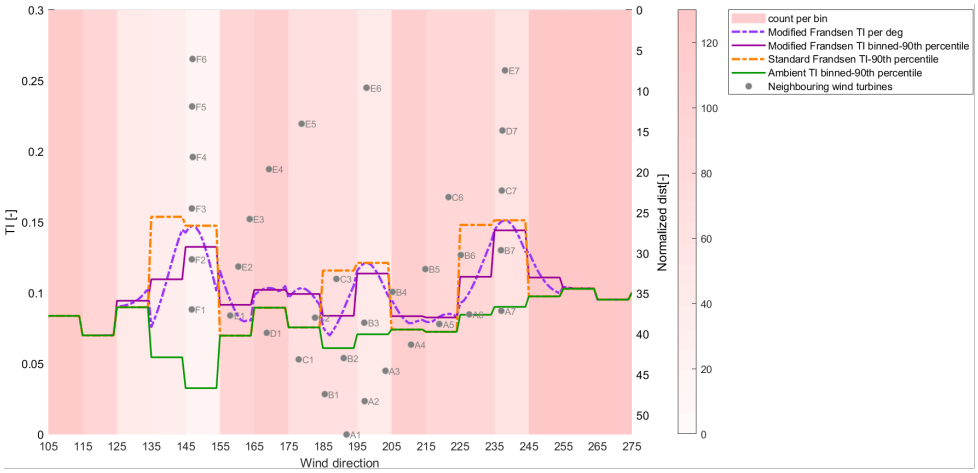

Figure 4.29: Representative directional turbulence intensity estimation from the Standard Frandsen and Modified Frandsen model for F07 in WMR at a wind speed of 9 m/s.

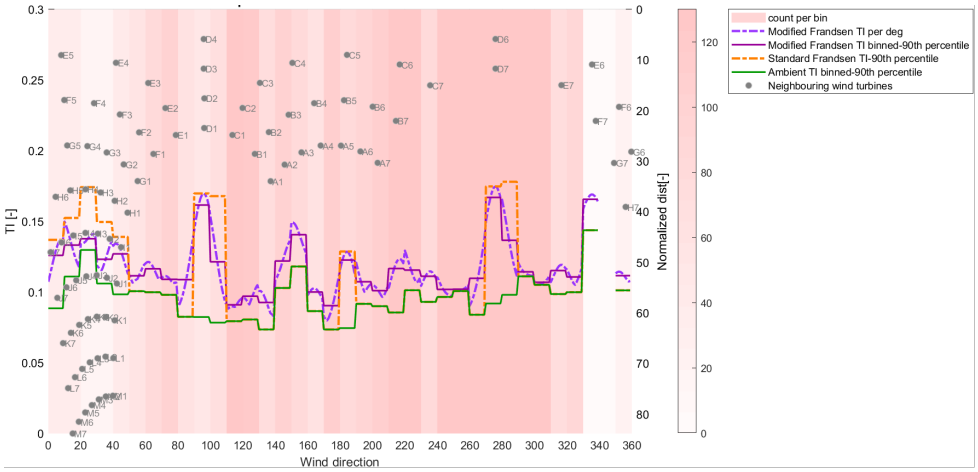

Figure 4.30: Representative directional turbulence intensity estimation from the Standard Frandsen and Modified Frandsen model for D05 in HR2 at a wind speed of 9 m/s.

The representative ambient turbulence intensity shown in Figure 4.27 and 4.28 is

used as an input in the turbulence models for calculating wake affected directional turbulence intensity. The Modified Frandsen model initially computes directional turbulence intensity per degree assuming a constant representative ambient turbulence intensity within each sector. Since the Modified Frandsen model assumes a bell-shaped added wake turbulence, a smooth variation can be seen in the per-degree-output from the model in Figure 4.29 and 4.30. On the contrary, across the sector Standard Frandsen model considers a constant added turbulence intensity, which compared to the Modified Frandsen model is the maximum of the bell shaped added wake turbulence. Since the modelled directional turbulence intensity is compared with the binned measured turbulence intensity, the per-degree-output from the Modified Frandsen model is averaged over each sector. The peaks in the modelled directional turbulence intensity correspond with the positioning of the nearest neighboring wind turbines shown by the grey dots. For WMR the Standard Frandsen modelled directional turbulence intensity represented by the dashed orange line only considers wake from F06, E06 and E07 (Figure 4.29). For HR2 the Standard Frandsen model considers added direct wake turbulence from E05, D04, C05 and D06 along with added wind farm turbulence for wind directions of 20-50 degrees. Figure 4.29 and 4.30 shows that, unlike the Standard Frandsen model, the Modified Frandsen modelled directional turbulence intensity in both wind farms also considers increased turbulence due to wake from upstream turbines positioned greater than 10D. For example for sectors 140-180 degrees for D5 in HR2 and 155-185 degrees for F07 in WMR, we can see that all wind turbines are positioned at a distance greater than 10D. The Standard Frandsen Model does not capture the peaks, while the Modified Frandsen model does.

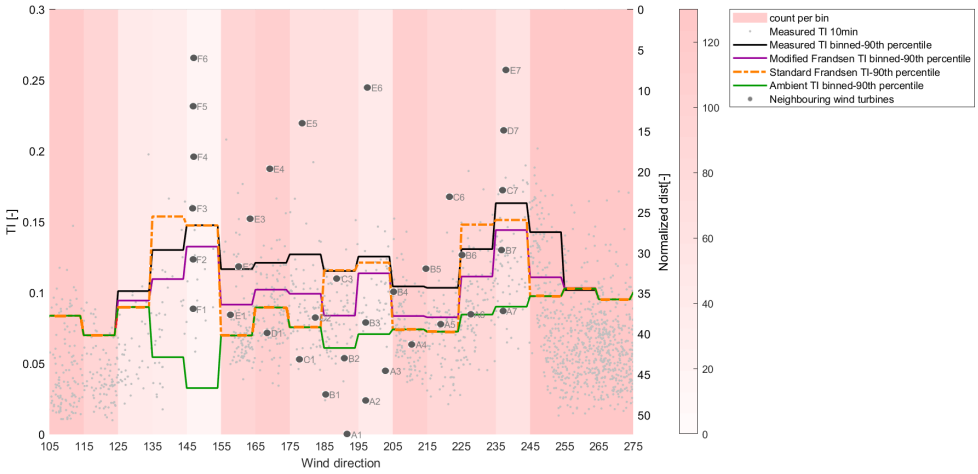

Figure 4.31: F07 in WMR: Comparison of the binned representative turbulence intensities from the Standard Frandsen and Modified Frandsen model with measured turbulence intensity

Figure 4.31 and 4.32 shows the measured directional turbulence intensity in comparison with the modelled results from the turbulence models. The Modified Frandsen modelled directional turbulence intensity is rather well reproduced in terms of shape for both the wind farms. For WMR the Modified Frandsen model consistently underestimates turbulence intensity across all wind directions. Where

as the Standard Frandsen model provides a better prediction of turbulence intensity in wind direction sector facing direct wake turbulence. The Standard Frandsen modelled directional turbulence intensity results for the wind direction of 135-155 in WMR show a better prediction of the turbulence intensity with respect to the observation, however due to lower number of observations within this sector no conclusion on the performance of the turbulence model can be made.

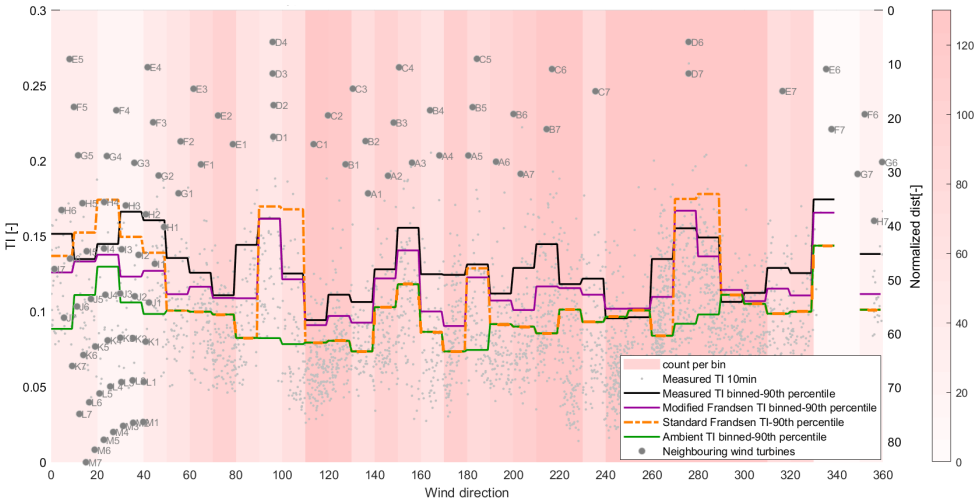

Figure 4.32: D05 in HR2: Comparison of the binned representative turbulence intensities from the Standard Frandsen and Modified Frandsen model with measured turbulence intensity

For HR2 the Standard Frandsen model, overestimates the direct wake turbulence intensity from D04 and D06. For direct wake flow from C05 located at a distance of approximately ten rotor diameters, the Standard Frandsen model gives a better prediction of turbulence intensity with respect to the observations. In the wind direction range where added wind farm turbulence intensity was considered the Standard Frandsen model initially over-predicts for the wind direction sector at 20 degree, followed by an underestimation of directional turbulence intensity. The Modified Frandsen model shows a better correlation with representative directional turbulence intensity for the direct wake sectors in HR2, however underestimating turbulence intensity in the wind directions with upstream turbines positioned greater than 10D.

Based on the comparative study of the wake added directional turbulence intensity in WMR and HR2, it can be concluded that for wind directions exposed to far wake turbulence, both turbulence models underestimate the turbulence intensity compared to the observations. However, the Modified Frandsen model provides a much better estimate of turbulence intensity compared to the Standard Frandsen model, which does not account for additional turbulence. However, for wind directions with direct wake turbulence, the Standard Frandsen model provides a better prediction of the turbulence intensity with respect to the observations compared to the Modified Frandsen model. It should be noted that the accuracy of

the predicted turbulence intensity from both turbulence models varies between the wind farms considered.

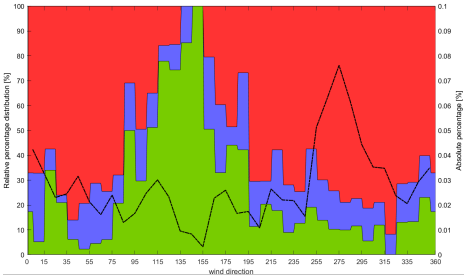

Figure 4.33: Relative atmospheric stability distribution in each wind direction sector observed in WMR for a wind speed of 9m/s

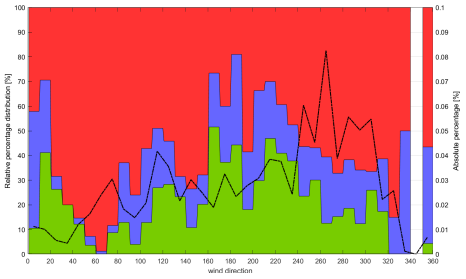

Figure 4.34: Relative atmospheric stability distribution in each wind direction sector observed in HR2 for a wind speed of 9m/s

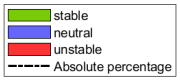

This varying performance of the Modified and Standard Frandsen model in both the wind farms for each wind direction can be explained by the atmospheric stability conditions being represented in the measured data. It is to be noted that in each sector different proportion of atmospheric stability conditions are found. The relative percentage of atmospheric stability conditions present in each of the defined wind sectors are shown in Figure 4.33 and 4.34. It is seen that the selected data for both the wind farms is mainly stable or unstable with a relatively smaller proportion of neutral conditions.

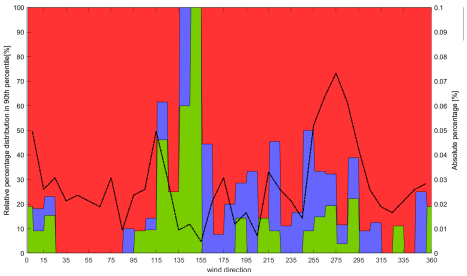

Figure 4.35: Relative atmospheric stability distribution in 90th percentile of turbulence data in each wind direction sector for WMR at a wind speed of 9m/s

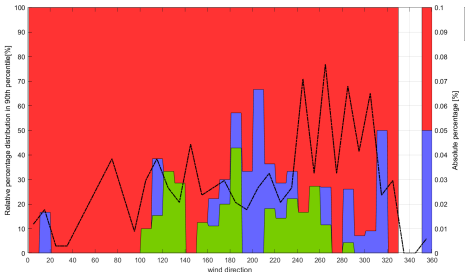

Figure 4.36: Relative atmospheric stability distribution in 90th percentile of turbulence data in each wind direction sector for HR2 at a wind speed of 9m/s

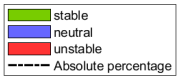

Since the comparative study is performed for the representative turbulence intensities the atmospheric stability distribution in the 90^{th} percentile of the data,

that is in the upper 10^{th} percentile of available data in each wind sector is more representative of the measured and modelled turbulence intensity as seen in Figure 4.31 and 4.32. The relative percentage of atmospheric stability conditions present in the 90^{th} percentile of data in each of the defined wind sectors in WMR and HR2 is shown in Figure 4.35 and 4.36. After correlating the atmospheric stability distribution in the 90^{th} percentile of the measured data with the modelled results of turbulence intensity in each wind direction sectors, the better performance of the Modified Frandsen model in the direct wake sectors in HR2 can be explained. The 90^{th} percentile of the measured data in the direct wake sectors in HR2 represent completely unstable conditions. This observation indicates that the Modified Frandsen model could be better at estimating directional turbulence under unstable conditions.

4.2.2 Turbulence models performance with respect to atmospheric stability conditions

In order to fully understand the performance of the turbulence models with varying atmospheric stability the measured and ambient turbulence data for the wind speed range of 7-9m/s are categorized into stable, neutral and unstable atmospheric stability conditions. Here, the considered wind speed range was extended to be able to have more measurement data. The relative percentage distribution of the atmospheric stability for each wind direction sector in WMR and HR2 for the selected wind speed range is presented in Figure 4.37 and 4.38. The overall variation in the stability conditions with respect to wind direction is very similar to what was observed with the data in the wind speed bin of 9m/s. However, an increase in the relative percentage of neutral conditions in each wind direction bin can be seen.

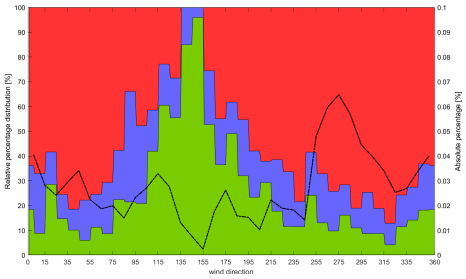

Figure 4.37: Relative atmospheric stability distribution in each wind direction sector observed in WMR for a wind speed of 7-9m/s

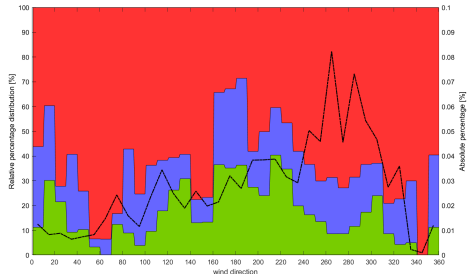

Figure 4.38: Relative atmospheric stability distribution in each wind direction sector observed in HR2 for a wind speed of 7-9m/s

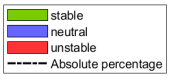

Figure 4.39 and 4.40 show the mean ambient turbulence intensity for each atmospheric stability per wind speed. In both wind farms, highest mean ambient turbulence intensity levels for the wind speed range of 7-9 m/s are observed under unstable conditions followed by neutral and then stable conditions representing

lowest ambient turbulence levels.

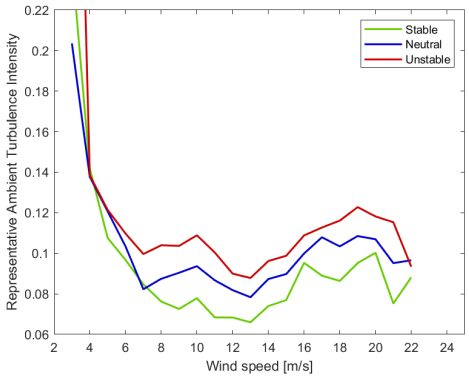

Figure 4.39: Mean ambient turbulence intensity for each atmospheric stability per wind speed for F07 in WMR

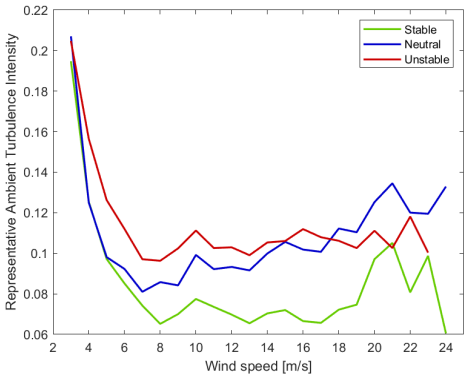

Figure 4.40: Mean ambient turbulence intensity for each atmospheric stability per wind speed for D05 in HR2

Figure 4.41 and 4.42 show the sector binned representative ambient turbulence under each stability condition for F07 in WMR and D05 in HR2. For WMR that is positioned relatively closer to the coast than HR2, the ambient turbulence intensity in each stability conditions are more or less the same for coastal wind directions ranging from 175-290 degrees. This observation can be as a result of coastal wind being dominated by the land effects such as roughness length and land-sea temperature variations. In contract to the observation for coastal wind directions, the ambient turbulence intensity under unstable conditions for the Easterly wind directions for F07 in WMR, is seen to be significantly higher than the turbulence under stable or neutral stability conditions.

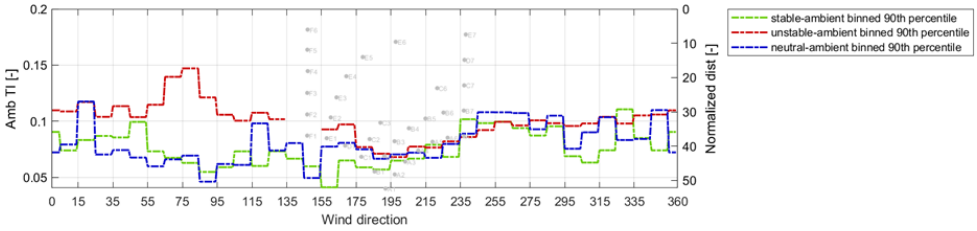

Figure 4.41: Binned representative ambient turbulence under each stability condition for F07 in WMR

For D05 in HR2 for the coastal wind directions a significant increase in stable ambient turbulence intensity is seen for wind directions ranging from 50-60 degrees that is mainly due to lower number of stable observations in this wind direction as seen in Figure 4.38. In addition an increase in unstable and stable ambient turbulence intensity is seen for wind directions from 110-160 degrees that can be as a result of wind being dominated by land effect in combination with additional turbulence from the wake of neighbouring wind farm HR. Lastly, for the open sea wind direction of 280-320 degrees an increase in neutral atmospheric turbulence

intensity is seen in Figure 4.42, that can be could be attributed to the increased offshore ambient turbulence intensity and higher number of neutral atmospheric stability distribution compared to the number of stable atmospheric stability distribution as seen in Figure 4.38.

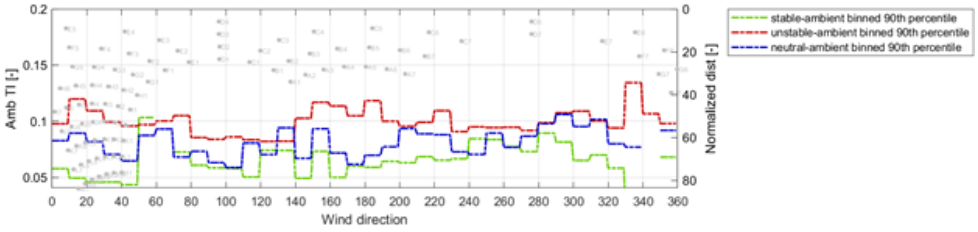

Figure 4.42: Binned representative ambient turbulence under each stability condition for D05 in HR2

This categorized representative ambient turbulence is used as an input into the turbulence models for estimating directional turbulence. Following this, the performance of the turbulence models is assessed by comparing:

1. Measured and modelled added turbulence intensity for each of the three atmospheric stability conditions.
2. Measured and modelled directional turbulence intensity with respect to ζ defining the degree of stability.

The purpose of this analysis is to understand the relationship between atmospheric stability and the performance of the turbulence model in predicting the 90^{th} percentile of directional turbulence intensity. Therefore, the comparative studies focused only on wind direction sectors with a sufficient number of observations and all stability conditions present in the 90^{th} percentile of the observed data (see Figure 4.43 and 4.44).

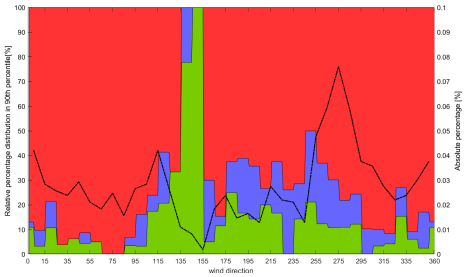

Figure 4.43: Relative atmospheric stability distribution in 90th percentile of turbulence data in each wind direction sector in WMR for a wind speed range of 7-9m/s

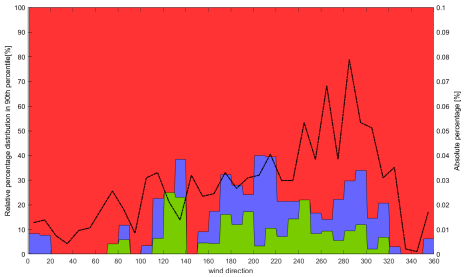

Figure 4.44: Relative atmospheric stability distribution in 90th percentile of turbulence data in each wind direction sector in HR2 for a wind speed range of 7-9m/s

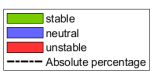

Added turbulence intensity comparison

Added turbulence intensities is calculated with reference to the representative ambient turbulence intensity levels:

$$I_{add} = \sqrt{I_{dir}^2 - I_{amb}^2} \tag{4.3}$$

The added turbulence represents the effects of the wind farm on the directional turbulence levels, independently of the variations caused by the changing ambient turbulence intensities. Figure 4.45 and 4.46 shows the calculated added turbulence intensity from the turbulence models at WMR and HR2. The turbulence models do not differentiate between each atmospheric stability as the added turbulence levels are similar for each stability conditions. Minor variations in the estimated added turbulence levels for each atmospheric stability from the Modified Frandsen model are observed. This variation is related to the term alpha (α - see equation 2.20) in the Modified Frandsen model, which is defined as a function of the representative ambient turbulence intensity. This results in a slightly lower added turbulence for stability conditions with lowest ambient turbulence intensity level in the investigated wind direction sector.

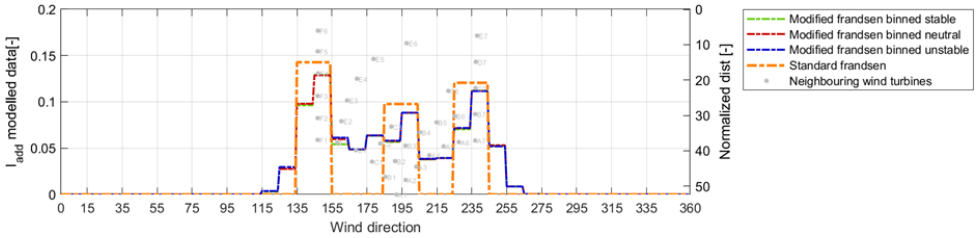

Figure 4.45: Added turbulence intensity calculated from the turbulence models for F07 in WMR for a wind speed range of 7-9m/s

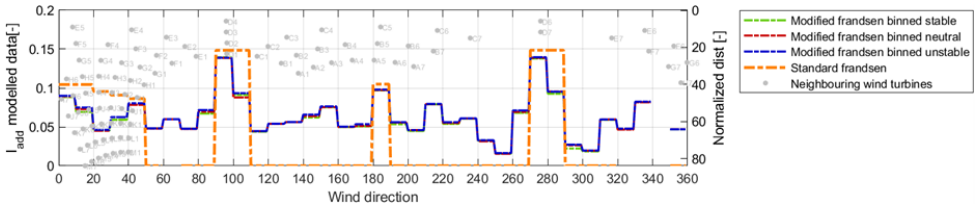

Figure 4.46: Added turbulence intensity calculated from the turbulence models for D05 in HR2 for a wind speed range of 7-9m/s

The added turbulence intensity from the turbulence models is seen to vary in magnitude with respect to the distance of the nearest wake inducing upstream wind turbine. The variation in magnitude of added turbulence with respect to upstream wind turbine distance was also observed in the measured results as seen in Figure 4.47 and 4.48. In addition, the measured results also presented a difference in the added turbulence levels for each atmospheric stability conditions. It is to be noted

that zero added turbulence within the wake flow of upstream wind turbine, as seen in Figure 4.47 and 4.48, is seen for sectors where the representative ambient turbulence was higher than what was measured. Therefore, the results from these wind direction sectors were disregarded from further analysis.

For F07 in WMR the added turbulence was recorded to be highest under stable conditions for direct wake situation from F6 and E7. The results for D5 in HR2 also showed maximum added turbulence under stable condition for direct wake from D6 (270-280 sector). However, this observation is not consistent for the wake flow from E5, D4 and C5.

To compare the modelled and measured added turbulence intensity, their dependence with respect to the atmospheric stability and the distance to the upstream wake-inducing wind turbine is investigated. In the case where several wind direction sectors have a common distance to the upstream wake inducing wind turbine, the maximum value of the added turbulence intensity for each atmospheric stability is chosen to be most representative of that distance of the upstream wind turbine.

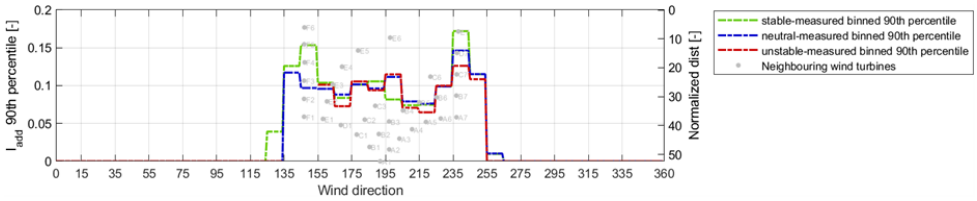

Figure 4.47: Added turbulence intensity calculated from the binned measured directional turbulence for F7 in WMR for a wind speed range of 7-9m/s

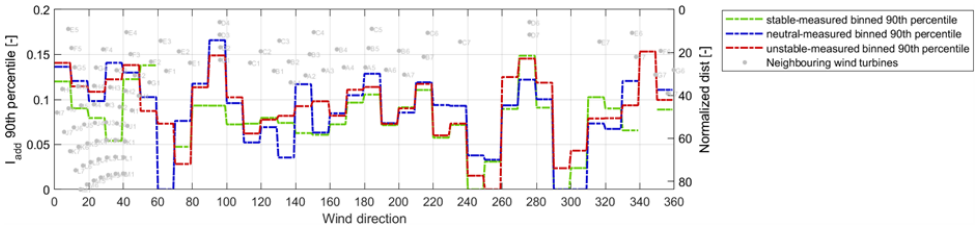

Figure 4.48: Added turbulence intensity calculated from the binned measured directional turbulence for D5 in HR2 for a wind speed range of 7-9m/s

For F07 in WMR this analysis showed consistent under-prediction of the added turbulence using the Modified and Standard Frandsen model (Figure 4.49). This under-prediction of the absolute value of added turbulence was seen to be greater for the distance of upstream wind turbine greater than 10D (far wake) in comparison with the distance of upstream wind turbine less than 10D (direct wake).

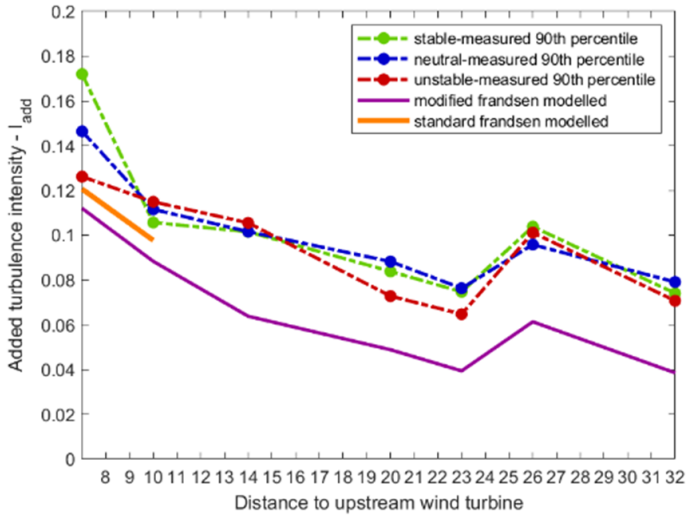

Figure 4.49: Added turbulence intensity calculated from the turbulence models and measured data-set for varying normalized distance of upstream wind turbines in WMR

For direct wake situation the under-prediction in the added turbulence was highest with respect to stable atmospheric conditions with an absolute difference of 0.0387 and lowest for unstable atmospheric condition due to lower added turbulence intensity with an absolute difference of 0.0204 as shown in Table 4.4. For far wake situation non significant difference was seen (Figure 4.49) in the under-prediction of added turbulence intensity for each atmospheric stability conditions. This observation is confirmed by the mean absolute difference between measured and Modified Frandsen model estimated added turbulence intensity (see Table 4.4), showing similar values with the relatively low under prediction of added turbulence for unstable conditions. The lower under-prediction of added turbulence intensity for unstable atmospheric conditions can be explained by increased mixing in the atmosphere due to the movement of the air parcels that resulting in increased wake recovery.

Table 4.4: Mean absolute difference between measured and Modified Frandsen model estimated added turbulence and directional turbulence intensity for F07 in WMR

Mean absolute difference between measured and Modified Frandsen modelled		Stable	Neutral	Unstable
Direct wake (upstream turbine <10D)	Added TI	0.0387	0.0288	0.0204
	Direction TI	0.0296	0.0237	0.0169
Far wake (upstream turbine >10D)	Added TI	0.0372	0.0378	0.0326
	Direction TI	0.0286	0.0255	0.0204

Figure 4.50 shows how these under-prediction of the added turbulence intensity translate in the comparison of directional turbulence intensity for each atmospheric stability condition with respect to distance of upstream wake inducing wind turbine. Here, in line with the observations from the comparative study of added turbulence intensity, both the turbulence models show an under-prediction of directional turbulence intensity. However, it is to be noted that the magnitude of the mean absolute difference between measured and Modified Frandsen model estimated

directional turbulence intensity is lower than the absolute difference of added turbulence intensity. Here, the lowest absolute difference of directional turbulence intensity is seen for unstable conditions, that is a result of low absolute difference of added turbulence intensity and high ambient turbulence levels.

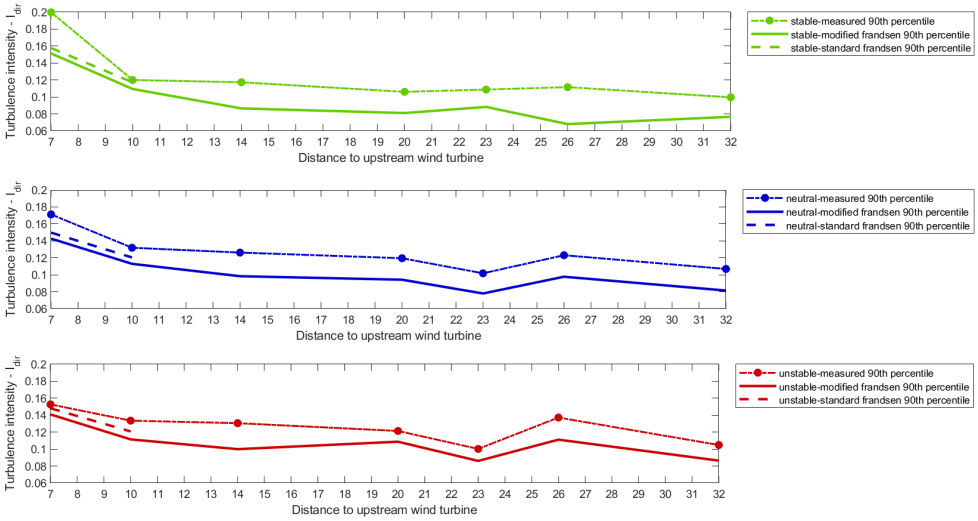

Figure 4.50: Directional turbulence intensity comparison for each atmospheric stability condition with respect to normalized distance of upstream wake inducing wind turbine in WMR

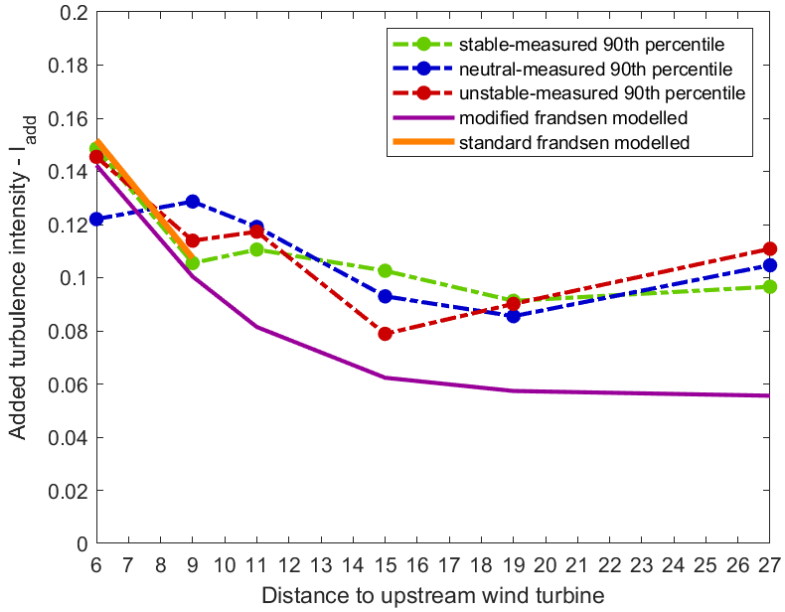

Figure 4.51: Added turbulence intensity calculated from the turbulence models and measured data-set for varying normalized distance of upstream wind turbines in HR2

For HR2 the results of this analysis are presented in Figure 4.51 and 4.53. Figure 4.51 shows the variation of the added turbulence intensity with increasing distance of upstream wind turbines excluding wind direction sector 20-50 degrees that are identified as facing wind farm turbulence by the Standard Frandsen model. For D5 in HR2 the Standard Frandsen model estimated added TI for distance of upstream wind turbines less than 10D is seen to provide a better estimation than Modified Frandsen model. The Standard Frandsen model estimated added turbulence is in line with the added turbulence calculated from measured data under stable atmospheric conditions. The modified Frandsen model consistently under-predicts added turbulence intensity except for neutral conditions when the upstream wind turbine is located at a distance of less than 7D. This under-prediction of the absolute value of added turbulence from the Modified Frandsen model was seen to be greater for far wake situations in comparison to direct wake situations as seen in Table 4.5. For far wake situations in HR2 similar observations as WMR can be made, since for both the wind farms the lowest absolute difference of added turbulence was seen for unstable conditions.

Table 4.5: Mean absolute difference between measured and Modified Frandsen model estimated added turbulence and directional turbulence intensity for D05 in HR2

Mean absolute difference between measured and Modified Frandsen modelled		Stable	Neutral	Unstable
Direct wake (upstream turbine <10D)	Added TI	0.0057	0.0243	0.0083
	Direction TI	0.0057	0.0242	0.0059
Far wake (upstream turbine >10D)	Added TI	0.0361	0.0364	0.0351
	Direction TI	0.0289	0.0208	0.0181

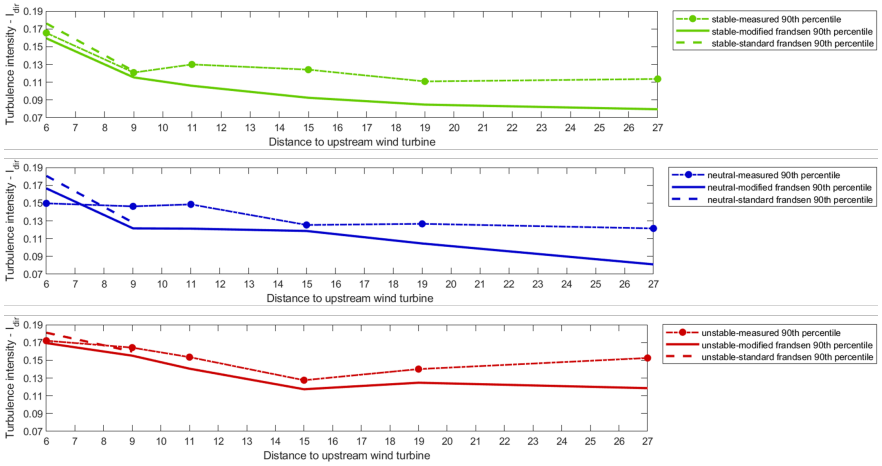

Figure 4.52: Directional turbulence intensity comparison for each atmospheric stability condition with respect to normalized distance of upstream wake inducing wind turbine in HR2

Figure 4.52 shows how the difference in the prediction of added turbulence intensity with respect to each atmospheric stability reflect into the comparison of directional turbulence intensity. Here, both the turbulence models show similar performance in estimating directional turbulence intensity as observed from the comparative study of added turbulence intensity at D05 in HR2. However it is to be noted that the

magnitude of the under-prediction of directional turbulence intensity, is significantly lower in comparison with the under-prediction of added turbulence intensity for unstable conditions in both far wake and direct wake situations(see 4.5). This drop in the under-prediction of directional TI and added TI can be explained by the higher ambient turbulence intensity levels for unstable conditions.

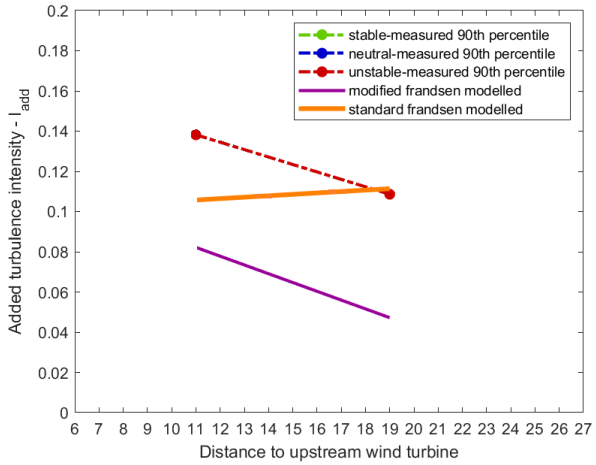

Figure 4.53: Comparison of measured and modelled wind farm added turbulence intensity for D05 in HR2 from wind direction sectors of 20-50 degrees with respect to normalized distance of upstream wake inducing wind turbine.

For the wind direction sectors (20-50 degrees) facing wind farm turbulence as identified by the Standard Frandsen model, both the considered turbulence model show an under-prediction of added turbulence intensity (Figure 4.53). However the Standard Frandsen model estimated added turbulence is relatively closer to the measurement based added turbulence. It is to be noted that there are only unstable conditions present in the 90th percentile of observed data in the wind direction sectors facing wind farm turbulence. The limitation of the data set makes it difficult to extract conclusions.

Directional turbulence intensity comparison

The comparative study of directional turbulence intensity is performed separately for the ranges of wind direction sectors facing a similar case as identified by the Standard Frandsen model. This comparison is performed with respect to varying degree of stability defined by $\zeta = z/L$. The compared directional turbulence intensity values are the 90th percentile of the 10 min data readings in a bin width of 0.2. It should be noted that the results shared in the Figures below labeled as modelled TI, refer to the directional TI calculated from the Modified Frandsen model.

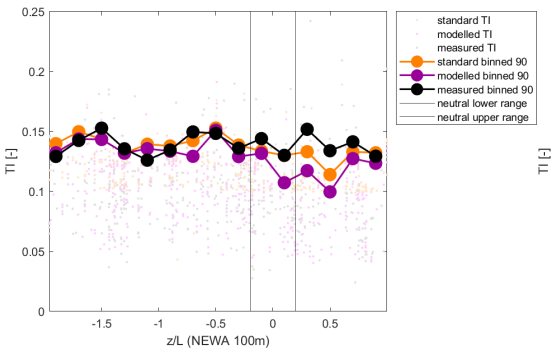

Figure 4.54: WMR directional turbulence intensity with respect to z/L for wind direction with distance of upstream wake inducing wind turbines less than 10D

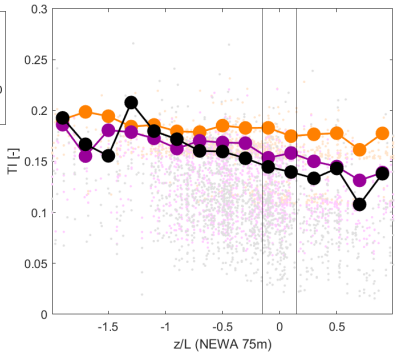

Figure 4.55: HR2 directional turbulence intensity with respect to z/L for wind direction with distance of upstream wake inducing wind turbines less than 10D

Figure 4.54 and 4.55 show the modelled and measured directional turbulence intensity for wind directions where the upstream wind turbines are positioned at less than 10 diameters away. For both WMR and HR2 under unstable conditions the modified and standard Frandsen model, estimate directional turbulence intensity around the measured value. However, under neutral and stable conditions different observations are made for both the wind farms. For WMR under neutral and stable conditions the standard and modified model underestimate the direction turbulence intensity. For HR2 under neutral and stable conditions the standard Frandsen model overestimate the directional turbulence intensity whereas the modified Frandsen provide a better prediction of turbulence intensity with respect to the observation.

Figure 4.56 and 4.57 show the modelled and measured directional turbulence intensity for wind directions where less than 5 upstream wind turbines are positioned more than 10 diameters away. For both WMR and HR2 an underestimation of the directional turbulence intensity is seen for all the atmospheric stability conditions. The directional turbulence intensity calculated by the Standard Frandsen model represents the ambient turbulence intensity as the it does not consider wake effects in the selected wind directions sectors. Here, for far wake situations the Modified Frandsen model provides better results of directional turbulence intensity for all stability conditions in comparison to Standard Frandsen model.

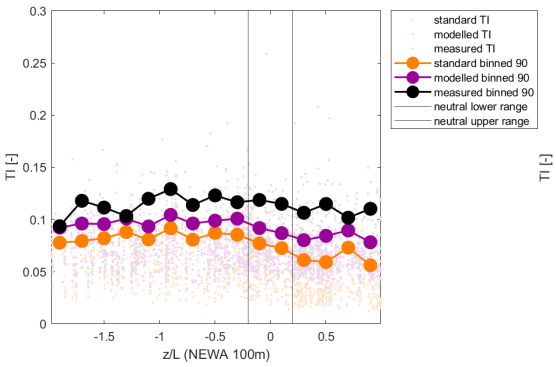

Figure 4.56: WMR directional turbulence intensity with respect to z/L for wind direction with distance of upstream wake inducing wind turbines greater than 10D

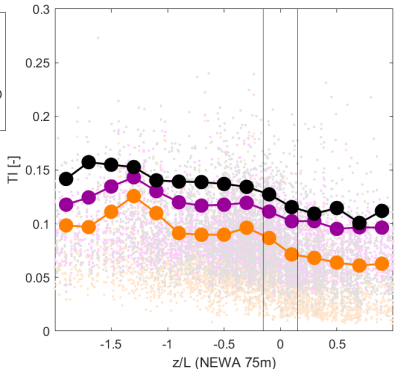

Figure 4.57: HR2 directional turbulence intensity with respect to z/L for wind direction with distance of upstream wake inducing wind turbines greater than 10D

Figure 4.58 shows the results of the comparative study of the directional turbulence intensity in the wind direction sectors (20-50 degrees) identified as facing wind farm turbulence as per the Standard Frandsen model. Overall Standard Frandsen model in comparison with modified Frandsen model is seen to provide a better estimate of measured directional turbulence intensity for all stability conditions. The modified Frandsen model consistently underestimates the directional turbulence intensity in all stability conditions. The Standard Frandsen model is seen to underestimated directional turbulence intensity under unstable and neutral condition, while providing a better prediction of TI with respect to the observations under stable conditions.

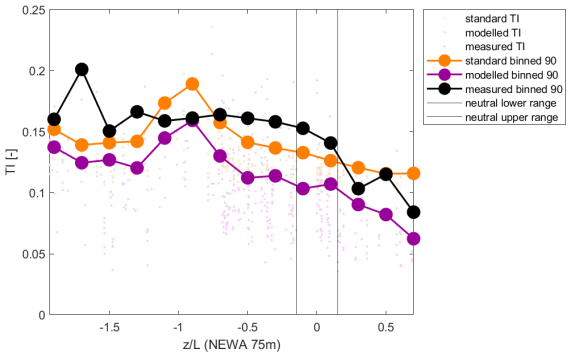

Figure 4.58: HR2 directional turbulence intensity with respect to z/L for wind direction face wind farm turbulence (20-50 degrees)

With limited number of measured TI values in each bin of z/L no definite conclusion can be drawn regarding the performance of the turbulence model from this comparative study. However, it is to be noted that most of the observation are in line with the observations made during the added turbulence intensity comparative analysis.

Chapter 5

Conclusion and Recommendations

Wind turbines in a wind farm are subjected to increased fatigue loads due to a proportional increase in turbulence in the wake of upstream wind turbines. In order to obtain an estimate of the increased fatigue loads for design purposes, Frandsen proposed a semi-empirical model to estimate the increased turbulence in the wake of upstream wind turbines as early as 1999 [3]. However, with the increasing size of wind turbines and wind farms, the accuracy of Frandsen's model became questionable. Therefore, this research focused on determining the accuracy of the Frandsen model for estimating directional turbulence intensity using measured data from two offshore wind farms: Westermost Rough and Horns Rev 2. In this chapter, conclusions based on the turbulence model validation study conducted in Chapter 4 are presented in relation to the research objectives (see Chapter 1). Recommendations for further research are also provided based on the conclusions.

5.1 Conclusion

The conclusions presented in this chapter answer the research question and objectives defined at the beginning of this project:

Is the Frandsen model accurate for estimating of turbulence intensity inside a wind farm under specific atmospheric stability conditions in a large offshore wind farm?

To answer this research question, a comparative analysis of the modelled and measured sectoral directional turbulence intensity for each atmospheric stability condition was performed. Based on this analysis, an objective answer to the main research question would be:

"The atmospheric stability distribution and the distance of upstream wake inducing wind turbine at the offshore site plays a considerable role in the accuracy of the estimated turbulence intensity from the Frandsen model. The Standard and Modified Frandsen model estimated directional turbulence intensity is not accurate for all atmospheric stability conditions. Both the turbulence models result in an

underestimation of turbulence intensity that is not preferred from a design point of view. The directional turbulence intensity estimation from the turbulence models was noted to be closest to the measured data under unstable conditions. This fact can be attributed to the presence of significant number of unstable conditions present in the offshore wind farms, that would have been used to design the semi-empirical Frandsen model."

Overall, based on the comparative study between measured and modeled directional turbulence intensity experienced at WMR and HR2, the following observations can be made regarding the performance of the turbulence models:

Modified Frandsen model:

- The directional turbulence intensity is consistently underpredicted for each atmospheric stability condition.
- The underprediction of directional turbulence increases with increasing distance from the upstream wake inducing wind turbine.
- It is found that the model performs relatively better than the standard Frandsen model for upstream wind turbines located at a distance greater than 10 diameters.

Standard Frandsen model:

- Similar to the Modified Frandsen model, the directional turbulence intensity is underpredicted for each atmospheric stability condition at WMR. However, a slight overprediction was found for stable conditions in HR2 for wind directions influenced by direct wake. This overprediction can be attributed to the significantly lower number of observed stable conditions and the different locations of the wind farm with a greater distance from the coast for HR2 compared to WMR.
- It shows relatively better performance than the modified Frandsen model for upstream wind turbines located less than 10D apart and for wind direction sectors identified as facing the wind farm turbulence.
- It fails to account for the added turbulence in wind direction sectors with fewer than five rows of upstream wind turbines located at a distance greater than 10 diameters.

It should be noted that there are several limitations associated with the obtained results:

1. Imperfect estimation of the values of turbulence intensity, wind speed and wind direction for free flow. These values are assumed to be constant over the scale of the wind farm.
2. The measured turbulence intensity is a function of the reduced wind speed in the wake of the upstream wind turbine. However, the modelled turbulence intensity is assumed to be a function of the wind speed in the free flow, resulting in increased turbulence intensity values.
3. Limited observational data for each atmospheric stability in each wind direction sector.

5.2 Recommendations

During this study, there were some limitations in terms of available data and some further assumptions were made considering the time frame of the project. Therefore, in order to confirm the findings obtained regarding the performance of the Frandsen model and to continue the research, some recommendations for further work can be made:

1. Analyse the accuracy of the Frandsen model for several large offshore wind farms with different atmospheric stability distributions to obtain clear conclusions. Applying this analysis to multiple sites would not only confirm the conclusion drawn from this study, but also increase the chance of identifying a trend in the accuracy of the estimated turbulence intensity.
2. Conduct the study in a wind farm with meteorological measurements of free wind flow at several heights from different locations in the wind farm. Consideration of meteorological measurements of free flow would remove uncertainty in the estimation of free flow conditions. These meteorological measurements could be from a met mast, SODAR or LIDAR.
3. Develop the external disturbance correction model for free wind flow, separately for each atmospheric stability. Since the wind speed and turbulence gradient present at the scale of the wind farm may be different for each atmospheric stability.
4. Perform a fatigue load analysis using the modelled turbulence intensity levels for each atmospheric stability. This analysis would provide information on how the difference between measured and modelled turbulence intensity levels is reflected in the fatigue load.
5. Develop a wake turbulence model that accounts for the effects of atmospheric stability distribution on the design site as it is concluded from this study affects the level of estimated turbulence.

Bibliography

[1] Paris agreement. UNTC XXVII 7.d.

[2] International Renewable Energy Agency. Future of wind: Deployment, investment, technology, grid integration and socio-economic aspects (a global energy transformation paper), 2019.

[3] Sten Frandsen and Morten L. Thøgersen. Integrated fatigue loading for wind turbines in wind farms by combining ambient turbulence and wakes. *Wind Engineering*, 23(6):327–339, 1999.

[4] Julia Gottschall and Joachim Peinke. How to improve the estimation of power curves for wind turbines. *Environmental Research Letters*, 3(1):015005, jan 2008.

[5] International Electrotechnical Commission (IEC). Wind energy generation systems - part 1: Design requirements, Feb 2019.

[6] Peter Argyle, Simon Watson, Christiane Montavon, Ian Jones, and Megan Smith. Modelling turbulence intensity within a large offshore wind farm. *Wind Energy*, 21(12):1329–1343, 2018.

[7] L.J. Vermeer, J.N. Sørensen, and A. Crespo. Wind turbine wake aerodynamics. *Progress in Aerospace Sciences*, 39(6):467 – 510, 2003.

[8] R. J. Barthelmie, K. Hansen, S. T. Frandsen, O. Rathmann, J. G. Schepers, W. Schlez, J. Phillips, K. Rados, A. Zervos, E. S. Politis, and P. K. Chaviaropoulos. Modelling and measuring flow and wind turbine wakes in large wind farms offshore. *Wind Energy*, 12(5):431–444, 2009.

[9] Fernando Porté-Agel, Yu-Ting Wu, and Chang-Hung Chen. A numerical study of the effects of wind direction on turbine wakes and power losses in a large wind farm. *Energies*, 6(10):5297–5313, 2013.

[10] Mahdi Abkar and Fernando Porté-Agel. Mean and turbulent kinetic energy budgets inside and above very large wind farms under conventionally-neutral condition. *Renewable Energy*, 70:142 – 152, 2014. Special issue on aerodynamics of offshore wind energy systems and wakes.

[11] Mahdi Abkar, Ahmad Sharifi, and Fernando Porté-Agel. Wake flow in a wind farm during a diurnal cycle. *Journal of Turbulence*, 17(4):420–441, 2016.

[12] Fernando Porté-Agel, Yu-Ting Wu, Hao Lu, and Robert J. Conzemius. Large-eddy simulation of atmospheric boundary layer flow through wind turbines and wind farms. *Journal of Wind Engineering and Industrial Aerodynamics*,

99(4):154 – 168, 2011. The Fifth International Symposium on Computational Wind Engineering.

[13] Linlin Tian, Weijun Zhu, Wenzhong Shen, Ning Zhao, and Zhiwei Shen. Development and validation of a new two-dimensional wake model for wind turbine wakes. *Journal of Wind Engineering and Industrial Aerodynamics*, 137:90 – 99, 2015.

[14] Takeshi Ishihara, Atsushi Yamaguchi, and Yozo Fujino. Development of a new wake model based on a wind tunnel experiment. 01 2004.

[15] Fernando Carbajo Fuertes, Corey D. Markfort, and Fernando Porté-Agel. Wind turbine wake characterization with nacelle-mounted wind lidars for analytical wake model validation. *Remote Sensing*, 10(5), 2018.

[16] Yu-Ting Wu and Fernando Porté-Agel. Atmospheric turbulence effects on wind-turbine wakes: An les study. *Energies*, 5:5340–5362, 12 2012.

[17] A. Crespo and J. Herna´ndez. Turbulence characteristics in wind-turbine wakes. *Journal of Wind Engineering and Industrial Aerodynamics*, 61(1):71 – 85, 1996.

[18] A. Crespo, J. Hernández, and S. Frandsen. Survey of modelling methods for wind turbine wakes and wind farms. *Wind Energy*, 2(1):1–24, 1999.

[19] Guo-Wei Qian and Takeshi Ishihara. A new analytical wake model for yawed wind turbines. *Energies*, 11(3), 2018.

[20] Ingrid Neunaber, Michael Hölling, Richard J. A. M. Stevens, Gerard Schepers, and Joachim Peinke. Distinct turbulent regions in the wake of a wind turbine and their inflow-dependent locations: The creation of a wake map. *Energies*, 13(20), 2020.

[21] B. Sanderse, S.P. van der Pijl, and B. Koren. Review of computational fluid dynamics for wind turbine wake aerodynamics. *Wind Energy*, 14(7):799–819, 2011.

[22] Richard J.A.M. Stevens and Charles Meneveau. Flow structure and turbulence in wind farms. *Annual Review of Fluid Mechanics*, 49(1):311–339, 2017.

[23] D.C. Quarton and J.F. Ainslie. Turbulence in wind turbine wakes. *Wind Engineering*, 14(1):15–23, 1990.

[24] A. Crespo and J. Herna´ndez. Turbulence characteristics in wind-turbine wakes. *Journal of Wind Engineering and Industrial Aerodynamics*, 61(1):71 – 85, 1996.

[25] A. Duckworth and R. Barthelmie. Investigation and validation of wind turbine wake models. *Wind Engineering*, 32:459–475, 10 2008.

[26] P. E. J. Vermeulen. An experimental analysis of wind turbine wakes. In *3rd International Symposium on Wind Energy Systems*, pages 431–450, January 1980.

[27] Shengbai Xie and Cristina Archer. Self-similarity and turbulence characteristics of wind turbine wakes via large-eddy simulation. *Wind Energy*, 18(10):1815–1838, 2015.

[28] Takeshi Ishihara and Guo-Wei Qian. A new gaussian-based analytical wake model for wind turbines considering ambient turbulence intensities and thrust coefficient effects. *Journal of Wind Engineering and Industrial Aerodynamics*, 177:275 – 292, 2018.

[29] P. B. S. Lissaman. Energy effectiveness of arbitrary arrays of wind turbines. *Journal of Energy*, 3(6):323–328, 1979.

[30] I. Katic, J. Højstrup, and N.O. Jensen. A simple model for cluster efficiency. In W. Palz and E. Sesto, editors, *EWEC'86. Proceedings. Vol. 1*, pages 407–410. A. Raguzzi, 1987. European Wind Energy Association Conference and Exhibition, EWEC '86 ; Conference date: 06-10-1986 Through 08-10-1986.

[31] Teknisk Grundlag. Rekommandation til teknisk grundlag (recommendation to design basis). *Energistyrelsen*, 1992.

[32] Sten Frandsen. Turbulence and turbulence-generated structural loading in wind turbine clusters, Jan 2007.

[33] Amin Niayifar and Fernando Porté-Agel. A new analytical model for wind farm power prediction. *Journal of Physics: Conference Series*, 625:012039, jun 2015.

[34] Sten Tronæs Frandsen and Peter Hauge Madsen. Spatially average of turbulence intensity inside large wind turbine arrays. In *Offshore wind energy in Mediterranean and other European seas. Resources, technology, applications*, pages 97–106. Univ. of Naples, 2003. European Seminar Offshore Wind Energy in Mediterranean and Other European Seas, OWEMES 2003 ; Conference date: 10-04-2003 Through 12-04-2003.

[35] R. J. Barthelmie, S. T. Frandsen, M. N. Nielsen, S. C. Pryor, P.-E. Rethore, and H. E. Jørgensen. Modelling and measurements of power losses and turbulence intensity in wind turbine wakes at middelgrunden offshore wind farm. *Wind Energy*, 10(6):517–528, 2007.

[36] Arno J. Brand and Jan Willem Wagenaar. Turbulent wind turbine wakes in a wind farm. In *Progress in Turbulence and Wind Energy IV*, pages 231–234, Berlin, Heidelberg, 2012. Springer Berlin Heidelberg.

[37] Gunner Chr. Larsen. *A simple stationary semi-analytical wake model*. Number 1713(EN) in Denmark. Forskningscenter Risoe. Risoe-R. Risø National Laboratory for Sustainable Energy, Technical University of Denmark, 2009.

[38] Tuhfe Göçmen and Gregor Giebel. Estimation of turbulence intensity using rotor effective wind speed in lillgrund and horns rev-i offshore wind farms. *Renewable Energy*, 99:524 – 532, 2016.

[39] Leonardo Chamorro and Fernando Porté-Agel. Turbulent flow inside and above a wind farm: A wind-tunnel study. *Energies*, 4:1916–1936, 12 2011.

[40] Leonardo Chamorro, Roger Arndt, and Fotis Sotiropoulos. Turbulent flow properties around a staggered wind farm. *Boundary-Layer Meteorology*, 141:349–367, 12 2011.

[41] Corey D. Markfort, Wei Zhang, and Fernando Porté-Agel. Turbulent flow and scalar transport through and over aligned and staggered wind farms. *Journal of Turbulence*, 13:N33, 2012.

[42] Søren Juhl Andersen, Jens Nørkær Sørensen, Robert Mikkelsen, and Stefan Ivanell. Statistics of LES simulations of large wind farms. *Journal of Physics: Conference Series*, 753:032002, sep 2016.

[43] Leonardo Chamorro and Fernando Porté-Agel. Effects of thermal stability and incoming boundary-layer flow characteristics on wind-turbine wakes: A wind-tunnel study. *Boundary-Layer Meteorology*, 136, 09 2010.

[44] Kurt S. Hansen, Rebecca J. Barthelmie, Leo E. Jensen, and Anders Sommer. The impact of turbulence intensity and atmospheric stability on power deficits due to wind turbine wakes at horns rev wind farm. *Wind Energy*, 15(1):183–196, 2012.

[45] Giacomo Iungo and Fernando Porté-Agel. Volumetric scans of wind turbine wakes performed with three simultaneous wind lidars under different atmospheric stability regimes. *Journal of Physics: Conference Series*, 524:012164, 06 2014.

[46] Mahdi Abkar and Fernando Porté-Agel. The effect of free-atmosphere stratification on boundary-layer flow and power output from very large wind farms. *Energies*, 6:2338–2361, 05 2013.

[47] Abkara. Mahdi and Porté-Agel. Fernando. Influence of atmospheric stability on wind-turbine wakes: A large-eddy simulation study. *Physics of Fluids*, 27, 2015.

[48] Adrian Sescu and Charles Meneveau. Large-Eddy Simulation and Single-Column Modeling of Thermally Stratified Wind Turbine Arrays for Fully Developed, Stationary Atmospheric Conditions. *Journal of Atmospheric and Oceanic Technology*, 32(6):1144–1162, 06 2015.

[49] Mahdi Abkar, Ahmad Sharifi, and Fernando Porte-Agel. Wake flow in a wind farm during a diurnal cycle. *Journal of Turbulence*, 17(4):420–441, 2016.

[50] V Sharma, Marc Calaf, Michael Lehning, and M. Parlange. Time-adaptive wind turbine model for an les framework. *Wind Energy*, 19, 07 2015.

[51] Rebecca Barthelmie, Ole Frost Hansen, Karen Enevoldsen, Jørgen Højstrup, Sten Frandsen, Sara Pryor, Søren Larsen, Maurizio Motta, and Peter Sanderhoff. Ten Years of Meteorological Measurements for Offshore Wind Farms. *Journal of Solar Energy Engineering*, 127(2):170–176, 04 2005.

[52] Matthias Türk and Stefan Emeis. The dependence of offshore turbulence intensity on wind speed. *Journal of Wind Engineering and Industrial Aerodynamics*, 98(8):466 – 471, 2010.

[53] Roland B. Stull. *An Introduction to Boundary Layer Meteorology*. Dordrecht: Kluwer Academic Publishers, Dordrecht, 1988.

[54] Ameya Sathe, J Mann, Thanasis Barlas, W Bierbooms, and Gerard van Bussel. Influence of atmospheric stability on wind turbine loads. *Wind Energy*, 16, 10 2013.

[55] Kurt Schaldemose Hansen, G Larsen, and S Ott. Dependence of offshore wind turbine fatigue loads on atmospheric stratification. *Journal of Physics: Conference Series*, 524:012165, 06 2014.

[56] American Meteorological Society. critical richardson number. `http://glossary.ametsoc.org/wiki/Critical_richardson_number`.

[57] Andrey Grachev and Chris Fairall. Dependence of the monin-obukhov stability parameter on the bulk richardson number over the ocean. *Journal of Applied Meteorology - J APPL METEOROL*, 36:406–415, 04 1997.

[58] Bernhard Lange, Søren Larsen, Jørgen Højstrup, and R. Barthelmie. Importance of thermal effects and sea surface roughness for offshore wind resource assessment. *Journal of Wind Engineering and Industrial Aerodynamics*, 92:959–988, 07 2004.

[59] J. A. Businger, J. C. Wyngaard, Y. Izumi, and E. F. Bradley. Flux-Profile Relationships in the Atmospheric Surface Layer. *Journal of the Atmospheric Sciences*, 28(2):181–189, 03 1971.

[60] U. L. F. Högström. *Non-Dimensional Wind and Temperature Profiles in the Atmospheric Surface Layer: A Re-Evaluation*, pages 55–78. Springer Netherlands, Dordrecht, 1988.

[61] A. A. M. Holtslag and H. A. R. De Bruin. Applied Modeling of the Nighttime Surface Energy Balance over Land. *Journal of Applied Meteorology*, 27(6):689–704, 06 1988.

[62] Andrey Grachev, Chris Fairall, and E. Bradley. Convective profile constants revisited. *Boundary-Layer Meteorology*, 94:495–515, 03 2000.

[63] Cristina L. Archer, Brian A. Colle, Dana L. Veron, Fabrice Veron, and Matthew J. Sienkiewicz. On the predominance of unstable atmospheric conditions in the marine boundary layer offshore of the u.s. northeastern coast. *Journal of Geophysical Research: Atmospheres*, 121(15):8869–8885, 2016.

[64] A.J.M. Van Wijk, A.C.M. Beljaars, A.A.M. Holtslag, and W.C. Turkenburg. Evaluation of stability corrections in wind speed profiles over the north sea. *Journal of Wind Engineering and Industrial Aerodynamics*, 33(3):551 – 566, 1990.

[65] M. Motta, R. J. Barthelmie, and P. Vølund. The influence of non-logarithmic wind speed profiles on potential power output at danish offshore sites. *Wind Energy*, 8(2):219–236, 2005.

[66] Sven-Erik Gryning, Ekaterina Batchvarova, Burghard Brümmer, Hans Jørgensen, and Søren Larsen. On the extension of the wind profile over homogeneous terrain beyond the surface layer. *Boundary-Layer Meteorology*, 124:251–268, 08 2007.

[67] Ameya Sathe, Sven-Erik Gryning, and Alfredo Peña. Comparison of the atmospheric stability and wind profiles at two wind farm sites over a long marine fetch in the north sea. *Wind Energy*, 14(6):767–780, 2011.

[68] U. Högström. Non-dimensional wind and temperature profiles in the atmospheric surface layer: A re-evaluation. *Boundary-Layer Meteorology*, 42:55–78, 1988.

[69] M Metzger, B.J McKeon, and H Holmes. The near-neutral atmospheric surface layer: turbulence and non-stationarity. *Philosophical Transactions of the Royal Society A: Mathematical, Physical and Engineering Sciences*, 365(1852):859–876, 2007.

[70] Daniel A. Rajewski, Eugene S. Takle, Julie K. Lundquist, Steven Oncley, John H. Prueger, Thomas W. Horst, Michael E. Rhodes, Richard Pfeiffer, Jerry L. Hatfield, Kristopher K. Spoth, and Russell K. Doorenbos. Crop Wind Energy Experiment (CWEX): Observations of Surface-Layer, Boundary Layer, and Mesoscale Interactions with a Wind Farm. *Bulletin of the American Meteorological Society*, 94(5):655–672, 05 2013.

[71] Laurent Beaudet (SGRE). private communication, 2019.

[72] *Report on WRF model sensitivity studies and specifications for the mesoscale wind atlas production runs: Deliverable D4.3*, volume D4.3. NEWA - New European Wind Atlas, 2019.

[73] Bruce Ratner. The correlation coefficient: Its values range between +1/1, or do they? *Journal of Targeting, Measurement and Analysis for Marketing*, 17:139–142, 5 2009.

[74] *Wind Characteristics and Resources, Wind Energy Explained*, chapter 2, pages 21–82. John Wiley Sons, Ltd, 2002.

TU Delft Delft University of Technology